Department of Electrical Engineering

Noise analysis of high voltage capacitors and dry-type air-core reactors

Marcin Hurkala

Aalto University

DOCTORAL DISSERTATIONS

Aalto University publication series
DOCTORAL DISSERTATIONS 155/2013

Noise analysis of high voltage capacitors and dry-type air-core reactors

Marcin Hurkala

A doctoral dissertation completed for the degree of Doctor of Science in Technology to be defended, with the permission of the Aalto University School of Electrical Engineering, at a public examination held at the lecture hall S1 of the school on 18th December 2013 at 12.

Aalto University
School of Electrical Engineering
Department of Electrical Engineering

Supervising professor
Professor Matti Lehtonen

Preliminary examiners
Professor Steffen Grossmann, Technische Universität Dresden, Germany
Doctor Kaj Juslin, VTT Technical Research Centre of Finland

Opponents
Professor Timo Vekara, University of Vaasa
Professor Steffen Grossmann, Technische Universität Dresden, Germany

Aalto University publication series
DOCTORAL DISSERTATIONS 155/2013

ISBN 978-952-60-5361-5
ISBN 978-952-60-5362-2 (pdf)
ISSN-L 1799-4934
ISSN 1799-4934 (printed)
ISSN 1799-4942 (pdf)
http://urn.fi/URN:ISBN:978-952-60-5362-2

Unigrafia Oy
Helsinki 2013

Finland

441 697
Printed matter

Author
Marcin Hurkala

Name of the doctoral dissertation
Noise analysis of high voltage capacitors and dry-type air-core reactors

Publisher School of Electrical Engineering

Unit Department of Electrical Engineering

Series Aalto University publication series DOCTORAL DISSERTATIONS 155/2013

Field of research Power systems and high voltage engineering

Manuscript submitted 14 June 2013 **Date of the defence** 18 December 2013

Permission to publish granted (date) 2 September 2013 **Language** English

☒ **Monograph** ☐ **Article dissertation (summary + original articles)**

Abstract

The goal for this work was to create new methods to study the noise production in some power system components, namely capacitors and reactors.

In the case of the capacitors the work was started by trying to create a FEM model of the individual capacitor element as well as each of the capacitor sides. In the end individual element proved to be too complicated to be modeled, but the sides were modeled using the assumption that they're individual clamped plates. To find out how the individual element behaves one was subjected to direct current of various amplitudes and the compression was measured with a dial indicator at various points. The compression was deemed to be linearly dependent on the distance from the middle point of the surface of the element.

In order to measure the response of the whole capacitor, a vibration measurement was used. Vibration transducer was used on each side to get the overall vibration response of each side when the capacitors were fed various inputs. The responses were measured in three different temperatures. The direct acoustic response was measured in the anechoic chamber. This yielded new information about the directivity of the noise produced by the capacitors at the different frequencies. The results of the vibration measurement could be also compared to the acoustic measurements. The comparison resulted in partially incoherent results. Final measurement related to the capacitors was one where the viscosity of the capacitor oil was measured. This allowed to partially explain the variations in the vibration response at the different temperatures.

The noise measurement of the reactors is difficult due to the high magnetic field caused by them. Since the direct measurement wasn't an option, a plastic tube extender was used to move the sound further away from the reactor where it could be then measured with regular microphone. The tube extender was used in one field reactor measurement, in one controlled reactor measurement, and its response was measured in the anechoic chamber. As a result it was found that the tube extender can be used in this kind of measurements, and perhaps could be in the future to use in recognizing the faults of the reactors before they become severe.

Keywords noise, capacitor, reactor

ISBN (printed) 978-952-60-5361-5 **ISBN (pdf)** 978-952-60-5362-2

ISSN-L 1799-4934 **ISSN (printed)** 1799-4934 **ISSN (pdf)** 1799-4942

Location of publisher Helsinki **Location of printing** Helsinki **Year** 2013

Pages 173 **urn** http://urn.fi/URN:ISBN:978-952-60-5362-2

Aalto-yliopisto

Tiivistelmä

Aalto-yliopisto, PL 11000, 00076 Aalto www.aalto.fi

Tekijä
Marcin Hurkala

Väitöskirjan nimi
Suurjännitekondensaattoreiden ja ilmasydämisten kelojen meluanalyysi

Julkaisija Sähkötekniikan korkeakoulu

Yksikkö Sähkötekniikan laitos

Sarja Aalto University publication series DOCTORAL DISSERTATIONS 155/2013

Tutkimusala Sähköverkot ja suurjännitetekniikka

Käsikirjoituksen pvm 14.06.2013 **Väitöspäivä** 18.12.2013

Julkaisuluvan myöntämispäivä 02.09.2013 **Kieli** Englanti

☒ **Monografia** ☐ **Yhdistelmäväitöskirja (yhteenveto-osa + erillisartikkelit)**

Tiivistelmä

Työn tavoitteena oli selvittää sähköverkossa käytettävien komponenttien, kondensaattorien ja reaktoreiden, melun syntymekanismeja sekä äänenhallintaa.

Kondensaattorien osalta työssä lähdettiin liikkeelle yrittämällä mallintaa ongelmaa FEMmallinnuksella. Yksittäistä kondensaattorielementtiä ja kondensaattorin sivuja yritettiin mallintaa, mutta kondensaattorielementti osoittautui liian monimutkaiseksi. Kondensaattorin sivut mallinnettiin käyttäen reunoistaan jäykästi kiinnitettyjen levyjen oletusta aikaisemman tutkimustiedon perusteella. Kondensaattorielementin käyttäytymisen selvittämiseksi mitattiin yksittäisen elementin painaumaa heittokellon avulla. Painauman havaittiin riippuvan lineaarisesti etäisyydestä elementin pinnan geometrisesta keskipisteestä.

Kokonaista kondensaattoria tarkasteltaessa lähdettiin liikkeelle sivujen värähtelymittauksesta. Kondensaattoriin vastetta mitattiin erilaisilla herätteillä. Kondensaattoreiden äänivastetta tutkittiin myös suoraan kaiuttomassa huoneessa. Tuloksena saatiin sekä tietoa siitä, miten kondensaattoreiden tuottama ääni suuntautuu, sekä voitiin vertailla äänimittauksia aikaisemmin tehtyihin värähtelymittauksiin. Vertailun tulokset olivat osittain ristiriitaisia. Lopuksi tutkittiin kondensaattoriöljyn viskositeettia. Mittauksella pyrittiin yhdistämään värähtelymittauksessa huomattuja vaste-eroja mittausten lämpötilaeroihin. Tulokset olivat lupaavia.

Reaktorien melumittaus on vaikeaa sen takia, että suuren magneettikentän takia normaalia mikrofonia ei voida käyttää suoraan. Työssä kehitettiin muovinen putkijärjestelmä, jonka avulla ääntä siirrettiin kauemmaksi reaktorista, jossa sitä voitiin mitata normaalilla laitteistolla. Putkijärjestelmä kalibroitiin akustisessa huoneessa, jonka jälkeen sitä käytettiin kahdessa kenttämittauksessa. Tuloksena havaittiin, että putkijärjestelmä soveltuu hyvin tämäntyyppiseen mittaukseen. Havaittiin myös, että tämäntyyppisen mittauksen avulla pystytään helposti havaitsemaan reaktorin äänen muuttuminen spektrianalyysin avulla. Tunnistaessamme äänen muutoksen ajoissa, voidaan mahdollisesti huomata alkavia vikoja ennen kuin ne kehittyvät vakaviksi

Avainsanat melu, kondensaattori, reaktori

ISBN (painettu) 978-952-60-5361-5 **ISBN (pdf)** 978-952-60-5362-2

ISSN-L 1799-4934 **ISSN (painettu)** 1799-4934 **ISSN (pdf)** 1799-4942

Julkaisupaikka Helsinki **Painopaikka** Helsinki **Vuosi** 2013

Sivumäärä 173 **urn** http://urn.fi/URN:ISBN:978-952-60-5362-2

Preface

As the communities gets more compact, the need of having power stations near the settlements increases. At the same time the need to understand how the power system components produce sound increases, as citizens do not want to listen to the noise the power stations produce around the clock. Until now the only solution has been to isolate the power station using enough dampening material between it and the inhabitants, but now thanks to the KOMPPI project it was possible to dive into the noise production of reactors and capacitors.

I would like to thank all the parties that financed the KOMPPI project: Tekes, Alstom Grid ("Alstom", formerly Nokian Capacitors), Fingrid and Helen Sähköverkko Oy.

For giving me the chance to work in this project I offer my sincere thanks to my supervisor, professor Matti Lehtonen.

For all the information given relating to the reactors and capacitors, as well as allowing the access to measure both reactors and capacitors I would like to thank Yrjö Enqvist, Jari Kotiniitty, Pekka Nevalainen, and Jussi Pöntys of Alstom Grid, and Timo Ojanen of Fingrid.

For the help in the measurements, without which I wouldn't have any results I would like to thank the following individuals working within the Aalto University: Ari Haavisto, Petri Hyvönen, Hannu Kokkola, Jouni Mäkinen, Tatu Nieminen, Veli-Matti Niiranen and Kari Nurminen of the Department of Electrical Engineering, Kari Kantola of the Department of Applied Mechanics, Symeon Delikaris-Manias, Javier Gomez Bolaños, Ilkka Huhtakallio, Henri Penttinen, and Tapani Pihlajamäki of the Department of Signal Processing and Acoustics, and also Juha-Pekka Pokki and Petri Uusi-Kyyny of Department of Biotechnology and Chemical Technology.

Erityiskiitokset Pirjo Heinelle, joka tutustutti minut tutkijan työnku-

vaan, Esa Pärnäselle, joka lukioajan esimerkillisellä opettamisella sai minut uskomaan, että fysiikka on kivaa, sekä ystävilleni, joiden tuki on ollut korvaamaton vuosien mittaan.

Wielkie dzięki dla mojej rodziny, która zawsze stała za mną i pomagała mi w tym czym się najwięcej interesowałem.

Helsinki, September 30, 2013,

Marcin Hurkala

Author's declaration

All the research and the work relating to post processing, analyses and conclusions in all the measurements is the sole work of the author.

The research group of High Voltage Engineering consisting of Petri Hyvönen, Jouni Mäkinen, Tatu Nieminen and Veli-Matti Niiranen helped me in the measurements of DC compression, vibration response of the capacitor sides and the acoustic response of the capacitor sides.

The team from Alstom Grid including Jari Kotiniitty, Pekka Nevalainen, and Jussi Pöntys helped with the measurements of acoustic response of the capacitor sides, reactor noise measurement in field, and reactor noise measurement in controlled environment.

In the DC compression of air filled element Kari Nurminen gave me the idea to start this type of measurements and Hannu Kokkola helped me with the measurements.

In the vibration response of the capacitor sides, Kari Kantola operated the measuring equipment and helped with preparation of the measurements.

Symeon Delikaris-Manias and Javier Gomez Bolaños from the Department of Signal Processing and Acoustics set up and operated the measuring equipment in the measurement of the acoustic response of the capacitor sides.

In the viscosity measurement Juha-Pekka Pokki and Petri Uusi-Kyyny of Department of Biotechnology and Chemical Technology helped with setting up the measurement. The author was responsible for operating the measuring device as well as calibrating it.

The idea for the tube extender came from Matti Lehtonen of the Department of Electrical Engineering and Henri Penttinen of the Department of Signal Processing and Acoustics. Measuring the response of the tube extenders was possible due to help of Tapani Pihlajamäki of the Department of Signal Processing and Acoustics.

Contents

List of symbols

Δ_m	Auxiliary variable
Δ_n	Auxiliary variable
ΔV	Change in volume
Δx	Total compression of capacitor elements
ε_0	Vacuum permittivity
ε_r	Relative permittivity
λ	Warburton's and Mitchell-Hazell's frequency parameter
λ_f	Wavelength
μ_0	Vacuum permeability
ρ	Density
ρ_{air}	Density of air
σ	Poisson's ratio
ω	Angular velocity

A	Area
a	Length of the plate edge
$A_{profile}$	Area of the bottom of the capacitor
b	Length of the plate edge
C	Capacitance
Cf_n	Cf unit's nominal voltage
Cf_r	Cf unit's real voltage
Cp_n	Cp unit's nominal voltage
Cp_r	Cp unit's real voltage
D	Flexural rigidity
d	Thickness
D_f	Largest dimension of the radiator
d_f	Fraunhofer distance
d_{jk}	Distance between the cables j and k
D_m	Maximum displacement
d_r	Diameter of the reactor
E	Young's modulus
E_{dstr}	Dielectric strength
F	Faraday
f	Frequency
F_x	Force in the x-direction
f_0	Natural breathing frequency of reactor

g	Standard gravity
G_x	Auxiliary variable
G_y	Auxiliary variable
h	Thickness of the plate
H_x	Auxiliary variable
H_y	Auxiliary variable
I	Electric current
i_j	Current in the cable j
i_k	Current in the cable k
I_N	Rated current
I_T	Reduced current
J_x	Auxiliary variable
J_y	Auxiliary variable
k	Stiffness
L	Inductance
l	Length of the cable
L_p	Sound pressure level in decibels
$L_{WA,IN}$	A-weighted sound power at rated current
$L_{WA,IT}$	A-weighted sound power at reduced current
m	Number of nodes
N	Number of windings
n	Number of anti-nodes
N_l	Number of windings per unit of length
P	Real power
p	pressure
p_n	Pressure at nominal voltage level
p_r	Pressure at real input voltage level
p_{ref}	Reference pressure
Q	Reactive power
r	Radius
t	Total number of capacitor elements
U	Electric potential
U_n	Nominal voltage
U_r	Real input voltage
v	Speed of air
X	Compression amount

List of abbreviations

AC	Alternate current
CSC	Compressible space component
DC	Direct current
FEM	Finite element method
FFT	Fast fourier transform
HVDC	High voltage direct current
MPP	Microperforated panel
SPL	Sound pressure level
THD	Total harmonic distortion relative to the fundamental frequency

List of Figures

List of Tables

1. Introduction

1.1 Background

High voltage capacitors (henceforth capacitors) and dry-type air-core reactors (henceforth reactors) are common components with multiple uses in power systems. They are both used for filtering [97], and compensating reactive power [102]. Reactors are in addition used for limiting current, and neutral-earthing.[99]

Even though these components are very common, the noise they produce hasn't been an object of much interest until lately. This is most probably due to the need for power increasing simultaneously with the overall building density, and thus the power stations have to be built closer to densely populated areas.

In addition to power stations moving closer to the customers, the capacitors and reactors themselves are nowadays often placed close to the customers as their efficacy is then heightened. When compensating reactive or capacitive load, placing the compensating component close to the load obviates the need of transferring the reactive load through the electric network, thus leaving more capacity for active load. If the customer has equipment that introduces harmonic frequencies to the network, they can be filtered immediately on site without disturbing the other customers. Also, if the customer has a large motor, its starting current can be limited by using a reactor on site.

These changes call for new innovations in energy engineering, since the closer the power stations are to the customers, the less overall noise they are allowed to produce. In the current situation, the noise problem is usually solved by using expensive sound proofing, for example by erecting concrete walls, to be sure that the standards are met. This suboptimal

situation results from the lack of a method that could be used to properly estimate the noise produced by the components.

The second gain to be had from knowing more about the reactor noise production related to the upkeep of the said components. In multiple cases the reactor using customer has noticed that increased sound production has pre-dated a mechanical breakdown. Thus the noise produced by reactor at a power station can also be an indicator of an upcoming problem, and it can perhaps be used to estimate when an inspection is warranted in order to prevent full-on failure.

1.2 State of the Art

The research relating to the sound production of compensation equipment is relatively new, but transformers have been a subject of this kind of research for a long time. Papers related to the subject have been published at least since the 1930s. The research's goal was at first to find the basic information about the noise production such as what actually caused the noise at the substations [1], the directivity of the transformer's noise [32] and what actually caused the sound inside the transformer [24] [27] [55]. After a while it was noticed that the contemporary noise standards weren't up to par when the urbanization picked up pace after the second world war and the substations were moved closer and closer to the load centers [72] [100] [61]. At the same time new materials and design practices both increased [12] and decreased [58] the noise production of transformers. The interest of finding out how the transformer noise could be lessened started to grow [4] [22] [23] [38] [47] [55] [69] [70] [83].

As the knowledge increased, new methods were developed to measure the sound more reliably [6] [29], even in a noisy environment [17] [46] [56] [57]. Gettys [33] invented a method of modeling transformer for the use of researching methods of sound isolation, such as enclosures. General Electric on the other hand constructed anechoic chamber for the sole purpose of transformer noise measurement [14]. The speed at which this field was developing illustrates the fact that from this era we have several [5] [18] [50] publications that try to summarize what have been done already in the field of transformer noise research.

Other research interests include Gordon [37] and Usry [96] presenting possible methods of estimating transformer sound without direct measurement, Ver [98] noticing that single decibel value doesn't tell the whole

truth about the noise of the transformer, and Ryder [82] proposing the use of fast fourier transform (FFT) to diagnose faults in transformers.

Most recently the transformer sound research has been focused on the actual design of the transformers. Kitagawa [59] and Shao [85] developed methods to better model the core of the transformer whereas Girgis [35] described engineering techniques at developing ultra-low noise transformer technology.

The first research found that concentrated on the noise of the capacitors was done by Cox et al. in 1994 [19]. This paper posits that the sides of the capacitors can be modeled as clamped plates. Based on Cox's paper this work also makes two other simplifying assumptions:

1. The capacitor is a linear system, and thus the result of the forces can be obtained by superimposing partial forces

2. The forces applied on each capacitor wall at the state of equilibrium after the capacitor is energized are uniform

In addition to Cox et al. the only papers published that were dealing explicitly with the sound radiating from the capacitors was by Peng [77] [76] and Shengchang [86], both working at the same university. Peng's papers concentrate on lessening the sound radiated from the capacitors. First of them states that due to the construction of the capacitor, the biggest vibrations, and therefore sound, comes from the top and bottom of the capacitor. In order to minimize the sound, the paper presents a microperforated panel (MPP) that is installed inside the capacitor. This panel is installed only at the bottom of the capacitor due to the concerns related to the electric field. Since the area of the bottom is relatively small, the thermal concerns are deemed to be insignificant. The paper assumes and verifies that the MPP is a band-stop filter, which effectively stops only a limited frequency range.

Second paper by Peng [76] presents new innovation to insert to the capacitor: A compressible space component (CSC) absorber. It is a sealed balloon filled with compressible gas that turns the vibration energy of the capacitor elements into heat. As the MPP, the CSC is also installed at the bottom of the capacitor. During the measurements it was found that this type of dampening not only reduces the vibration of the bottom plate, but also the larger sides. When compared to the MPP it was found that

CSC manages to dampen the sound at a wide frequency as long as the frequency is higher than the CSC's absorption frequency threshold.

For the information relating to the reactor, this work bases most its information on the master's thesis by Verbruggen from 2007 [99]. In addition to providing us the basis for further analysis on our own, Verbruggen's thesis shows a method for modeling a reactor using FEM simulation. Unfortunately that work includes no direct method of calculating noise resulting from the vibrations of the reactor.

Other previous work in this field includes single paper by Hagiwara [41], which presents the methods of constructing a more silent shunt reactor. It takes into account the vibration in the magnetic shield as well as in the reactor tank. Kendig on the other hand noticed [56] that reactors can be a major source of noise at the substation. There are also two more recent papers by Gao [31] [30] which go into more basic reactor theory and state that there's a significant correlation between the hardness of the construction of the reactor, and the noise it emits. They also find that there seem to be an optimal value to the hardness to minimize the noise.

Since capacitors resemble closely cuboids, it was assumed in this work, that the sides of the capacitors could be separately modeled as clamped plates. This paved the way to connect this work to extensively researched field of characteristics of plates. It was found out that a plate with all edges clamped is mathematically relatively easy to solve for resonance frequencies[65], so this field yielded plenty of papers.

The papers on this subject tend to concentrate on frequency parameter from which one could calculate the resonance frequency instead of the resonance frequency itself since frequency parameter is independent of the material of the plate. The most common approach to solving the resonance frequencies is using set of beam functions and then using the Rayleigh-Ritz method. Other methods include among others method of finite differences[3] and variational method [44]. Some papers [7] [21], [39] [65] [105] present their results as calculated frequency parameters for number of first modes for number of different ratios of plate, and some [13] concentrate on finding the range in which the frequency parameters can be found. Yet others concentrated on developing the calculation theory[3], [44] [84] [94] [95]. There was also number of papers illustrating the modes visually [10] [90]. For a reader who wants to have a good overview of the basics without going through all the references, there's an excellent, although bit dated, work by Leissa[64] available. It includes e.g. results

originally published in German by Janich in 1962.

Since this work was mostly interested in engineering applications of the resonance formulas, it concentrated on Warburton's work from 1954 Warburton, which had presented equations to calculate clamped plate's resonance frequencies[101]. Another set of even simpler equations were found in the work of Mitchell et al. from 1987 [71]. These two works mostly agree with each other, and later this work presents the comparison of results between these two works, and the values obtained by FEM simulation.

The other necessary constituent in capacitor in addition to the elements themselves, and the enclosure, is the impregnating oil. The oil's most important function is its viscosity as it defines the movement rate and therefore it was assumed that it would affect the sound of the capacitors as well. In the literature there are various branches being investigated over time. Recently there are new methods of measuring the viscosity being developed [28] [52] [53]. Previously most of the research concentrated on either measuring and presenting the viscosity of an oil [11] [79], fitting it with Arrhenius' equation [2] [8] or comparing the values of viscosities of two or more oils [40] [42] [54] [63] [62] [104]. Recently the mixtures of oils have been a focus in the research endeavors [20] [26] [67] [78]. Other papers compare the viscosity of the oil to other characteristics as a function of temperature [91], show how the viscosity is affected by aging [60] or show the correlation between high viscosity and water treeing [9].

In addition to these previous endeavors in research, we are aware of the basic mechanical and electrical structures of the capacitors and reactors. We can assume that we know the loading situation of the network, which can be then simulated by using similar frequencies and amounts of current in the laboratory measurements. We also know that the sound is caused by the vibrations in the structures, which are then caused by the forces related to the pulsing electromagnetic fields.

1.3 Aim of the research

The goal of this dissertation is twofold:

1. To model the sound production of a capacitor

2. To find a connection between the noise of reactor, and a malfunction within

If successful, the results could then be further utilized in the development of capacitors in order to make them less noisy, and thus more friendly for the surrounding environment. The successful deployment of analyzing method for reactors could be used to save non-trivial amounts of money in avoided interruptions and repairs.

1.4 Challenges of the research

Each capacitor units are composed of multiple rolled capacitor elements, which are connected together to form the unit. Each rolled capacitor element is a combination of sheets of aluminum and plastic impregnated with oil. Reactors consists of non-magnetic support structure, and individually insulated aluminum cables, which are impregnated with epoxy resin.

This multiple level construction means that simulating a whole component with a FEM software would require very high amount of calculating power, or even prove impossible with the current methods. For the capacitor this called for limiting the complexity of the research problem by concentrating on simulating single wall of the capacitor and its resonance frequencies to avoid the intrinsic complexity of the whole unit. In the case of the reactor this research decided to concentrate on developing a method that would allow the direct measurement of noise in the magnetic field caused by the reactor. The traditional method of using a microphone next to the target to be measured wasn't valid in this case as traditional microphones cannot withstand the massive magnetic field, and the ones which can are prohibitively expensive.

1.5 Contribution

As a contribution of this dissertation we have achieved new knowledge about vibration and sound response of the compensation capacitor as a function of frequency. Additionally we have a new methodology to measure the noise of compensation reactors, and a possible use for noise spectrum in fault diagnostics. More details of the contribution can be found below.

1. Compression in a single element of the capacitor

Compression in a single element when a voltage is applied to it is not uniform across the whole area. Instead the compression is linearly dependent on the distance from the middle point of the element.

2. Vibration response of the capacitor

   Based on the theoretical research, it was expected that the vibration response of the capacitors has big spikes in amplitude on resonance frequencies of the capacitor sides. When the measurements were carried out, there was no sign of any of these calculated and simulated high amplitude points. This was deemed to be so due to the internal dampening of the capacitor caused by the insulation oil.

3. Effect of the oil viscosity on the vibration response of the capacitor

   The changes in the oil viscosity caused by the various temperatures can be tied to the vibration response of the capacitor as long as we're in the frequency domain where the response is linear. This linear response domain seems to end soon after we exceed 700 Hz.

4. Source of noise of the capacitor unit

   The noise of the capacitor unit is caused primarily by the vibration of the bottom side of the unit.

5. Measurement of reactor noise by the use of tube extender

   Using a simple tube extender composed of simple disposable parts, it is possible to measure the differences in reactor noise from safe distance without use of specialized equipment.

6. Relating reactor noise and faults

   When measuring the change in reactor noise in controlled environment, it was shown that the microphone can "hear" the changes in the reactor noise at least as well as human ear can when a fault is introduced to the reactor.

2. Methods

2.1 Basics of the acoustics

2.1.1 Human perception of sound

What is sound? And how are we able to perceive sound? We know that humans can generally sense vibrations in the frequency range between 20 Hz and 20 kHz as sound. Different animals, such as dogs, can hear different frequency ranges. We also know that sound caused by a fluctuation of pressure [25][68]. Thus without medium to propagate the pressure fluctuation there is no sound. This is why there's no sound in space – it's too sparse to propagate the wave.

The visible part of human ear serves the purpose to both collect the sound waves, and to help us determine the location of the sound's source. The sound is then passed through the auditory canal to our eardrum, where with the help of the smallest bones in the human body – ossicles – it's transferred from the air medium to fluid medium into cochlea. In the cochlea the vibration is transferred into neural impulses with the help of hair cells through a chemical reaction and is sent to the cochlear nerve, which is also called auditory nerve.[15][16][45]

When we hear sound, we differentiate between the different amplitudes in sound. We call these differences 'loudness'. But we must note here that loudness is very subjective, and it behaves very differently from the objectively measurable sound qualities such as sound pressure and intensity [16][45][68]. The perception varies very much as a function of both sound pressure level, waveform and frequency [74]. The loudness of pure tones can be measured in phons[15][68]. Figure 2.1 (original by Peter J Skirrow, in public domain) illustrates the complex connection of loudness of pure

tones to SPL and frequency. The curves are defined by ISO 226 standard [51].

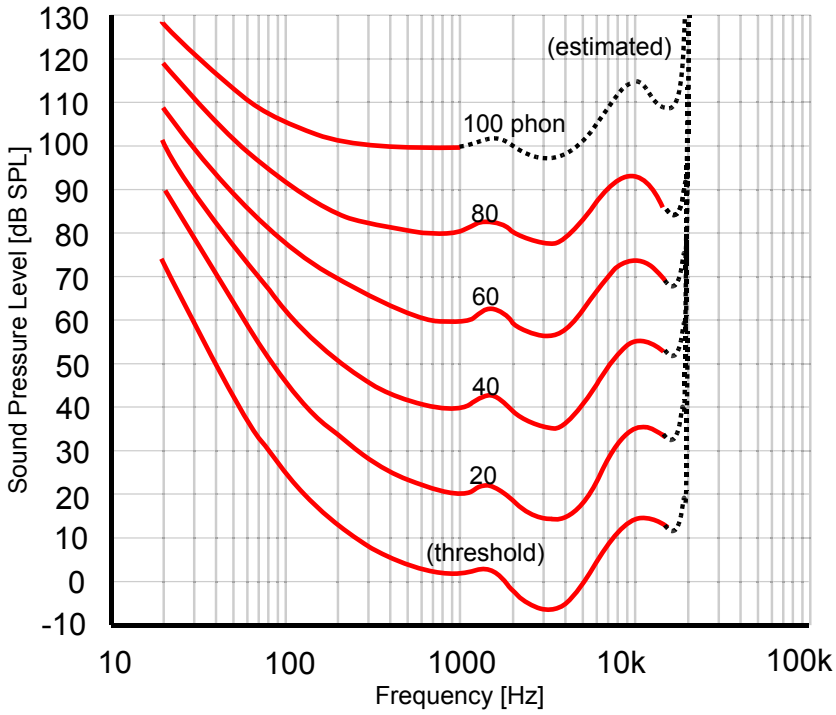

Figure 2.1. Equal loudness curves in respect to SPL and frequency.

2.1.2 Sound pressure, power and intensity

As mentioned in the Section 2.1.1, while loudness is subjective, sound can be measured objectively using sound pressure, power and intensity. Sound pressure is the pressure the wave of sound causes in a measuring point, sound power is the total power the source emits in its surroundings, and the sound intensity is the power divided by the area.

Sound pressure level (SPL) is defined by the Equation 2.1 [15][16][25] [43][45][68] as a relation of the absolute pressure to reference pressure. Sound power level (L_W) is defined in Equation 2.2 [16][25][45] as a relation of the absolute power to reference power. As both sound pressure and sound power tend to have very wide ranges of absolute values, the decibels are more widely used.

$$L_p = 10 \cdot log(\frac{p_{rms}^2}{p_{ref}^2}) = 20 \cdot log\frac{p_{rms}}{p_{ref}} \tag{2.1}$$

where L_p is the sound pressure level in decibels, p_{rms} the sound pressure

value, and p_{ref} the reference pressure value. p_{rms} is commonly set to be 20 μPa [25][43][68].

$$L_W = 10 \cdot log \frac{W}{W_0} \tag{2.2}$$

where L_W is the sound power level in decibels, W the sound power value, and W_0 the reference power value. W_0 is commonly set to be 1 pW [25][45].

Since the definitions of the two decibels are different, it's very important to know which value we're talking about when comparing different sound sources. When talking about the SPL, 3 dB change in the pressure causes a $\sqrt{2}$ change in the pressure level, whilst 3 dB change in the power level doubles the wattage. Similarly 10 dB change causes $\sqrt{10}$ change in the pressure level, but factor of 10 change in the power level.

2.1.3 Sound weighting methods

The measurements presented in this work are presented not weighted if possible. This is done to maintain the usability of them as much as possible. The standard way of weighting the sound is currently A-weight, but it has numerous problems [80], namely the insensitivity to noise below 100 Hz and above 1000 Hz. A-weighting doesn't take into account the wide frequency noise effect nor high volume sounds either as it's based on the equal loudness contours which assume pure tones and relatively low sound amplitude. If weighting is needed to obtain a single comparable number, in the International Telecommunication Union's recommendation ITU-R 468-1[93] there's an improved method, which is based on the human hearing response. This method is based on the BBC's Engineering Division's work[92] which researched how human ear reacts to different sounds. All the weightings are done to the SPL values of the sound. Figure 2.2 shows how the two weighting systems compare to each other.

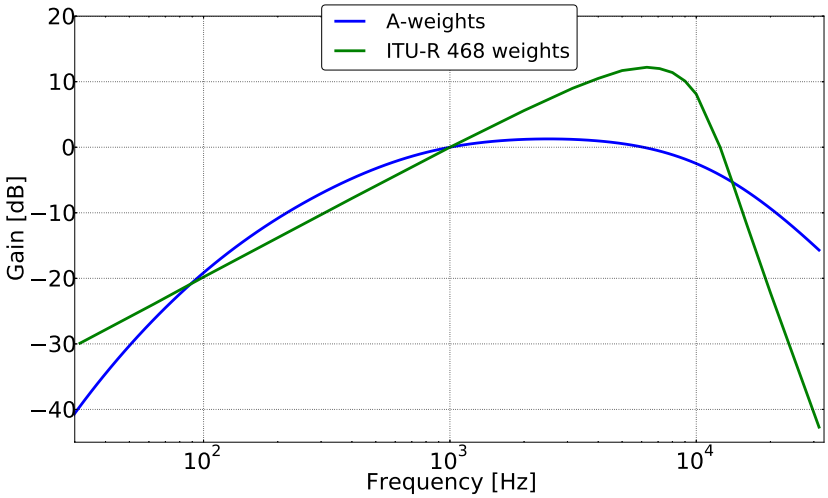

Figure 2.2. The differences between A-weighting and ITU-R 486 weighting.

2.1.4 Near and far field

If we start from the most simple sound emitter – a point – we can assume that it emits the sound pressure universally across the whole spherical volume. Thus we can easily calculate the values we want as long as we know our distance from the point, and we know the area that is affected by the emitted sound. When we move from the ideal, simple case, towards a real life physical, tangible items, we quickly realize that they are often complex to model, and we can't fully understand how they propagate sound.

We can consider the item to be composed of differentially small points of which all cause sound on their own. Each of these points' pressure waves have their own directivity and amplitude. As they collide, interference occurs. Whether it's constructive or destructive depends on the phase and amplitude of the fields included. The area in which we are close enough to the source that we have to take these interferences into account is called near field. When we go far enough from the source so that the item seems to be a single source instead of multiple smaller ones, we are in the far field. This principle is shown in the Figure 2.3.[81]

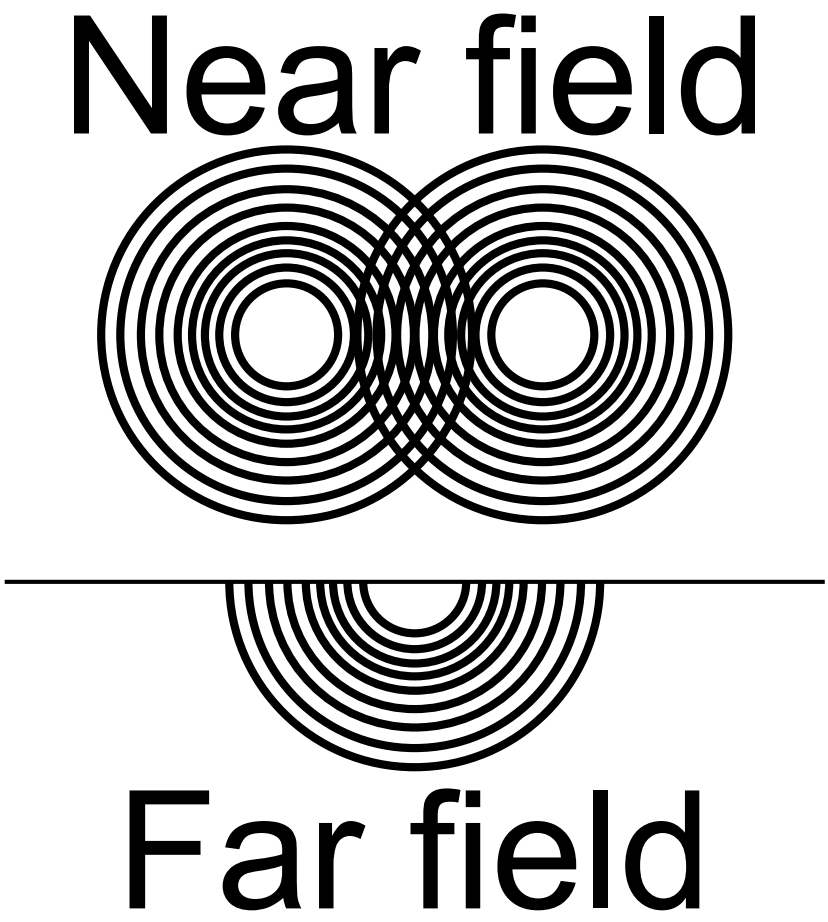

Figure 2.3. Basic difference between near and far field.

When defining whether we're in the near or far field, we may first refer to radio wave propagation where we have to first define whether we have electromagnetically short or long antenna. For these calculations we assume that the surrounding medium is air. Roughly speaking the break point between electromagnetically short and long antenna is half of the wavelength they emit. Since the basic frequency a power system component emits is double the input frequency as will be shown in Sections 2.2 and 2.3, our component's main emitting frequency will be 100 or 120 Hz. Half of the wavelength of the 100 Hz sound wave in air is roughly 1.72 m. As we rise in the frequency, the wavelength will get gradually shorter, and at 3rd and 7th harmonic inputs of 150 and 350 Hz, the respective half wavelengths have shrunk to 0.57 and 0.25 m. Thus we can see that by the definition it's not clear whether the capacitor should be considered an electromagnetically short or long antenna.

The limit where the near field becomes far field is called the Fraunhofer

distance. For electromagnetically long antennas, this distance d_f can be calculated from the first part of the Equation 2.3. Additionally for the wave to be in the far field, it has to met the two other criteria posited in this equation. Unfortunately a 1 m tall capacitor emitting a 100 Hz wave (3.43 m wave length) yielding Fraunhofer distance of 0.58 m doesn't satisfy the two other parts of the Equation 2.3, so we're not in the far field.[87]

$$\begin{cases} d_f = \frac{2D_f^2}{\lambda_f} \\ d_f >> D_f \\ d_f >> \lambda_f \end{cases} \tag{2.3}$$

where d_f is Fraunhofer distance, D_f the largest dimension of the radiator and λ_f the wavelength.

If we assume the antenna to be of the short type, the limit for the near field to turn into far field is triple of the wavelength emitted. Thus again at 100 Hz we might be in near field, but when we move to higher frequencies, we'd slip partially into the far field. This is exactly why much care has to be taken when measuring sound at various frequencies to distinguish between near and far field characteristics. What these changes mean in practice will be shown in the Section 3 where the results will be presented.[48]

When we have a situation where we have multiple sound sources, and we want their total sound pressure level, we treat them similarly as in the case when we move from the near field to far field in a single source case. As we move further away from the system comprised of individual sources, the system starts behaving as if it was a single source.

At that point, in order to calculate the total sound pressure level, we can simply add the levels of individual sources together using Equation 2.4 [43]:

$$SPL_\Sigma = 10 \cdot log_{10}(\frac{p_1^2 + p_2^2 \dots p_n^2}{p_{ref}^2}) \tag{2.4}$$

where L_Σ is the total sound pressure level in decibels, p_1, p_2, p_n are individual pressure levels, and p_ref is the pressure reference often set as 20 μPa.

To make the calculation easier we can use Equation 2.1 to write the following:

$$\frac{p_i^2}{p_{ref}^2} = 10^{\frac{SPL_i}{10}} \tag{2.5}$$

where p_i is the individual pressure level, p_{ref} is the reference pressure, and L_i is the sound pressure level in decibels.

Finally combining Equations 2.4 and 2.5 allows us to calculate the total pressure level in decibels from the individual pressure levels [16][43]:

$$SPL_{\Sigma} = 10 \cdot log(10^{\frac{SPL_1}{10}} + 10^{\frac{SPL_2}{10}} + \dots 10^{\frac{SPL_i}{10}}) \tag{2.6}$$

2.1.5 Resonant frequencies

When talking about resonance it's best to start with a simple example: a string, which is attached to a wall from other end. When this string is shaken from the free end at specific frequency, it creates a standing wave with nodes that have zero amplitude, and anti-nodes, where the amplitude is at its maximum. We can make the case two dimensional by using a membrane instead of a string. If we want to add the third dimension, we have to add thickness. Thus from strings we get bars, and from membranes we get plates.[81]

Since the object is more prone to vibrate at a specific frequency, those frequencies are called resonant frequencies. Input at frequencies can produce bigger oscillations and thus movement in the objects than what they were specified at, thus causing more sound, and possibly even breaking them in case of for example bridges. Due to these reasons resonant frequencies cannot be ignored in the planning phase, as in an electric system even though the fundamental frequency might not excite the system much, a harmonic frequency might do so.

In Figure 2.4 have been presented the two first resonance modes of a plate. We can clearly see that in the left image we have one anti-node, and in the right one we have two of them. As we would increase the frequencies, we'd get more and more complicated resonance modes. The calculation of these resonance mode frequencies have been studied, and they can be also simulated using a computer software.[71][101] The different resonance modes have been an interesting study target for a long time, as they constitute to an important part of how musical instruments work[81]. In the Section 2.5.1 the simulation results and the theoretical formulas have been compared to see how accurate they really are.

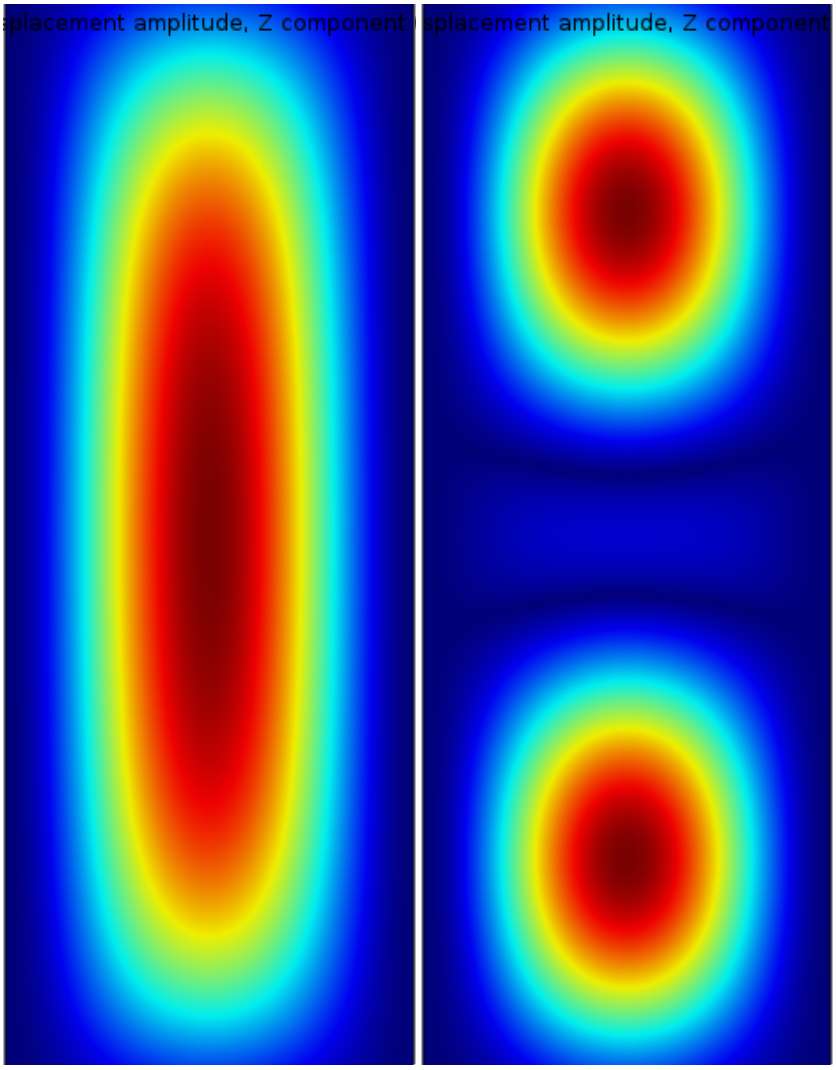

Figure 2.4. Two first modes for a plate sized 1060 mm times 350 mm at 50 Hz and 100 Hz.

2.1.6 Sound in power systems

When we enter the domain of power systems and high voltage engineering, we usually deal with limits related to the thermal and electrical properties of the components we use. Those properties can be generally fairly easily calculated theoretically or tested for empirically. If we are interested in the sound propagation with the power system component as a source, the issue is much more complicated. The basic idea of how the sound is produced in the compensation capacitors and reactors is shown in the Figure 2.5. In case of the reactor we have multiple current conduc-

tors, and according to the definition of the ampere[75] we must have force between two current conductors, these currents must therefore cause internal forces when the component is energized. In capacitor units on the other hand the variable voltage causes electrical forces between the electrodes of the capacitor element. As we well know, the force causes acceleration, and therefore motion. Finally motion causes pressure in the surrounding environment. This pressure is called sound when it occurs in at the frequency and amplitude range we can hear in the medium next to our ear.

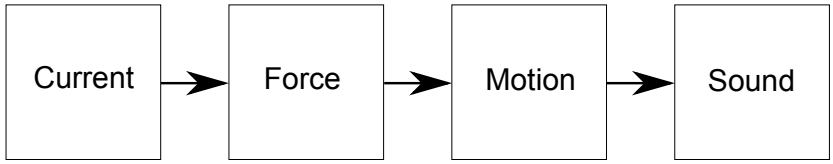

Figure 2.5. Flowchart showing how electric current causes sound.

2.2 Physics of the capacitor

Let's start by introducing the basic laws that define the characteristics of capacitors. Capacitor's characteristic parameter is its capacitance which defines how much electric charge Q the capacitor can hold using certain electric potential U:

$$C = Q/U \tag{2.7}$$

Based on on Equation 2.7 we should try to maximize the capacitance in order to store as big an electric charge as possible with using the lowest possible electric potential. In this thesis, the capacitors studied can be presented electrically as a simple capacitor with two parallel plates with area A and distance d. Between these two plates is material, which relative permittivity is ε_r. For this kind of capacitor, the capacitance can be calculated from Equation 2.8.

$$C = \varepsilon_0 \varepsilon_r A/d \tag{2.8}$$

where $\varepsilon_0 = 8.854$ x $10^{-12} Fm^{-1}$. Since the distance d is divisor in the Equation 2.8, it would seem that the easiest way to increase capacitance would be to decrease the distance between the plates. While this is true, this brings up another problem relating to the physical nature of materials. Namely, the materials are only able to withstand electric potential U up

to a certain limit. This limit, called dielectric strength (E_{dstr}) can be calculated from Equation 2.9.

$$E_{dstr} = U/d \tag{2.9}$$

As we see, the smaller the distance d is, the faster the limit for dielectric strength is reached. Thus to increase the capacitance C we need either materials that have high dielectric strength, high relative permittivity ε_r or both. Simultaneously we can use a roll-like structure presented in Figure 2.6 to maximize the area.

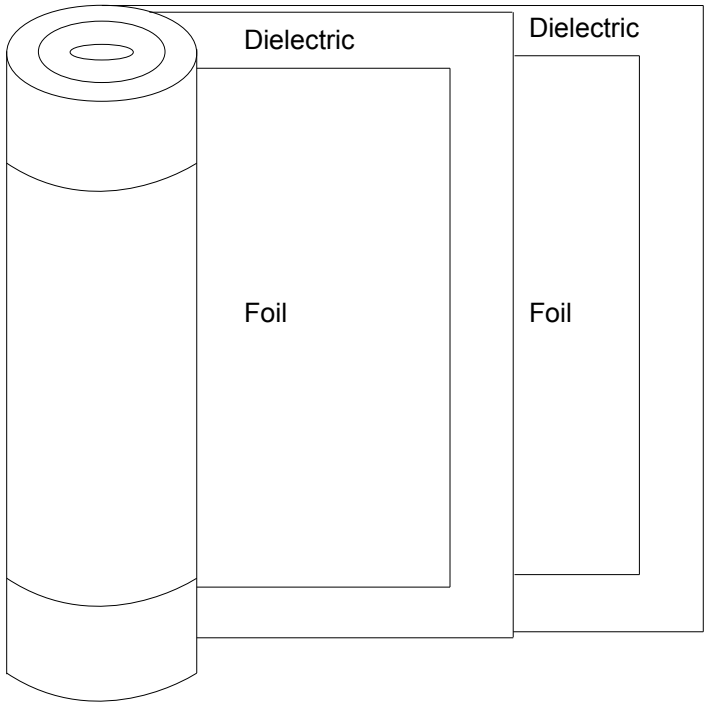

Figure 2.6. Basic concept behind rolled capacitor

The capacitance of rolled capacitor can be easily solved by using the simplified model. This model assumes that all the layers of the capacitor are identical, and that they can be represented as a series connection of a number of capacitors equal to the number of layers in the rolled capacitor. The equivalent model for a single layer is showed in the Figure 2.7. Figure 2.8 further explains why rolled capacitor is an excellent choice

when maximizing the area of a capacitor. When another layer is added on top of the existing capacitor, it produces not one, but two equivalent capacitors. Whole rolled capacitor is made up of usually hundreds of layers, which translates into hundreds of equivalent capacitors. Even though the equivalent model can look like a series connection of capacitors due to layers being on top of each other, the equivalent capacitors are in parallel connection, since the voltage foil and ground foil are the same in the whole rolled capacitor. The equivalent model for a whole rolled capacitor can be seen in Figure 2.9.

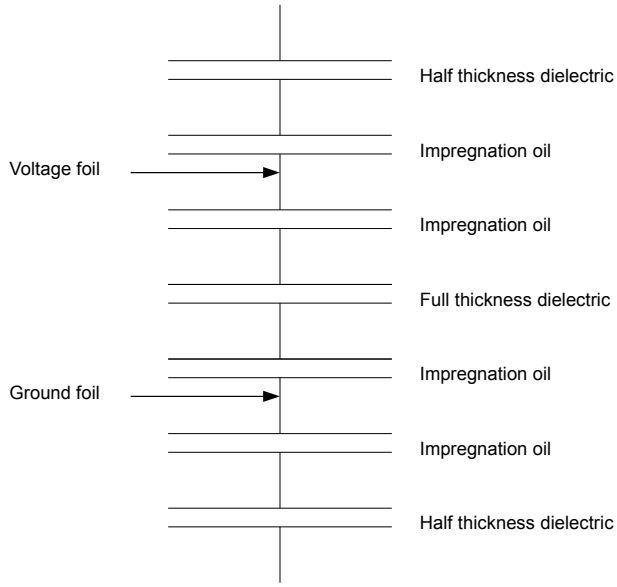

Figure 2.7. Equivalent model for a layer of a rolled capacitor

To understand the forces between different layers, Figure 2.10 which

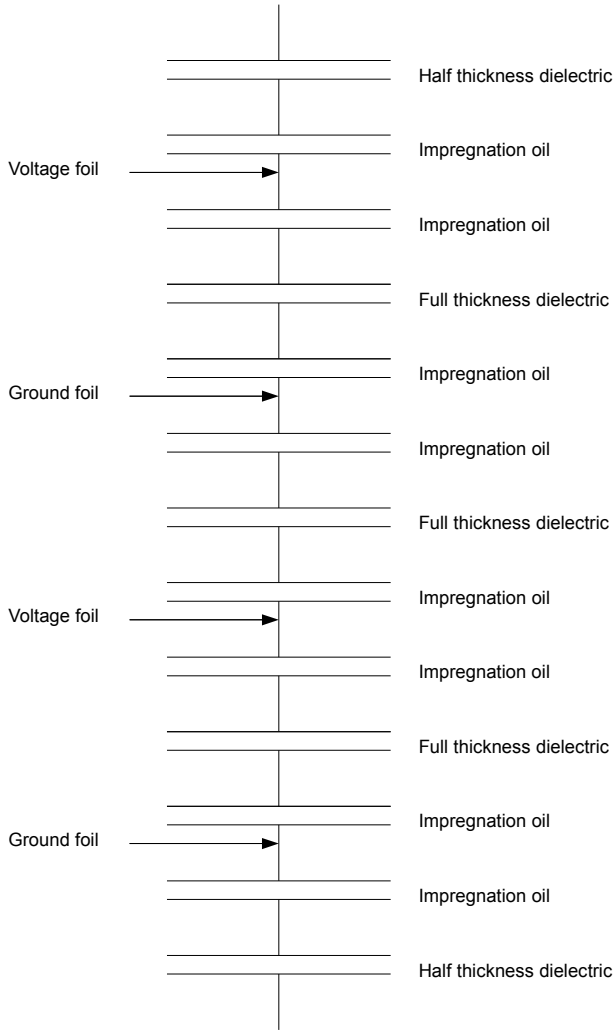

Figure 2.8. The advantage of rolled capacitor

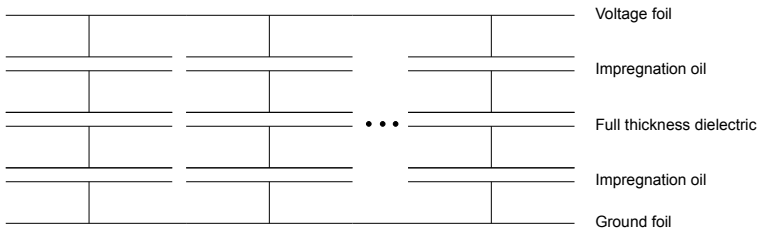

Figure 2.9. Equivalent model for whole rolled capacitor

shows how the layers of aluminum are entwined in a single element is used here. From the image we can see that the negative polarity (illustrated as gray line), and positive polarity (black line) are one on top of the other. We can calculate the force between them from Equation 2.10.

$$F_x = \frac{U^2 \varepsilon A}{2d^2} \tag{2.10}$$

where U is the voltage between the two plates, ε is the permittivity of the isolating material, A is the area of between the plates, and d the distance between the two plates.

Since the layers are on top of each other as seen in the picture 2.10, we can deduce that there is force between them. We can also deduce that since the distances between the layers are equal, as are the voltages, area, and ε, thus the forces are also equal. Consequently, the whole element becomes compressed when the voltage is applied to it, and the compressions within each layer should be even. This evaluation is valid for any given moment in time, but when we take into account that the voltage U is oscillating at the rate of 50 Hz per second, we can see that the force F_x is oscillating at the rate of 100 Hz per second.

Figure 2.10. Polarities of entwined aluminum layers in a single element

In order to calculate the vibration from the power, we're interested in how much the capacitor elements compress when they come under stress. To calculate this we assume that both the capacitor oil and aluminum are incompressible, and just the polypropylene film is responsible for all the compression. This simplification can be made as the Young's modulus (E) for polypropylene is 1.5 GPa[66] and aluminum's value significantly higher at 70 GPa. To calculate compression we use Hooke's law, which is

presented as Equation 2.11:

$$F_x = kX \tag{2.11}$$

where F_x is the force applied, k is the stiffness, and X is the compression amount.

Stiffness is defined as shown in the Equation 2.12:

$$k = \frac{AE}{l} \tag{2.12}$$

where A is the cross-sectional area, E is Young's modulus and l is the length.

If we combine Equations 2.10, 2.11 and 2.12, we'll get Equation 2.13 which we can use to calculate the total compression X of a single layer of the capacitor.

$$X = \frac{U^2\varepsilon}{2Ed} \tag{2.13}$$

where X is the total compression, U is the voltage between the plates, ε is the permittivity of the isolating material, E is the Young's modulus, and d is the distance between plates.

As we could see in the Figure 2.8, each additional layer of the rolled capacitor produced two partial capacitors. Thus if we know the total length and width of the layered materials, we can calculate the total change of volume of a single element when we combine this information with Equation 2.13 to yield the following Equation 2.14.

$$\Delta V = \frac{U^2 A\varepsilon}{Ed} \tag{2.14}$$

where ΔV is the change in the volume, U is the voltage between the plates, A is the total area of the foil of a capacitor element, ε is the permittivity of the isolating material, E is the Young's modulus, and d is the distance between plates. We notice that 2 has been removed from the equation due to the reason discussed previously.

Since the capacitors usually include multiple elements, and we're mostly interested in the total compression perpendicular to the bottom of the capacitor, Equation 2.14 becomes Equation 2.15:

$$\Delta x = t \times \frac{U^2 A\varepsilon}{EdA_{profile}} \tag{2.15}$$

where Δx is the total compression, t is the total number of elements, U is the voltage between the plates, A is the total area of the foil of a capacitor element, ε is the permittivity of the isolating material, E is the Young's

modulus, d is the distance between plates and $A_{profile}$ is the area of the bottom of the capacitor.

As an example of how much the volume of a typical capacitor element changes volume due to these forces we use an example where A = 10 m^2, U = 3500 V, ε_r = 2.2, E = 1.5 GPa, d = 30 μm and $A_{profile}$ = 0.07 m^2. Calculating using the Equation 2.15, the total compression would be roughly 0.76 μm in the direction perpendicular to the bottom of the capacitor. We will compare theoretically calculated value to the measurements in the section 3.2.

In the above calculations we assumed that the layer of isolating material is homogenous like in the Figure 2.11 in order to calculate the compression amount directly. Unfortunately the case isn't always this simple. If polypropylene film is used as insulating material, its surface can be made rough on purpose for the impregnation oil to fill the cavities and make the structure more homogenous overall. Example of how this could look like is shown in the Figure 2.12.

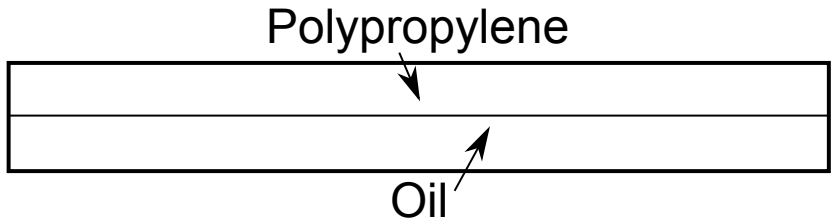

Figure 2.11. Polypropylene/oil interaction in an idealized case.

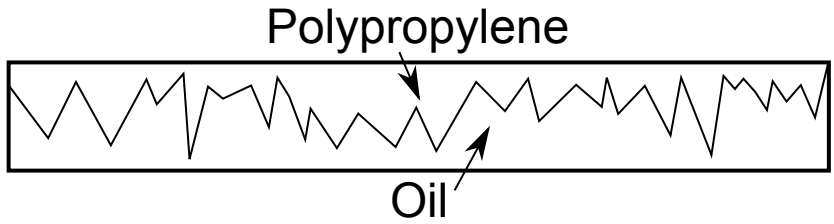

Figure 2.12. Polypropylene/oil interaction in real life.

2.3 Physics of the reactor

Since this work concentrates on modeling sound production for capacitor, and only tries to find application for sound measurement in reactors, the reactor physics background will be based on the previous work done by Verbruggen [99].

The most defining characteristic of a reactor is its inductance, which calculation is somewhat complicated. From Verbruggen's work we learn that there are two common approaches to calculating inductance of a reactor: One presented by Nagaoka in 1909 [73] and one by Wheeler in 1928 [103].

Nagaoka [73] states that there's an older Equation 2.16 which allows calculating inductance of very long reactors. The work of Nagaoka presents Equation 2.17 to calculate the inductance, which introduces new coefficient K, which takes into equation the shape of the reactor.

$$L = 4\pi N_l^2 A l \tag{2.16}$$

where N_l is the number of turns per unit length, A is the area of cross section and l is the length of the reactor.

$$L = 4\pi N_l^2 A l K \tag{2.17}$$

where N_l is the number of turns per unit length, A is the area of cross section, l is the length of the reactor and K is the Nagaoka's coefficient. The coefficient is highly dependent on the dimensions of the reactor, and its values are tabled in the original paper [73].

Since the Nagaoka's equation requires the usage of a fairly complex coefficient, it isn't the easiest way of calculating inductance. To remedy this situation, Wheeler presented [103] Equations 2.18 and 2.19, which are meant for every day use in the laboratory. They can be used to easily calculate the inductance of a reactor within reasonable accuracy. The two equations have different fields of application. The first, Equation 2.18 is meant for use where the thickness of the windings, d is roughly equal to the radius of the reactor r and length of the reactor l. The latter, Equation 2.19 is meant for reactor with single layer, and when $l > 0.8\ r$. Both equations are accurate within about 1 % within these limits. Figure 2.13 demonstrates the differences between the applicabilities of these two equations.

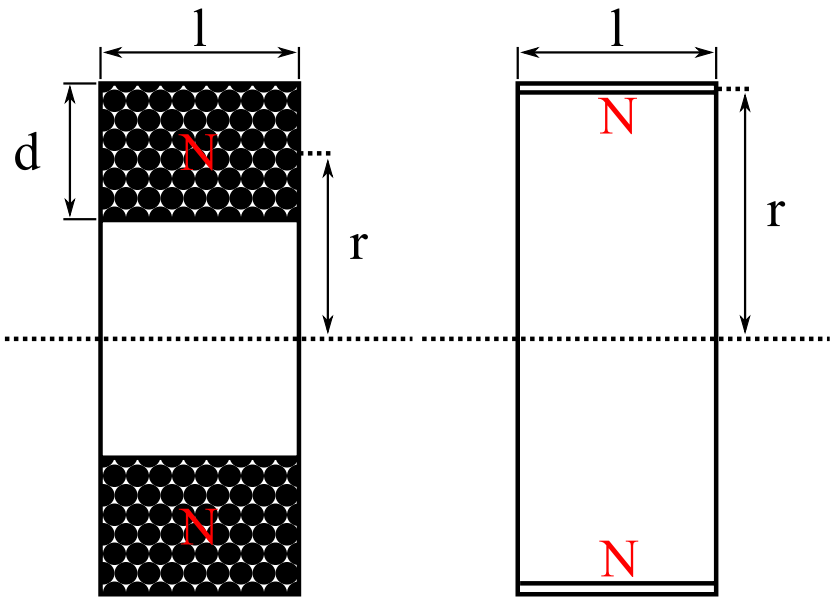

Figure 2.13. Differences in applicabilities in the Wheeler equations.

$$L = \frac{0.8r^2N^2}{6r + 9l + 10d} \tag{2.18}$$

where L is the inductance, r is the radius of the reactor, N is the number of windings, l is the length of the reactor, and d is the thickness of the windings. The dimensions in this formula are given in inches, and the inductance result is in microhenries [μH].

$$L = \frac{r^2N^2}{9r + 10l} \tag{2.19}$$

where L is the inductance, r is the radius of the reactor, N is the number of windings, and l is the length of the reactor. The dimensions in this formula are given in inches, and the inductance result is in microhenries [μH].

From Equation 2.20, we can see that force between two conductors causing a current is relative to the product of the two currents involved. The currents in reactor are either identical (single phase reactor) or phase shifted by $\frac{2}{3}\pi$ in relation to each other, but have similar amplitude (three phase reactor). Thus we can see that the force has double the frequency compared to the currents.

$$F = \frac{\mu_0 i_j i_k l}{2\pi d_{jk}} \tag{2.20}$$

where μ_0 is vacuum permeability, i_j and i_k are currents in cables j and k,

l is length of the cable, and d_jk is distance between cables j and k.

Due to the layout of the windings of the reactor, the ones which are immediately next to each other carry the current in the same direction whilst the ones of the opposite ends carry the current in the opposite direction. Due to these currents the windings which are side by side attract each other whilst the ones that are on the opposite ends of the reactor repel each other. These forces cause the reactor to move from neutral shape to barrel shape at the double frequency compared to the one that is fed to the reactor. This act of shape shifting is demonstrated in the Figure 2.14, which is based on Verbruggen's[99] figure.

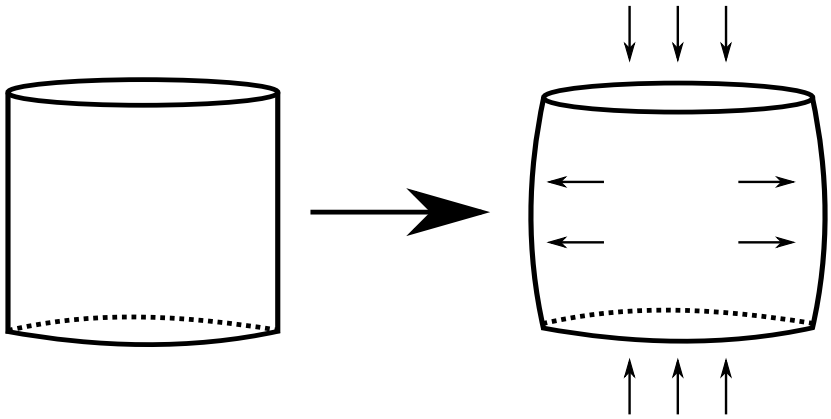

Figure 2.14. Basic idea behind the breathing mode of the air core reactor

The difference between this idealized case and real life is that a real reactor has so called "spider arms" at the top and the bottom. These are illustrated in the Figure 2.15. The aim of these supports is to bolster the mechanical strength of the reactor. By doing this, they are also changing the pulsing mode of the reactor, so the pulses do not cause equal deformation in all directions, but more like the one shown in that figure. Since the reactor deforms outwards, it has to also affect its height. This causes the reactor to move between the cylindrical shape (neutral position) to barrel like shape (deformed position) cyclically.

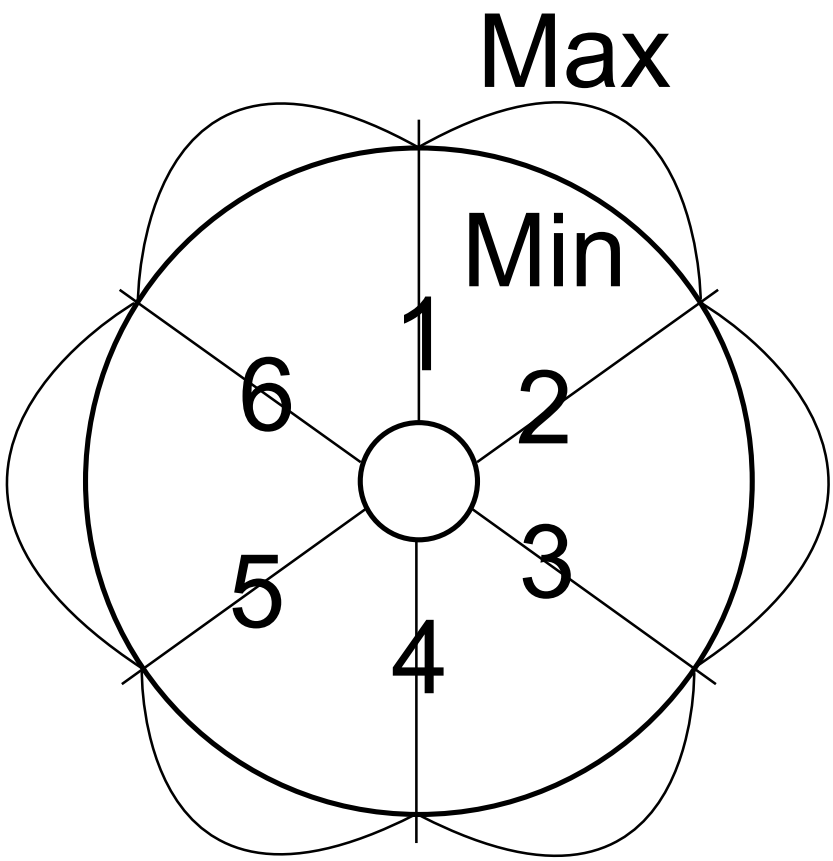

Figure 2.15. The six numbered spider arms and their effect on the breathing mode

The natural breathing frequency is the frequency at which the reactor has tendency of strengthening the forced mechanical movements caused by the electrical currents. This frequency can be calculated from the Equation 2.21. From it we can see that the material of the reactor is a major factor with diameter of the reactor being second. It's worth noting that the height of the reactor has no effect on the natural frequency.[88]

$$f_0 = \frac{1}{\pi \cdot d_r}\sqrt{\frac{E}{\rho}} \tag{2.21}$$

where f_0 is the natural breathing frequency, d_r is the reactor's diameter, E is the Young's modulus and ρ is the density of the reactor material.

Since we're interested primarily in the sound produced by the reactor, we should examine the formula for sound intensity I, which is given by the Equation 2.22 [99].

$$I = \frac{(2\rho_{air} v \pi D_m f)^2}{2\rho_{air} v} \tag{2.22}$$

where ρ_{air} is density of air, v is speed of air, D_m is the maximum displacement, and f is frequency.

After we simplify the Equation 2.22 for sound intensity into Equation 2.23 we notice that the sound intensity is relative to the frequency squared. This is a general equation, which can be used for both capacitors and reactors. Additionally in the reactors' case we can see that since according to the Equation 2.20 force is related to the product of the two currents, which is directly related to the displacement D_m. Thus either increasing the frequency or the current should increase the sound intensity.

$$I = 2\rho_{air} v \pi^2 D_m^2 f^2 \tag{2.23}$$

2.4 Measurements

2.4.1 DC compression of air filled capacitor element

In order to compare air filled and oil filled elements, and to determine the maximum expected amplitude of compression in the elements, the element was tested using DC (direct current) voltage, and the compression was measured. Draft image of the measurement set-up can be seen in the image 2.16. To measure how the element compresses when the voltage is applied, the element was divided into square shaped portions, which are visible in the image. In this measurement the size of each measurement square was 20mm x 20mm. The error marginal was $\pm$ 1mm. Since the element is a flattened rolled capacitor (2.6), its longer edges are different from the middle portion, and thus have been not taken into account in the measurement, and are marked as "safety area" in the picture. The short edges of the element have also been partially marked as "safety area", since the homogeneity of the material, and the thus the repeatability of the measurement was an issue. The width of this safety area was defined as being more than half, but less than full width of each square measurement section that the element was divided into, in this case it ended up being 1.2$\pm$1 mm.

In this measurement a 20x20x5 mm $\pm$ 1 mm piece of PVC plastic was put on top of a measurement square. Then a voltage was applied, and displacement of the plastic piece was measured using a dial indicator. After taking the measurement, the element was allowed to decompress until

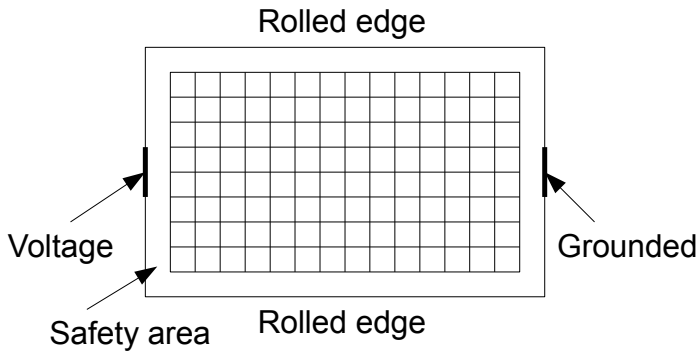

Figure 2.16. Air filled element DC compression measurement

the dial indicator's dial wasn't visibly moving any more. The measurement was repeated at the measuring square until at least three consecutive samples with spread of under 0.03mm were obtained. The precision of a single measurement was $\pm$0.01mm. After reaching acceptable result the measurement was moved to next measurement square. The measurement was repeated later for some squares, as it was observed that even though the spread for consecutive measurements was small, the results for a single point could vary even over 30% if the measurement was repeated later. This lead to choice that the results were studied using statistical methods. The dial indicator was calibrated each time the measuring square was changed by making one test run before the actual measurements were started.

To make the measurements easier, a hypothesis was made that the measuring area can be divided into four symmetrical parts. This division was based on x- and y-axial symmetry. The dividing point, origin, is shown as the black dot in the Figure 2.17.

Compression measurements at 3.2 $\pm$ 0.1 kV were conducted for various symmetrical points in the element in order to test the symmetry hypothesis. These results were also used to compare the compression at this voltage level to compression at lower voltage levels in order to verify the non-linear relation between the voltage and the compression, which is caused by the force. Non-linear relation was expected based on the Equation 2.10. The other voltage levels used to confirm this non-linear connection were 2.6 and 2.0 $\pm$ 0.1 kV.

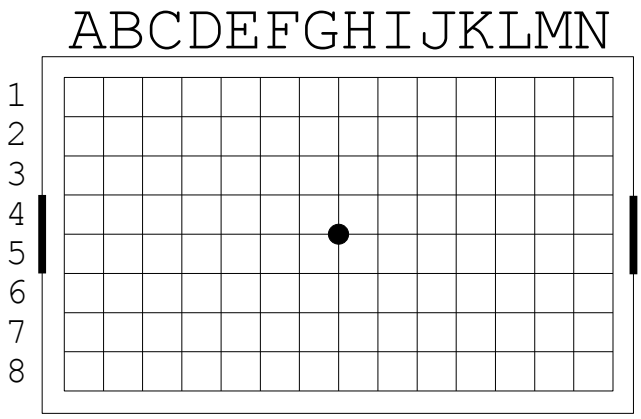

Figure 2.17. Division of the air filled element for DC measurement

2.4.2 Vibration response of the capacitor sides

In order to verify the presence of the resonance frequencies mentioned in Section 1.2, it was decided that vibration measurements of the capacitor sides would be the best approach. The measurement was done in co-operation with Mr. Kari Kantola from the Department of Applied Mechanics of the Aalto University. The main measuring position can be seen in the Figure 2.18. This position was chosen as the main measuring position instead of the standard installation position seen in the Figure 2.19 since the capacitor wouldn't fit in the Department of Applied Mechanics' "fridge" used to cool down the capacitor in one part of the measurements.

When using the main measuring position, the capacitor was placed on the two pieces of wood in order to further isolate it acoustically from the ground. Other reason for using wood instead of rubber was that we needed more space underneath the capacitor in order for the bottom accelerometer to fit there. The metal under the capacitor is an engine bed weighing roughly a tonne. In addition to these preparations, the other machines in the machine hall weren't in use during the measurements in order to avoid disturbances.

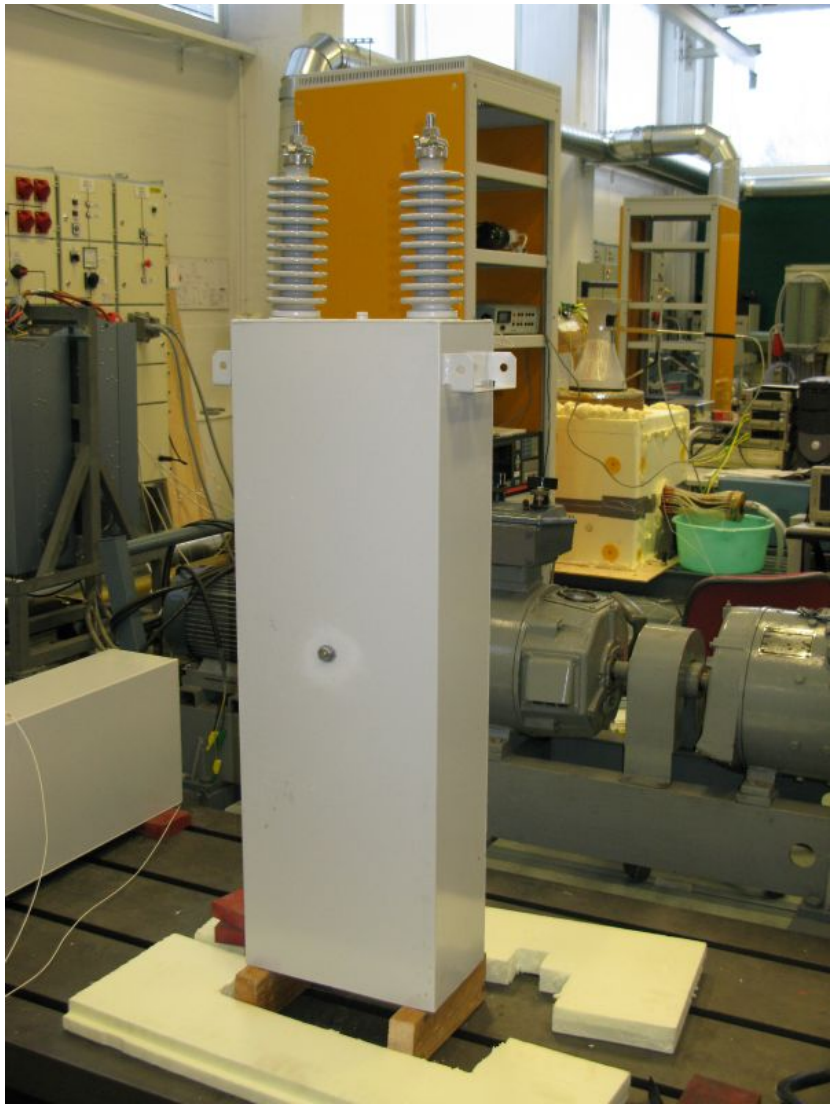

Figure 2.18. Capacitor in the main measuring position

The metal colored item placed approximately in the middle of the of the capacitor in the Figure 2.18 is a base for accelerometer. This base is glued to the surface of the capacitor after the paint has been removed. The accelerometer is then screwed to this base. The attached accelerometer can be seen in the Figure 2.20. The red objects that can be seen under the capacitor in the Figures 2.19 and 2.20 are industrial rubber, which is also used for dampening the outside vibrations.

There were total two capacitors, four different states for both of them, and two different measurements which will be reported here. The capacitors were mechanically almost identical, as both had the same width (350

mm) and depth (200 mm). The first capacitor (C1, 12.7 μF) was 1060 mm tall, and weighed 102 kg, and second one (C2, 38.8 μF) was 1000 mm tall, and weighed 101 kg. The main difference between the capacitors was that the elements inside were connected differently in series and parallel resulting in different capacitance and voltage rating. Out of the four different cases, two were in the room temperature (+20 °C) with the difference being the position: One was in the main measuring position shown in the Figure 2.18 and other was in the standard installation position shown in the Figure 2.19. The reasoning between these two cases was to see whether or not there's a difference in the vibration when the position is changed. In order to get reliable results, the capacitor was left overnight in the new position before making the measurements. The two other cases were -44 °C and +47-48 °C. These variation of temperature were made in order to see how the vibration of the capacitors change with respect to the temperature.

Figure 2.19. Capacitor in the standard installation position

The two different measurements were "sweep" and "high frequencies". In the sweep measurement, a constant voltage level (173 V) was fed, and then frequency was increased over time. Waveform was pure sine wave for all measurements. For the C1, the sweep range was from 50 to 600 Hz, and for C2 it was from 50 to 350 Hz. The different upper limit was due to the fact that C2's capacitance was higher, and thus the power supply's

limit was reached faster. The frequency change rate was done manually, and was roughly 0.3 Hz per second in 0.1 Hz increments. Only difference between the various measurements had to be introduced in the C2's cold measurement, as the temperature caused the capacitor to take more power out of the power supply, and thus the voltage level had to be decreased to 170 V. The measurement was done using peak-hold averaging, and there were approximately 70 thousand averages in each sweep.

In the second measurement the voltage level was kept at 150 V for C1, and 80 V for C2. In this measurement singular sine waves were fed in individually. The measurement frequencies were from 1000 to 1450 Hz every 50 Hz. The maximum was chosen so that the results could be plotted into the same figure without having issues with the 3rd harmonic of the first input frequency coinciding with the 2nd harmonic of the last input frequency. Also in this measurement there was one exception that had to be made, since the 1450 Hz level for C2 in the cold temperature caused over current protection in the power supply to trigger. Thus for the C2 cold measurements the frequency range is from 1000 to 1400 Hz.

If one looks at the Figure 2.20, one might wonder why the accelerometer isn't in the middle. This isn't a mistake, but instead all three accelerometers used are similarly bit off to the side. This is since if the accelerometer would be in the very middle, it would measure only that singular point's vibrations. This is an issue since the middle point is one where nodes and anti-nodes are frequently formed. This would cause a situation where we would get very detailed data of a single point, but almost no generally usable data. The point selected is one where we should get good average results of how the whole plate moves, and whether or not the individual resonance frequencies affect the whole plate, or are they very local and insignificant when considering the overall vibration levels.

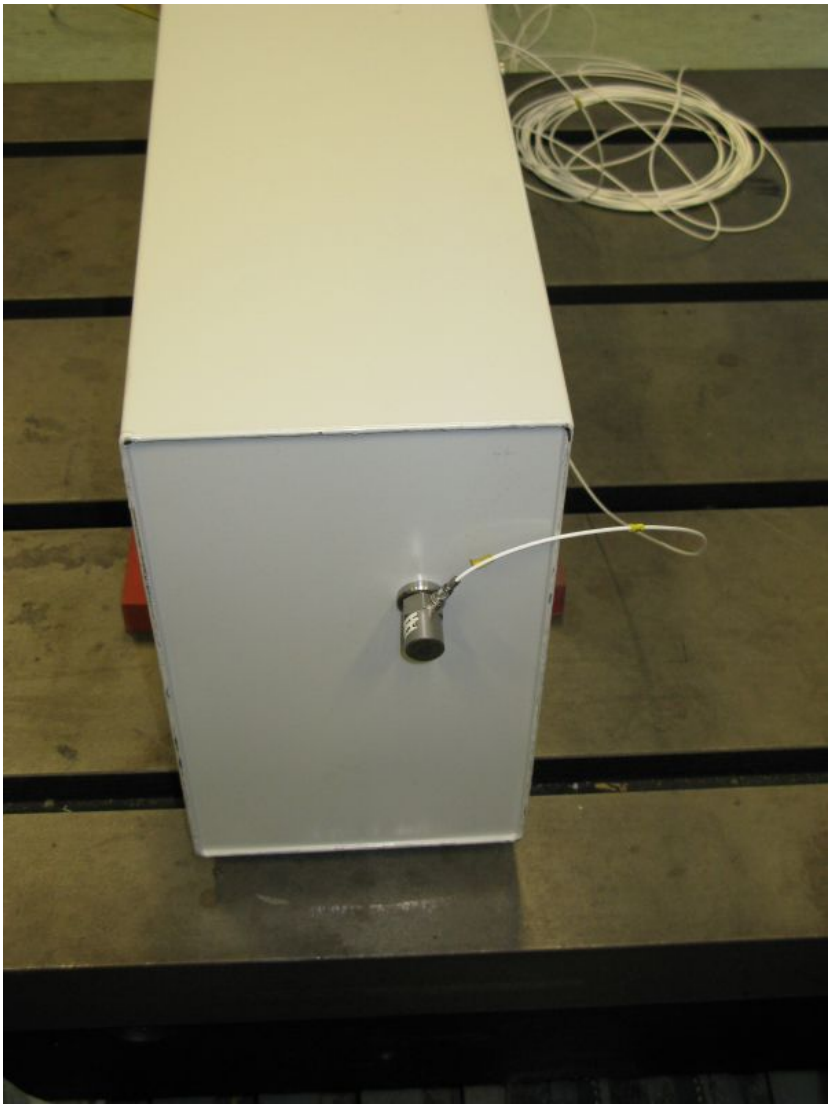

Figure 2.20. The bottom of the capacitor with the accelerometer installed

2.4.3 Acoustic response of the capacitor sides

After vibration measurements the next logical step was to try and compare those results with direct acoustic measurements. Also since using the vibration measurements we couldn't really say anything about the directivity of the capacitors, we decided to measure it as well. Since our power supply limited the power levels far below the nominal specifications of the capacitors, the problem was that the sound levels were very low. To compensate for that we co-operated with the Department of Signal Processing and Acoustics of the Aalto University in order to make mea-

surement in their anechoic chamber. This chamber is a concrete cube with 10 m sides, which is padded with special soft material inside so that the sound is absorbed in the walls instead of producing an echo. Overview of this chamber can be seen in the Figure 2.21. As from this figure can be also seen, the “ground“ is made of steel wire web, to further decrease the echo.

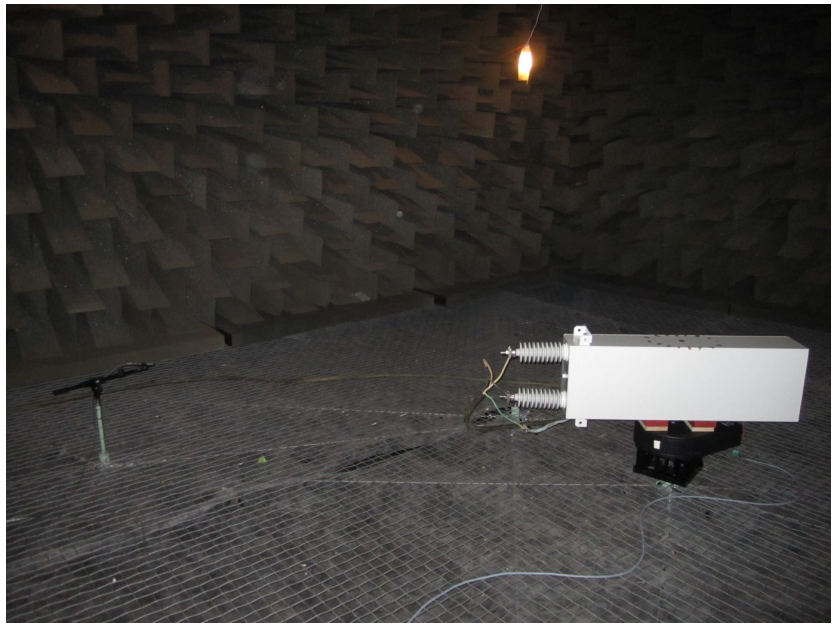

Figure 2.21. Overview of the 2 m measurement

This portion of measurements was composed of two disparate portions. The first portion’s goal was to determine the capacitors’ sound propagation as a function of frequency and position. This measurement was conducted for two capacitors which both were 200 mm deep and 350 mm wide. Their other parameters were: 820 mm tall with 23.3 μF capacitance (Cp) and 1060 mm tall with 12.7 μF capacitance (Cfo). The overall shape of the two capacitors was same except for the difference in height. As can be seen in the Figure 2.22, on the thin side of the capacitor there were marks for the center point of the capacitor as well as for the different angles. Since the manufacturer of the capacitor had previously indicated that according to their measurements the directivity of the capacitor was symmetrical, we measured only 180° of the capacitor. We started with the side with the bushings as can be seen in the Figure 2.21, and finished with the microphone pointing directly to the bottom of the capacitor. With this measuring set-up we ended up measuring nine (9) points per capacitor for

each frequency.

Figure 2.22. Close-up of the capacitor during the acoustic measurements

The input signals were decided in such a way that they would resemble the frequencies and voltages that the capacitor could encounter in the power system during its lifetime. Unfortunately due to the limitations of the power supply, we couldn't go as high voltage wise as we would've wanted. Fortunately though we managed to secure a small transformer, so we could use that to increase the voltage up to over 700 V compared to the 300 V the power supply could normally provide. Since the transformer was meant for 50 Hz use, and our input signals were from 60 to 480 Hz, we measured the output voltage to verify what is actually going to the capacitor. The list of the measured output voltages as a function of frequency can be found in the Table 2.1.

Table 2.1. Inputs for the acoustic directivity measurement

f [Hz]	U_820 [V]	U_1060 [V]
60	740,5	739,6
90	674,3	742,1
120	500,5	744,1
150	461,6	707,8
180	466,3	616,2
210	449,7	530,5
240	423,7	465,9
270	401,5	469,9
300	381,8	474,4
330	327,7	289,8
360	343,4	299
390	177,0	155,3
420	154,1	107,9
450	84,0	62,94
480	23,6	20,21

The second portion's goal was to compare the direct measurements of sound, and then previously measured vibrations. In order to do this we measured the sound levels 2 cm away from the bottom at high frequencies from the same spots where the accelerometers had been using the same inputs as in the vibration measurements. In this measurements we did not use the transformer. Detail of this measurement can be seen in the Figure 2.23 where cross has been marked where an accelerometer was glued in the previous measurement. Since we wanted to compare the results, we measured the same capacitors as in the directivity measurement, but also the 1040 mm tall one with 38.8 μF capacitance (Cfb) that was used in the vibration measurements. Furthermore the requirement to be comparable restricted our voltage ranges, and thus 1060 mm capacitor was measured at 150 V voltage level, 1040 mm at 80 V, and 820 V at 140 V except for the 1450 Hz level, at which only 135 V was input due to power supply restrictions.

In addition to these high frequency measurements at 2 cm, we measured the 1040 mm tall capacitor's acoustic response at frequencies from 60 to 330 Hz every 30 Hz at 173 V as we did during the vibration measurement. Finally we also measured the high frequency response of the 1060 mm tall capacitor at 1 m to see what effect would the increase of sound have.

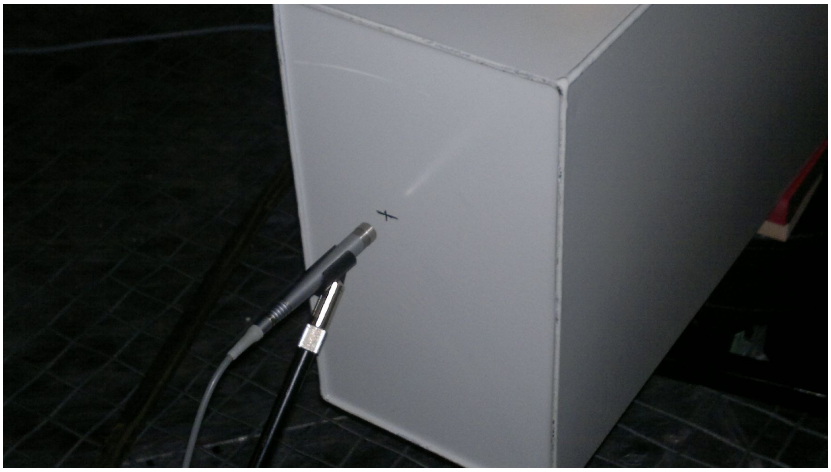

Figure 2.23. Detail of the 2 cm measurement

Finally in order to verify that we really know what we're inputting to the capacitors, we measured the THD and three first significant harmonics using a Fluke 43B power quality analyzer. Since this power quality analyzer was made for low voltage usage, we measured the THD values from low voltage side when we used the transformer, but the voltage was measured from the high voltage side. During the high frequency measurements, the two values were naturally measured from the same side as there was no transformer in use during those measurements. All the measured values can be seen in the Table 2.2, and can be considered generally to be very low, and having little to no effect on our measurements.

Table 2.2. THD values for different input voltages

f [Hz]	Measured U [V]	THD [%]	3rd [%]	5th [%]	7th [%]
60	740,5	0,3	0,1	0,1	0
90	674,2	0,2	0,1	0,1	0,3
130	500,5	0,5	0	0,2	0,4
150	461,6	0,2	0,1	0,3	0,1
180	466,2	0,2	0	0,1	0,1
310	449,7	0,2	0,1	0,1	0
340	432,7	0,7	0,6	0,1	0,1
370	401,5	3,1	3,1	0,1	0,1
200	281,8	3,2	3,2	0,3	0,1
220	237,7	1,6	1,6	0,1	0,1
260	242,4	1,4	1,4	0,1	0,1
290	177,0	1,5	1,4	0,2	0,3
430	154,1	1,5	1,4	0,2	0,1
450	84,0	3,3	3,1	0,6	0,2
480	32,6	2,2	2,3	0,7	0,1
1000	150,6	0,4	0,2	0	0
1050	150,7	0,4	0,2	0	0
1100	150,6	0,4	0,2	0,1	0
1150	150,5	0,4	0,4	0,1	0
1300	150,5	0,4	0,2	0,1	0
1350	150,4	0,2	0,2	0	0
1200	150,2	0,4	0,2	0	0
1250	150,3	0,4	0,2	0	0
1400	150,3	0,5	0,4	0,1	0,1
1450	150,1	0,5	0,4	0,1	0

Since during our measurements in the anechoic chamber of the university we could input only a portion of the nominal voltage to the capacitors, the people from Alstom kindly made their own measurements using a rack of six Cp type capacitors at nominal voltage of 7.3 kV and 60 Hz. The principle figure of this rack is shown in the Figure 2.24. These measurements were unfortunately not as exact as the one done at the anechoic chamber due to suboptimal surroundings, which may have caused some echoes. Also, since there was significant background noise, the noise made by the 60 Hz component was measured at 1 m distance instead of the 2 m distance that was used for other measurements. Further analysis of the results can be found in the Section 3.3.

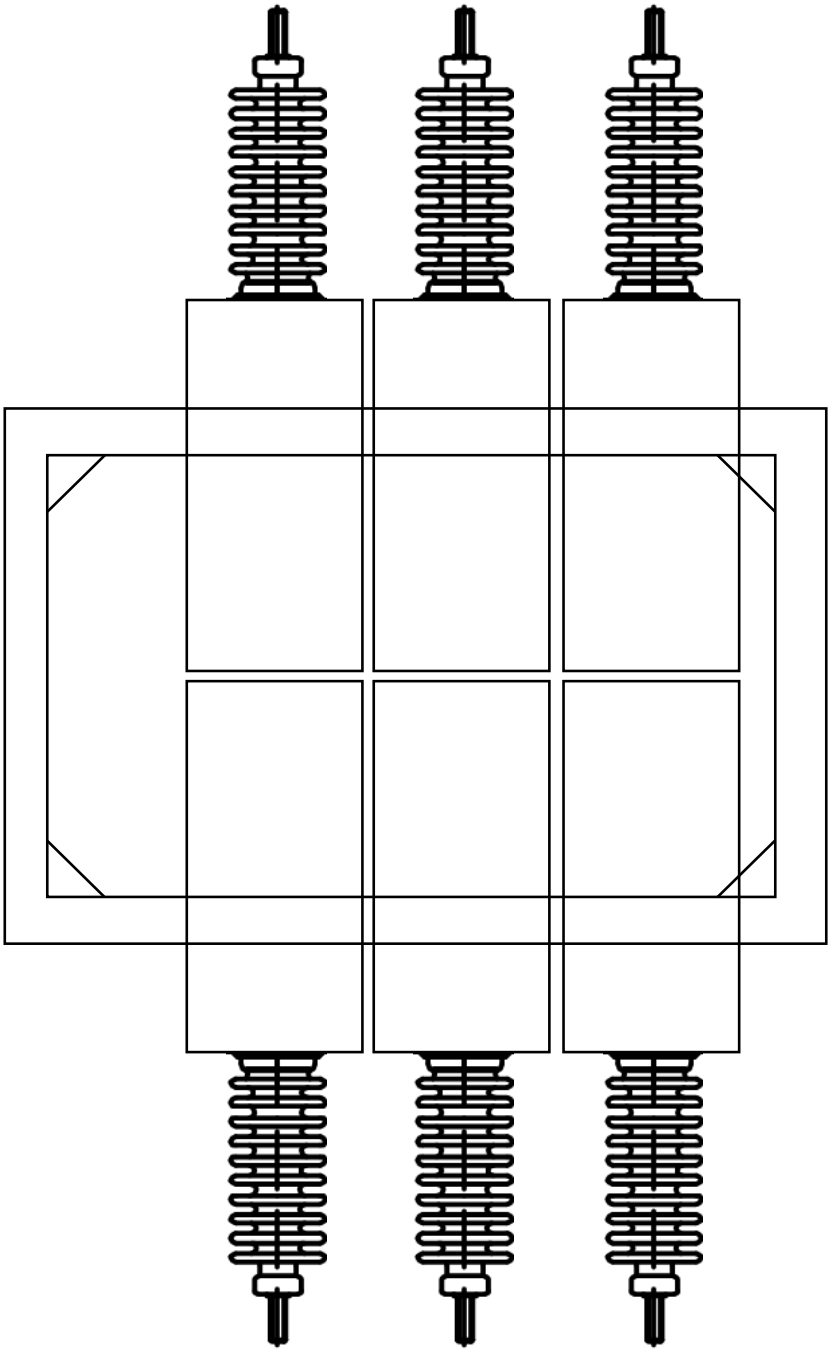

Figure 2.24. Diagram of the measured rack of six Cp type capacitors

Another difference in these measurements was that since the measurement methodology was different, the results were measured using third-octave bands. The capacitors were assumed to produce mainly three different frequencies when fed with nominal frequency. Those frequencies

Table 2.3. Output frequencies and third-octave bands used to measure them at Alstom

$Output \quad frequency$	$Measuring \quad band$
120	$112.2 - 141.3$
360	$281.8 - 354.8$
360	$354.8 - 446.7$
480	$446.7 - 562.3$

along with the output frequencies caused and third-octave bands used to measure them were presented in the Table 2.3. It should be noted that since 360 Hz output frequency caused by the 180 Hz third harmonic of the 60 Hz was almost precisely between the two third-octave bands, it was measured using both of them.

2.4.4 Viscosity of the capacitor oil

Figure 2.25. Viscometer used in the viscosity measurements

In Section 2.4.2 we measured the vibration response of the capacitors. It was assumed that the viscosity of the capacitor oil changes as a function of temperature, and that this variation explains most of the differences of the vibration response in the different temperatures. The reasoning behind this assumption was that the movement of oil inside the capacitor unit is similar to the one inside a shock absorber, where the shock is dampened as the oil flows through the valves. As the temperature changes, so does the viscosity of the oil, thus changing the stiffness of

the shock absorber. In a resembling fashion, it was assumed that the internal dampening of the capacitor changes as the characteristics of the oil fluctuate.

Since the viscosity data in the respect to the temperature wasn't readily available, it was decided that it needed to be measured. The viscosity measurements were carried out using a Brookfield DV-E viscometer belonging to the Department of Biotechnology and Chemical Technology of the Aalto University.

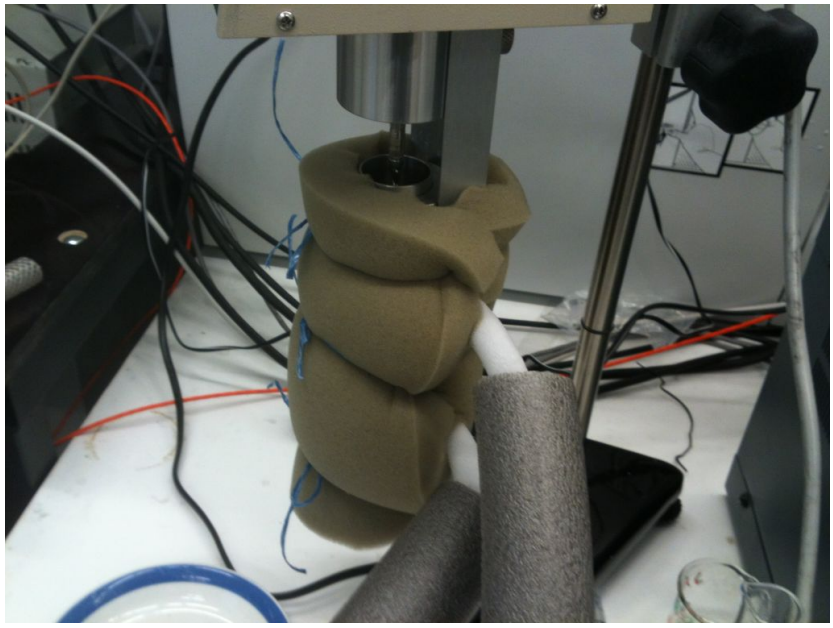

Figure 2.26. Close-up of the spindle used in the measurement

The viscometer can be seen in the Figure 2.25. It's fully digital device in which one selects the rounds per minute (RPM), and spindle they're using, and then the device gives the result directly in cP (equal to $mPa \cdot s$). Since we were interested in the capacitor oil's viscosity in extreme temperatures, we needed to use an insulated thermal unit which included a heat exchanger. This limited the selection of the spindles to a single one. The equipment that was used can be seen in the Figure 2.26. In this figure it's used in the lower temperatures, and thus is heavily insulated to minimize the heat gain, which was here assumed to be zero. A better overview of the insulation, and the whole system can be seen in the Figure 2.27.

Figure 2.27. Overview of the viscosity measurement at the low temperatures

Prior to starting the measurements, the device was calibrated first. After running multiple test runs with various RPMs using 1-butanol, and 1-decanol as calibrating liquids, it was deemed that the results are too large by roughly 10% and thus 10% will be deducted from the results in order for them to be of correct magnitude. This isn't ideal solution, but we believe it yields acceptable results. While calibrating it was also noted that whilst according to the instruction manual a 10% torque would still yield acceptable results, the limit was observed to be closer to 20%, and below this limit the accuracy started to decrease.

Figure 2.28. Temperature control unit in the low temperature measurement

The measurements for the capacitor oil were done in two parts: in the first part water was used as heating and cooling liquid, and the temperatures measured were from +15 °C to +60 °C. In the second part glycerol liquid was used, and the temperature range was from -42.4 °C to +19.3°C. The overlap was intentional to compare the accuracy of the two fluids. One fluid couldn't be used to measure the whole range since water freezes at subzero temperatures, and glycerol starts to evaporate at higher temperatures. The error in the temperature measurement was deemed to be no larger than $\pm$ 0.1 °C. The temperature controller used in the cold temperature measurement can be seen in the Figure 2.28.

2.4.5 Response of the tube extender used for measuring the reactor noise

The second part of this thesis is related to the reactors, and especially how their sound production could be linked to fault detection. The first issue we came across in our research is that the measuring of sound itself proved to be problematic. Due to the high magnetic fields the reactor causes around itself, no ordinary microphone can be used for measurements as it would be destroyed. One could buy specially made non-metal microphones for a significant sum of money, but this would be counter-intuitive since widely used solutions can't be prohibitively expensive. In

order to solve this problem, we decided to try another approach. Since we couldn't bring the microphone to the sound source, we decided to bring the sound to the microphone.

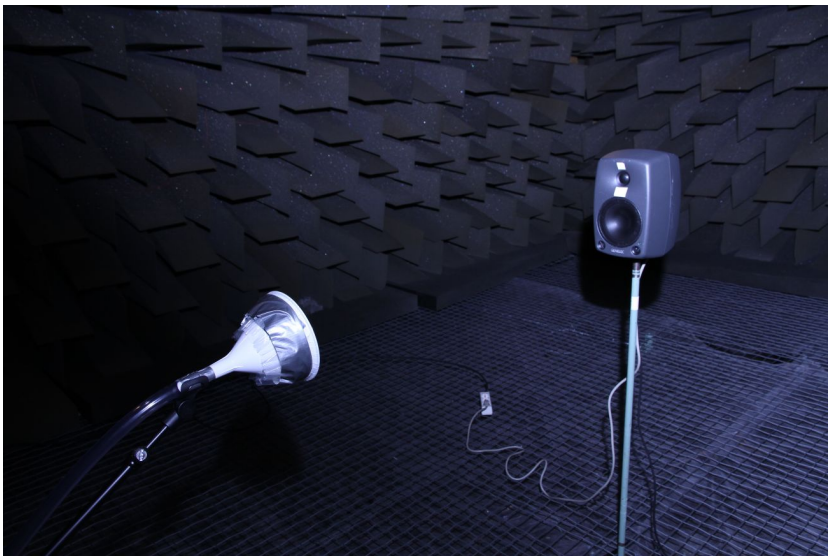

Figure 2.29. Overview of the tube extender response measurement

In order to do these acoustic measurements, we co-operated with Department of Signal Processing and Acoustics of the Aalto University as we did in Section 2.4.3, and made measurements in their large anechoic chamber. In order to bring the sound to the microphone, we went for a very simple idea: A plastic pipe with a funnel on the other end, which has a plastic membrane covering the open end. The overview of the funnel end can be seen in the Figure 2.29. The silver tape was used to secure the membrane to the funnel so that it would have even tension. With the funnel secured in one spot using a microphone stand, a Genelec 8030A speaker was then placed 1 m away from the funnel in order to produce steady pressure level of sound over a frequency range. The frequency range used in these measurements was 50-5000 Hz, and the signal was 5 second in length total. The reference level was 96 dB SPL, and the signals we used for measuring were -10, -22, and -34 dB relative to this level. The -10 dB was selected so that we would have ample difference from the maximum output of the speaker, and the two other levels were 12 dB away from each other, which means quadrupling pressure level.

Figure 2.30. Microphone end of the tube extender

The measurement had three goals: To determine how the tube extender changes the sound as a function of frequency, how do the changes vary based on the parameters of the tube, and what uncertainties making the tube extender by hand causes. The variance of frequency was covered by using vast frequency range in the input signal. The variance caused by the length was taken into account by using three different lengths: 5 m, 7.5 m and 10 m. Finally the issue of hand-made parts was investigated by making three copies of each of the tube extender lengths. The raw materials used in each extender were naturally identical. The microphone end of the tube extender can be seen in the Figure 2.30. As we were making the measurements, it was noted that it would be a good idea to test how the response changes if the microphone end of the tube extender is insulated. This is due to the fact that closing the end causes the pressure at the end to double.[81] The image of this case is pictured in the Figure 2.31.

Figure 2.31. Insulated microphone end of the tube extender

2.4.6 Reactor noise measurement in the field using the tube extender

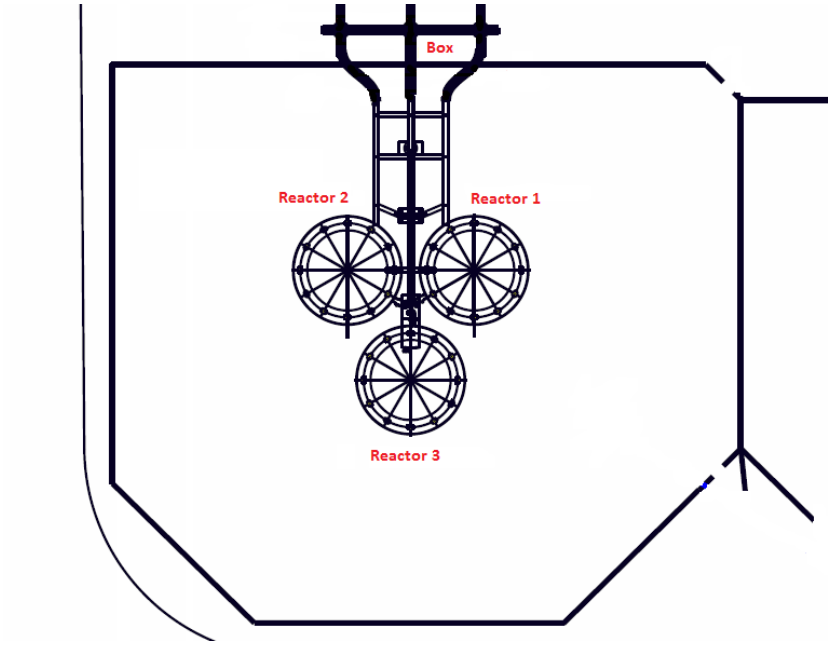

Figure 2.32. Birds eye view of the relative positions of reactors and the measurement box

In order to verify the usability of the tube extender in the field, we co-operated with the Finnish national grid operator Fingrid in order to do a

test installation in the field. The goal for this measurement was to determine whether or not we could measure the difference between the background and operational noise of the reactor in a real environment. Our target for the installation was power station in Keminmaa, a municipality in Lapland, northern Finland. Fingrid had scheduled an interruption in the power supply to one set of three reactors on the site, and allowed us the time to make installation during this period. In the Figure 2.32 we see the birds eye view of the reactor area. Reactors that were measured are numbered, as is the measuring box ("Box") under the bus bars. The black enclosing around the reactors is the safety fence outside which everyone must be when the reactors are turned on. On the right edge of the figure we can see the start of the next enclosure, which contains a second set of reactors, which were on during the time we installed the extenders, and made the measurements.

Figure 2.33. Overview of the reactors from the side with the tube extender installed

In the Figure 2.35 we see an overview of the reactors under which the tube extenders were installed. As can be seen, we used planks to create a T-shaped construction in order to place the funnel end of the tube extender at the very middle of each reactor. Details of this construction can be seen in the Figure 2.34, where we see that there's ample amount of space below the reactor in order for us to install the tube extenders. Also, it can be seen that we used the plank to further support the soft tube so that we could

shorten its total length.

Figure 2.34. Tube extender installed below a reactor

Figure 2.35. Soft tube attached to the concrete below the reactor

One can see more details of the installation in the Figures 2.35 and 2.36 where it's shown how the soft tube is lead to the drainpipes for further protection. In order to preserve the sound we needed to avoid sharp corners, and thus we had to support the tube using copper conduit clips. When we got to the ground level, we used plastic drain pipes to further protect the soft tubes from weather and trampling.

Figure 2.36. Drainpipes protecting the tube extender up to the safety fence

The end of the drainpipes can be seen in the Figure 2.37 where soft tubes emerge again before they are connected to the weather resistant plastic box. When the box is opened, normal microphones can be connected to a laptop computer, and used to record the sound of the reactors from a safe distance. The tube extenders used in this measurement were almost identical to the ones measured in Section 2.4.5, but due to the experimental nature of the measurement the lengths of the tubes were different. The reactors' 1 and 2 from Figure 2.32 had identical tube extenders, but since reactor 3 was further away, its extender was different. Also, in this measurement the ends of the tubes weren't insulated. Overall these limitations were of little concern, as this measurement's goal was to verify whether or not we could use the tube extenders in field measurements to differentiate between the background and operational noise.

Figure 2.37. Sealed weather resistant box to which the tube extenders are terminated

2.4.7 Reactor noise measurement in a controlled environment using the tube extender

Figure 2.38. Overview of the controlled environment measurements

After we verified the usability of the tube extender in a field environment, and measured the tube extender's response, we decided to do a controlled measurement. The goal for this measurement was to see whether we could add a controlled fault to the reactor, which would produce an audible noise that could be detected by noise measurement and analysis. If such a fault could be produced, it would signify that there's a high chance of being able to use sound as a method of fault detection in the future. The overview of this measurement can be seen from the Figure 2.38. We used 10 m long tube extenders in order to measure the reactor's sound from a safe distance while the measurer was sitting inside a forklift's cabin. Since reactor of this size causes a big variance to the local reactive power balance, it had to be compensated using capacitors seen in the Figure 2.39.

Figure 2.39. Capacitor battery that was used to compensate the reactor being measured

Figure 2.40. Cable ties were used to minimize the vibrations of the input cables

Since the measurements were carried in the yard of the manufacturer, there were multiple challenges in measuring. First of all the location was in the middle of an industrial area, and thus the traffic from the nearby road was one cause of concern. Secondly, the capacitors used for the compensation also produced sound. Finally, the other work being done in the factory also produced some sound. In order to minimize the effects of these factors, the measurements of the sound were done when no traffic was passing by, and as an average over a period of roughly ten seconds. Also when analyzing the results, the measured background noise was deducted from the measured operating noise to minimize its effect. To fur-

ther reduce the effect of outside noise, we used cable ties as can be seen in Figure 2.40 to reduce possible vibrations of the input cables.

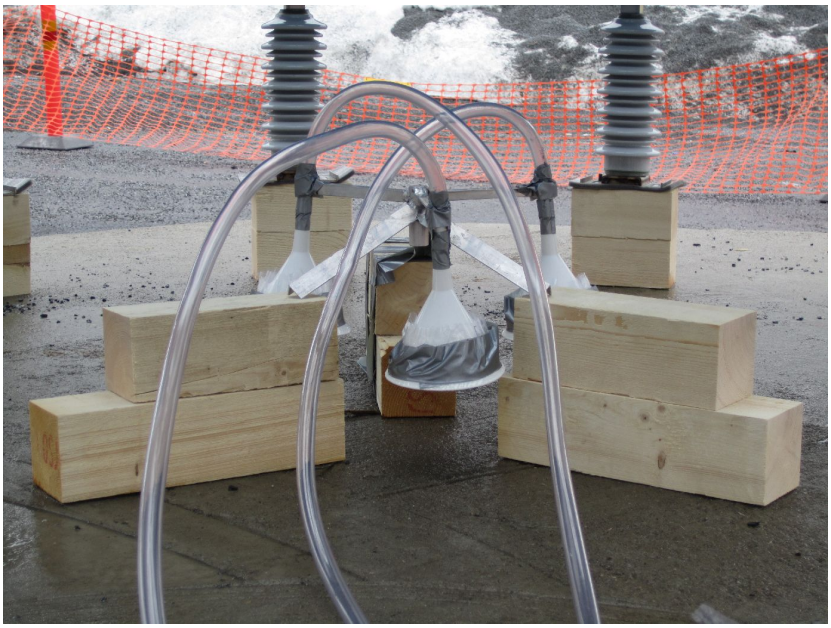

Figure 2.41. Tube extenders' position was experimented with by putting them upside down

Since this time we could do any number of interruptions in the reactor operation, we decided to experiment a bit with the position of the tube extenders. In the Figure 2.41 it's shown that we used three tube extenders at once with the help of custom made aluminum tube extender holder. This allowed us to measure from three separate spots at the same time, and thus to study how much small differences in location matter when measuring reactor noise. Also, since in this reactor the ground was concrete instead of gravel as it was in Section 2.4.6, we decided to see how much the tube extenders would "hear" when turned upside down. This was mostly interesting since then the funnels would probably last more due to membranes not being directly exposed to weather.

When the tube extenders were in this position, we did three measurements. First we measured the background noise, then the normal operating noise of the reactor, and finally we loosened few bolts at the top of one insulator according to the Figure 2.42. After these measurements we moved away from this experimental position, and continued the same was as we had started in Section 2.4.6.

Figure 2.42. Insulator's bolts were loosened to create a minor fault

Since in the previous measurements we measured the sound with the tube extenders pointing upwards, we decided to measure most of the cases using this position as well. The position can be seen from the Figure 2.43. The position is considered here more usable as the base of the reactor has little effect on the noise measured unlike in the downward position. To start off with this position, the fault presented in the Figure 2.42 was fixed in order to measure the background and normal operating noises. After measuring these two we did two series of tests in which we started adding new faults little by little.

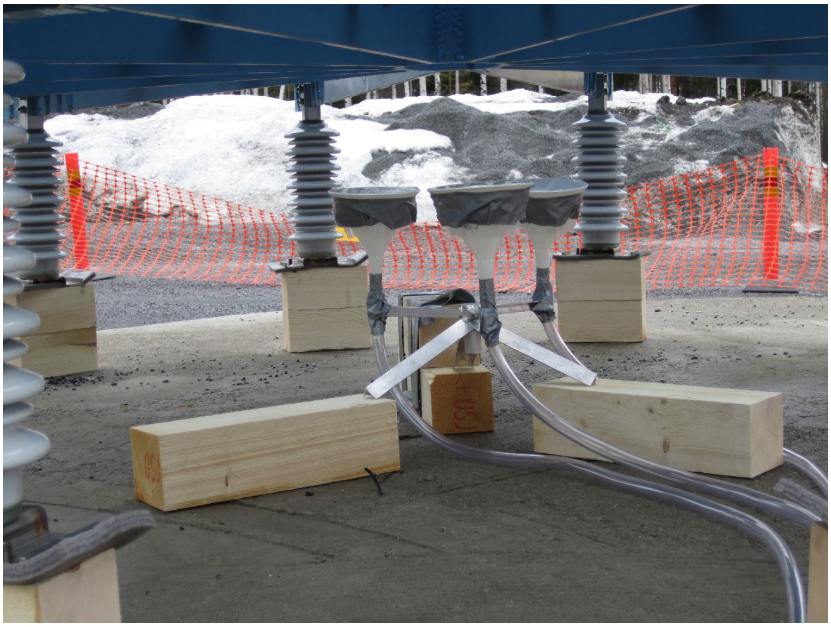

Figure 2.43. Most of the measurements were done when the tube extenders were in upwards position

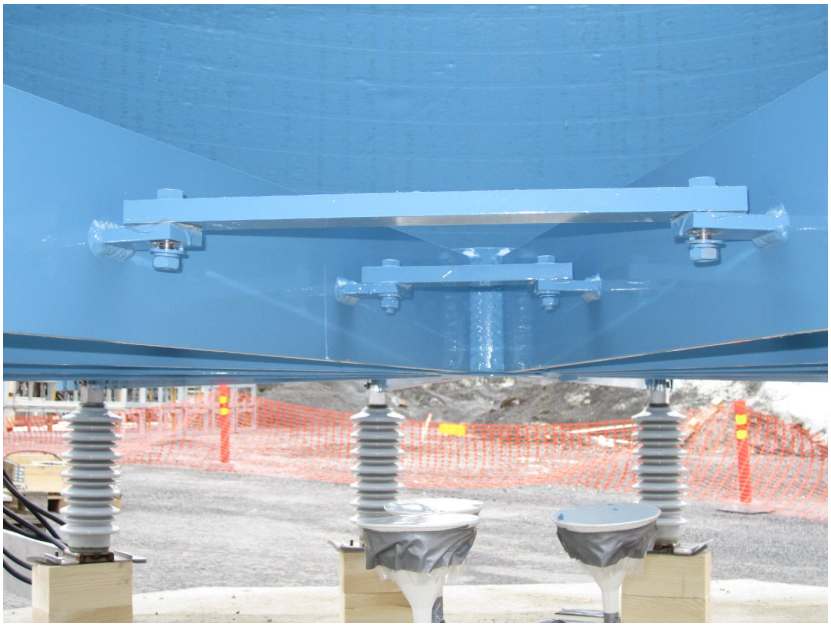

Figure 2.44. The supporting bar's bolts loosened for the experiment

At first we loosened some bolts of the supporting bar according to the Figure 2.44. After measuring these, we went on to loose the bolts of the middle pipe as can be seen in the Figure 2.45. Following these two cases, we went on to loosen up the bolts of the lifting lug as presented in the

Figure 2.46. After these three cases it was time to refasten the loose bolts, and start testing from the start again.

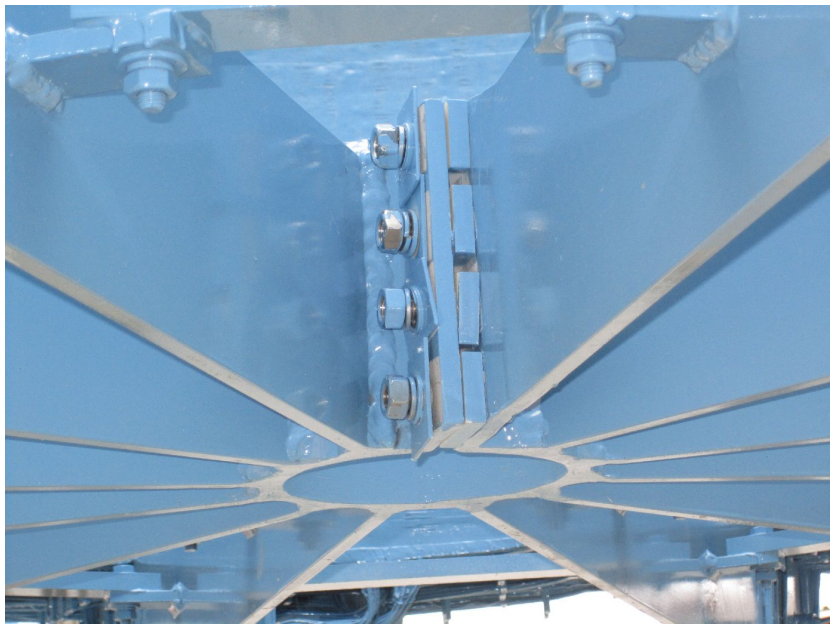

Figure 2.45. Middle pipe's bolts were loosened in order to create sound

Figure 2.46. Lifting lug's bolts were loosened to create audible noise

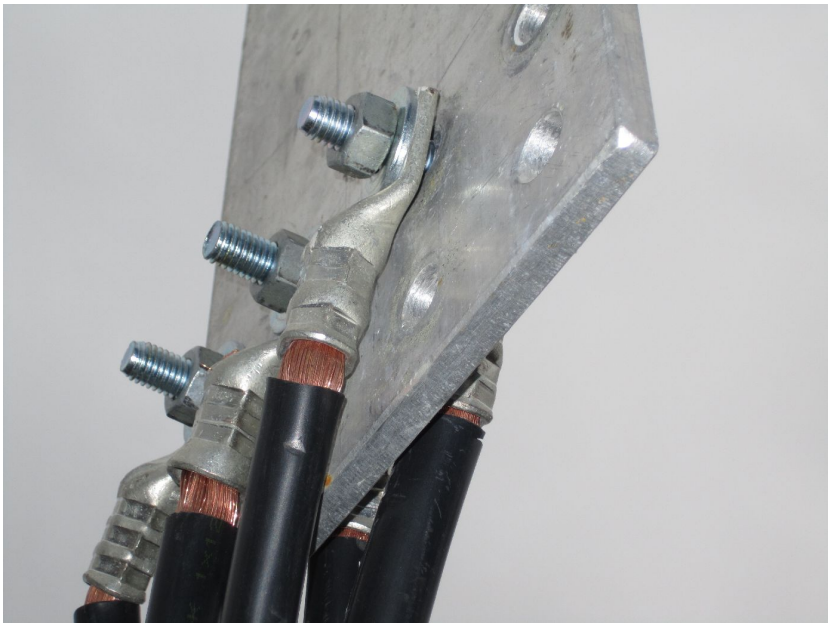

Figure 2.47. Input cable's bolts were loosened to see whether it would create noise

While in the first set of measurements we concentrated on the structure of the reactor itself, we moved on to search for the possible sources of sound in the input cables for the second set. First of all we loosened the bolts of one of the three bolts that was responsible for holding two of the six input cables securely in place as can be seen in Figure 2.47. Secondly we added two loose bolts made of regular steel, which should be more susceptible to the magnetic field, and thus not usually used in the installation. These bolts can be seen in the Figure 2.48. The results from these measurements can be found in Section 3.6.

Figure 2.48. Finally loose bolts were added near the input to see if they create noise

2.5 Simulating resonance frequencies of capacitors

2.5.1 Comparing simulation results with the literature

As we discussed in the Section 1.2, there are two publications that present the equations needed to calculate the resonance frequencies of a clamped plate with any dimensions. Since these equations are based on the basic physical equations, we will see in this section how good results they give in simple cases, such as the left hand side of the Figure 2.49. In this figure red color represents the maximum displacement, and blue the minimum displacement. If we want to move to more complicated cases, such the right hand side of Figure 2.49, we have to move towards simulation techniques, as the theoretical equations do not handle these cases well.

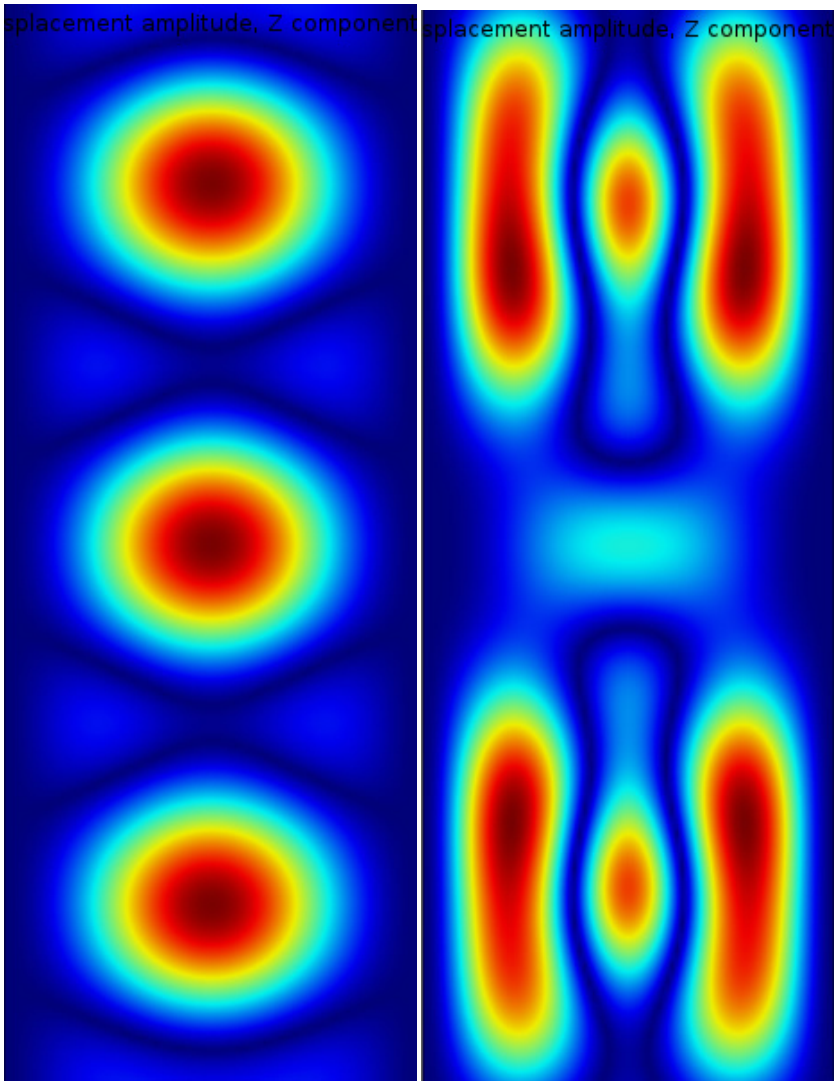

Figure 2.49. Two different resonance images obtained via simulation at 200 Hz and 400 Hz inputs.

This section presents the two theoretical equations in detail, and compares the results they give with the first ten resonance frequencies obtained from the simulation software. The software used was COMSOL 4.2a, and the plate used to represent the capacitor bottom was 200 mm x 350 mm x 1.9 mm plate made out of UNS S40900 steel. During the simulation all the edges were fixed to obtain results equivalent to the “all sides clamped“ situation. The mesh used was set to “finer“, and temperature to 20°C. The material properties used were taken from the material library included in the software.

The first set of equations, presented by Warburton in his work in 1954

[101], is the more complicated of the two. The full equation to obtain frequency parameter λ is shown in the Equation 2.24.

$$\lambda^2 = G_x^4 + G_y^4 \frac{a^4}{b^4} + \frac{2a^2}{b^2}[\sigma H_x H_y + (1-\sigma) J_x J_y] \tag{2.24}$$

Luckily for this particular case, in case of a plate clamped from all sides, $J_x = H_x$ and $J_y = H_y$. Thus we can simplify the equation into the form shown in the Equation 2.25. In this equation a and b are the lengths of the sides of the plate in meters, where a is the smaller dimension. Other parameters are more complicated, and will be explained below in the Equation group 2.26.

$$\lambda^2 = G_x^4 + G_y^4 \frac{a^4}{b^4} + \frac{2a^2}{b^2} H_x H_y \tag{2.25}$$

In order for Warburton's equation to give a result, we need to know the amount of nodes that the resonance frequency creates in the plate in both x- and y-directions. For example in the left side image of the Figure 2.49 we have two nodes in the x-direction (the sides of the plate), and four in the y-direction (the sides, and the two nodes between the anti-nodes). In Warburton's equation the nodes in the x-direction are represented by m, and the nodes in the y-direction by n. Now we can calculate other parameters needed for the Equation 2.25.

$$\begin{cases} G_x = 1.506,\ if\ m = 2,\ else\ G_x = m - 0.5 \\ G_y = 1.506,\ if\ n = 2,\ else\ G_y = n - 0.5 \\ H_x = 1.248,\ if\ m = 2,\ else \\ H_x = (m - \frac{1}{2})^2 [1 - \frac{2}{(m-\frac{1}{2})\pi}] \\ H_y = 1.248,\ if\ n = 2,\ else \\ H_y = (n - \frac{1}{2})^2 [1 - \frac{2}{(n-\frac{1}{2})\pi}] \end{cases} \tag{2.26}$$

With all the parameters calculated, we've obtained λ, which allows us to move to the last equation needed in order to obtain the resonance frequencies. It should be noted that in order to calculate λ we do not need to know what the plate is made of. We only need its physical dimensions. In the last Equation by Warburton's (2.27), h is the thickness of the plate, a is the length of the longer side, E is the Young's modulus, g is the standard gravity, ρ is the density of the plate, and σ is the Poisson's ratio.

$$f = \frac{\lambda h \pi}{a^2} \sqrt{\frac{Eg}{48\rho(1-\sigma^2)}} \tag{2.27}$$

As can be deducted from the name of the publication (“A simple frequency formula for clamped rectangular plates“), the equation presented by Mitchell and Hazell is much simpler than the one presented above. In the Equation for λ (2.28) we have have very similar looking symbols, but this time they have a bit different meaning. λ is once again frequency parameter. a and b are the lengths of the shorter and longer edges respectively. m and n are the numbers of *anti-nodes* in x- and y-direction respectively. Using the left side of Figure 2.49 as an example again, this means m would be 1 and n would be 3 in this case.

$$\lambda = a^2\pi^2[\{(m + \Delta_m)/a\}^2 + \{(n + \Delta_n/b\}^2] \tag{2.28}$$

The meanings of parameters Δ_m and Δ_n can be found in the Equations 2.29 and 2.30 below. As can be seen, they are much simpler than the corresponding parameters in the Warburton's equation.

$$\Delta_m = ((na/mb)^2 + 2)^{-1} + (0.017/m) \tag{2.29}$$

$$\Delta_n = ((mb/na)^2 + 2)^{-1} + (0.017/n) \tag{2.30}$$

After the Equation 2.28 yields the λ we can use Equation 2.31 in order to calculate the resonance frequencies. The D in the equation is the flexural rigidity, which can be calculated using Equation 2.32. Please do note that similarly as in the Equation 2.25, the value of λ is not dependent on the material of the plate, only on the physical dimensions of it.

$$\lambda = \omega a^2\sqrt{\rho h/D} \tag{2.31}$$

$$D = \frac{Eh^3}{12(1 - \sigma^2)} \tag{2.32}$$

If we substitute D by its equation in the Equation 2.30, substitute ω by $2\pi f$, and then solve the f, we obtain final Equation 2.33. It's almost the same as Warburton's final Equation 2.27, with just the π being in the denominator instead of the numerator. All the other values and symbols are the same, but there's a catch: the a in this equation is the length of the shorter edge as it was in the Equation 2.28 instead of being the longer edge as it was in the Equation 2.27.

$$f = \frac{\lambda h}{\pi a^2}\sqrt{\frac{Eg}{48\rho(1 - \sigma^2)}} \tag{2.33}$$

The results given by the theoretical equations are dependent on the material values of real life materials. Since those values have a variance[89], it was decided to give the frequency value not only for the average values, but also for the values that would yield the minimum and maximum frequency. In the Table 2.4 it can be seen that the difference between using the values at the extreme ends of the spectrum can affect the end results up to about 6%. As can be deducted from Equations 2.27 and 2.33 the maximum values occur when Young's modulus is at it's maximum value, and the density and Poisson's ratio are at their minimum values. Naturally minimum values occur in the exact opposite situation.

Table 2.4. Variation in the yielded resonance frequencies due to variance in the input data

a =	0,2	b =	0,35				
h =	1,90E-03	g =	9,8				
ρ_avg =	7865	ρ_min =	7700	ρ_max =	8030	ρ_COMSOL =	7700
E_avg =	2,00E+011	E_min =	1,90E+011	E_max =	2,10E+011	E_COMSOL =	2,20E+11
σ_avg =	0,29	σ_min =	0,27	σ_max =	0,30	σ_COMSOL =	0,29
D_avg =	124,4	D_min =	129,5	D_max =	119,3	D_COMSOL =	137,3

Warburton m&n = 2,3,4...

f_avg	f_max	f_min	λ	m	n	G_x	G_y	H_x, J_x	H_y, J_y
300,1	309,4	290,9	2,6	2	2	1,5	1,5	1,2	1,2
419,5	432,5	406,6	3,6	2	3	1,5	2,5	1,2	4,7
627,3	646,7	608,0	5,4	2	4	1,5	3,5	1,2	10,0
763,4	787,0	739,9	6,6	3	2	2,5	1,5	4,7	1,2
877,9	905,0	850,9	7,6	3	3	2,5	2,5	4,7	4,7
919,9	948,4	891,7	7,9	2	5	1,5	4,5	1,2	17,4
1071,7	1104,9	1038,8	9,2	3	4	2,5	3,5	4,7	10,0
1292,9	1332,9	1253,2	11,2	2	6	1,5	5,5	1,2	26,7
1349,6	1391,4	1308,1	11,6	3	5	2,5	4,5	4,7	17,4
1460,0	1505,2	1415,1	12,6	4	2	3,5	1,5	10,0	1,2

Mitchell m&n = 1,2,3...

f_avg	f_max	f_min	λ	m	n	Δ_m	Δ_n
291,8	300,8	282,8	25,4	1	1	0,4	0,2
405,1	417,7	392,7	35,3	1	2	0,3	0,4
604,6	623,3	586,0	52,7	1	3	0,2	0,4
745,7	768,7	722,7	64,9	2	1	0,5	0,1
853,8	880,2	827,5	74,4	2	2	0,4	0,2
887,5	914,9	860,2	77,3	1	4	0,2	0,5
1042,4	1074,7	1010,4	90,8	2	3	0,4	0,3
1249,9	1288,6	1211,5	108,9	1	5	0,1	0,5
1310,4	1351,0	1270,1	114,1	2	4	0,3	0,4
1426,4	1470,5	1382,5	124,2	3	1	0,5	0,1

After doing the research on the general values of the steel used in the capacitors, the values used by COMSOL were determined, and used to calculate the resonance frequencies using both Warburton's and Mitchell-Hazell equations. The differences between the resonance frequencies obtained from the simulations and the theoretical equations are shown in

the Table 2.5. It can be seen that the older Warburton's equation yields fairly even 2.5% difference compared to the simulation whereas Mitchell-Hazell equation results in frequencies that are mostly within a single percent from the simulation results. It should be also noted that whilst Warburton's equation yields larger values than the simulation, Mitchell-Hazell equation yields smaller values than the simulation.

Table 2.5. Differences between resonance frequencies obtained from the theoretical equations and the simulations

#	COMSOL	Mitchell	Diff %	Warburton	Diff %
1	311,4	309,8	0,5	318,6	2,3
2	434,7	430,1	1,1	445,3	2,4
3	649,7	641,8	1,2	666,0	2,5
4	791,9	791,6	0,0	810,5	2,3
5	909,1	906,4	0,3	932,0	2,5
6	952,2	942,2	1,1	976,7	2,6
7	1110,3	1106,7	0,3	1137,8	2,5
8	1338,1	1327,0	0,8	1372,6	2,6
9	1397,5	1391,2	0,5	1432,8	2,5
10	1531,5	1514,3	1,1	1550,0	1,2

2.5.2 The idiosyncrasies of clamped plates' resonance frequencies

As could be seen from the Section 2.5.1, we can calculate as many resonance frequencies as we want to. What is even more interesting than at which frequencies those resonances are, is what effect they have on the plate. The theoretical equations do not give us any information on how much the amplitude changes if we apply the same force on different frequencies. While simulations won't give us the absolute values of the displacement amplitudes, we can still obtain the relative values of displacement at each frequency. This section concentrates on the idiosyncrasies of clamped plates' resonance frequencies, as they are more complicated as one might think when first encountering them.

The first demonstration concentrates on the relative amplitudes around the three first resonance frequencies. This raw amplitude response can be seen in the Figure 2.50. We can see one peak at around 300 Hz, and another one at around 650 Hz. It was mentioned that this figure shows the data around the first *three* resonance frequencies though. So what is the issue here?

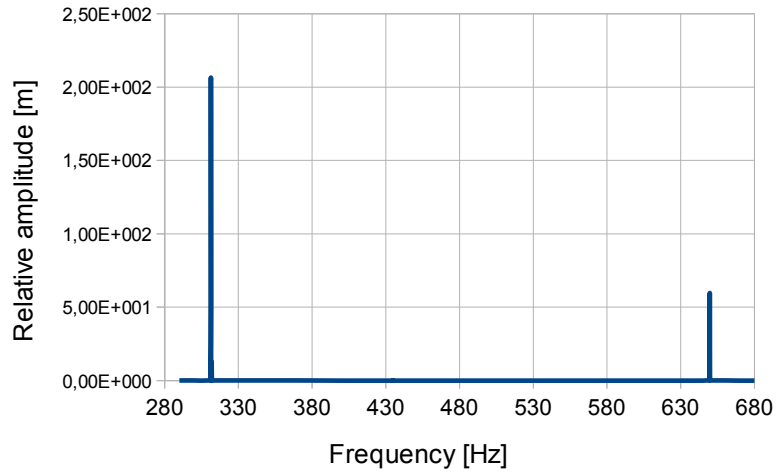

Figure 2.50. Raw amplitude response of the plate around three first resonance frequencies

As we can see from the Figure 2.50, the amplitudes of the displacement are seemingly zero elsewhere except at the two peaks mentioned. This isn't the whole truth though, as it just means that the variance in the displacement is extremely large. We can demonstrate this by post-processing the relative amplitude data a bit. In the Figure 2.51 it is shown how the above figure changes when it's multiplied by a large enough number to scale all the measuring points above 1, and then a logarithm is applied to it. Now we can clearly see the second resonance peak as well. For the further discussion, please do note that the relative level of amplitude outside peaks is roughly between one and three.

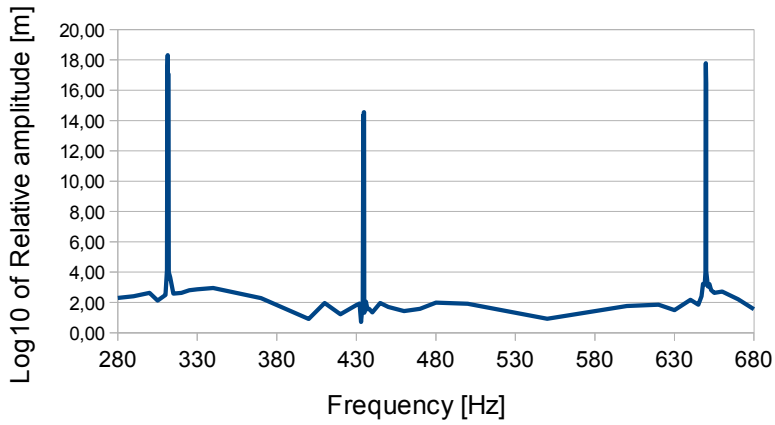

Figure 2.51. Post-processed amplitude response of the plate around three first resonance frequencies

When looking at a larger number of resonance frequencies, we can see from Figure 2.52 that their amplitudes vary somewhat, but are generally above the “background noise“ of one to three. But how does this relate to capacitors?

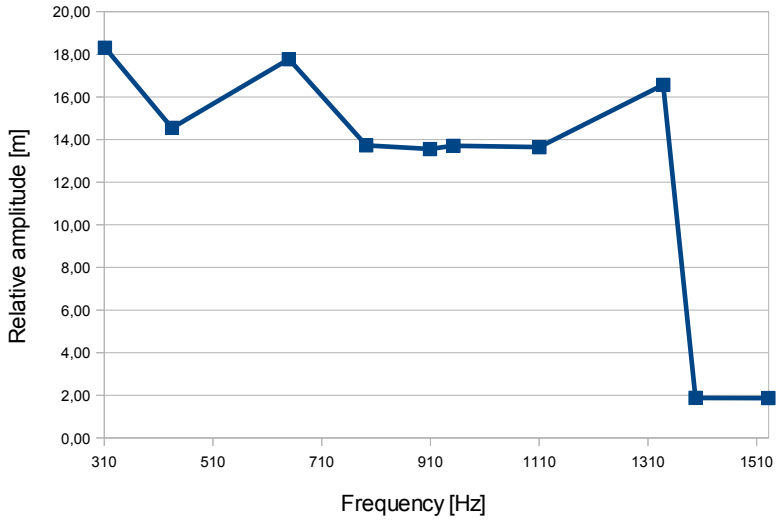

Figure 2.52. Post-processed amplitude response of the plate at the resonance frequencies

Since the nominal frequency of the power systems is usually 50 Hz or 60 Hz, the existing frequencies in the power system are the multiples of these two fundamental frequencies. In order to see whether or not these frequencies should excite the capacitor bottom, the response of the multiples of these fundamental frequencies up to 1560 Hz were simulated, and then plotted into the Figure 2.53. If we compare these levels to the Figure 2.51 shown before, we can conclude that all but one are on the equal level to the “background noise“. Even the one at 650 Hz, which is just 0.3 Hz away from the calculated resonance at the 649.7 Hz isn’t even close in the amplitude to the nearest peak. This train of thought will be continued later on in the Section 4.2 where vibration response of a real capacitor will be studied.

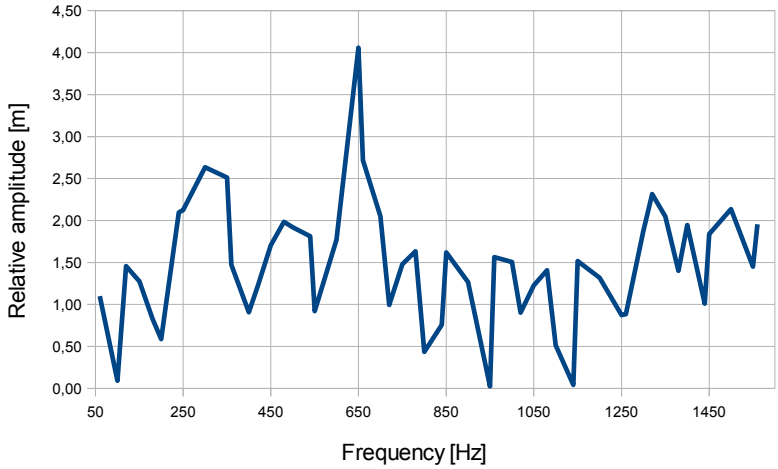

Figure 2.53. Post-processed amplitude response of the plate at the harmonic frequencies of 50 and 60 Hz

For the data used in drawing the graphs in this section, please consult appendix B.

3. Results

3.1 DC compression of air filled capacitor element

The first measurements aimed to provide insight to the symmetry hypothesis by measuring whether the distance from the origin, and the compression measured correlates. The results, along with a linear curve fitted to these results, are presented in the Figure 3.1. The correlation between the Pythagorean distance, and the compression value was -0.77. The square unit used to present the distance from origin is 20 mm long as mentioned in the Section 2.4.1.

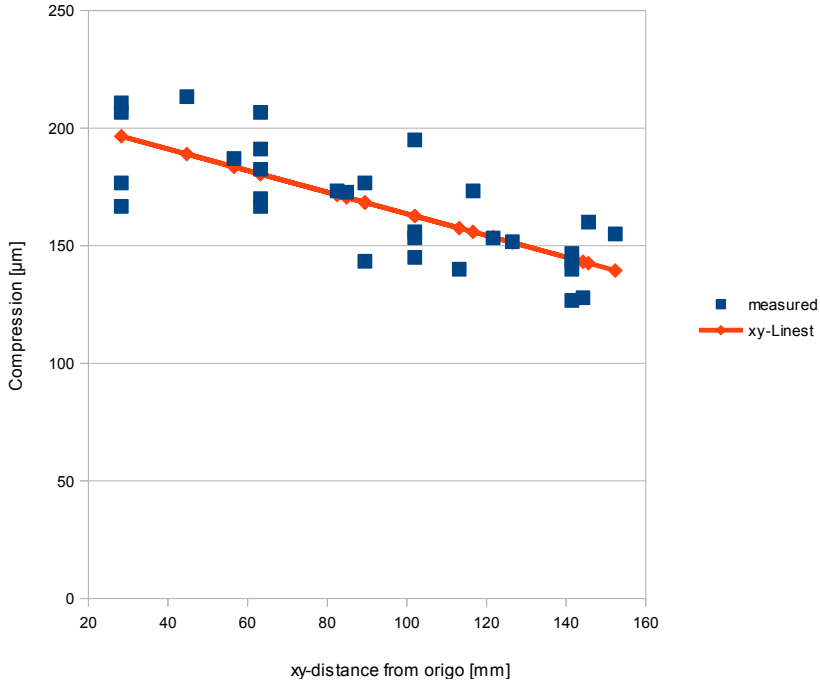

Figure 3.1. Measuring points and fitted linear curve for air filled element at 3.2 kV DC

The results for the two other measurements, done at 2.6 and 2.0 ± 0.1 kV are shown in the Figures 3.2 and 3.3. The correlation between Pythagorean distance and the compression was -0.78 and -0.83 respectively.

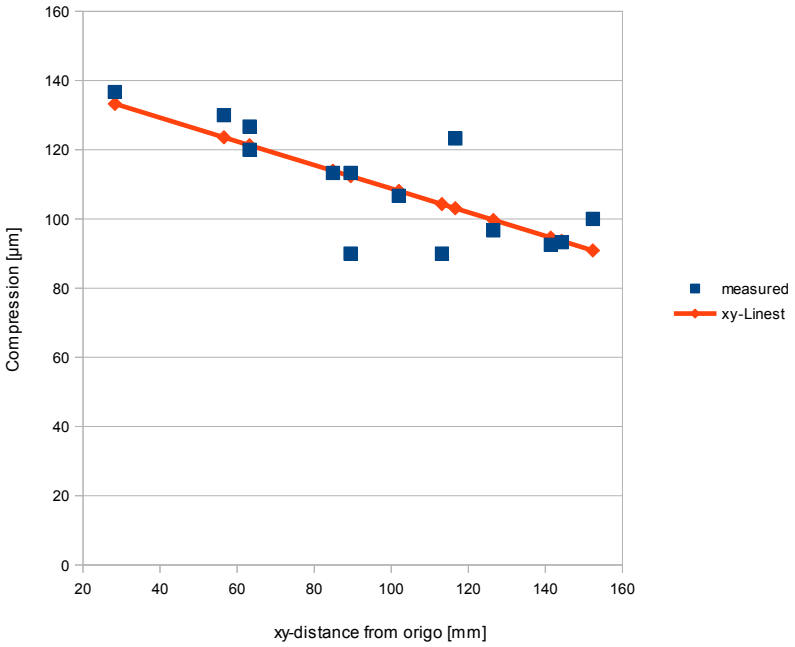

Figure 3.2. Measuring points and fitted linear curve for air filled element at 2.6 kV DC

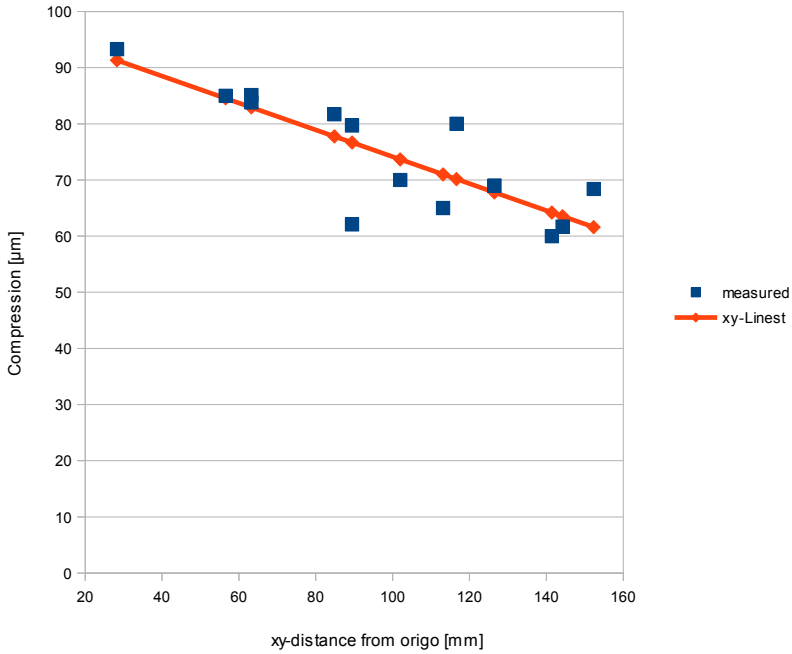

Figure 3.3. Measuring points and fitted linear curve for air filled element at 2.0 kV DC

To better see the differences in the compressions between these three voltage levels, the linear estimations for the measurements are all plotted in the same Figure 3.4.

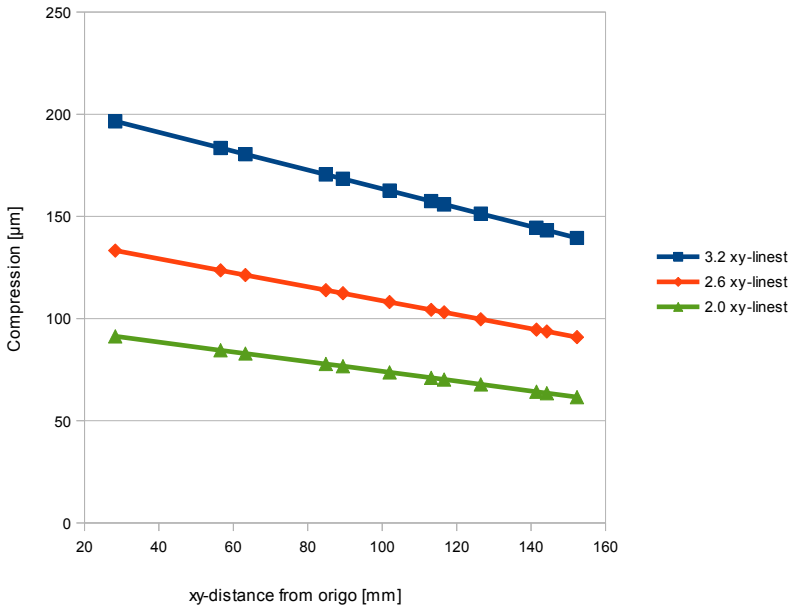

Figure 3.4. Fitted linear curves for air filled element at different DC voltage levels

3.2 Vibration response of the capacitor sides

In this measurement there were two capacitors (C1, 12.7 μF and C2, 38.8 μF). Each capacitor has a measurement on each of the three sides, so there are six figures per each measurement. We'll start with sweep measurements, in which the input was 173 V for both capacitors, and the frequency varied between 50 to 600 Hz for C1 and between 50 to 350 Hz for C2.

To compare the theory with the measurements we first present Figure 3.5 in which we see the displacement of the 38.8 μF C2's bottom plate as a function of frequency. In this figure we have also drawn additional line which corresponds to the calculated value of the vibration based on the Equation 2.15. The values used are below:

t = 56, U = $\frac{173}{4}$ V = 43.25 V, A = 10.032 m^2, ε_r = 2.2, E = 1.5 GPa,
d = 30.4 μm, $A_{profile}$ = 0.07 m^2

where t is the total number of elements, U is the voltage between the plates, A is the total area of the foil of a capacitor element, ε is the permittivity of the isolating material, E is the Young's modulus, d is the distance between plates and $A_{profile}$ is the area of the bottom of the capacitor.

Voltage is quarter of the 173 V used in the measurement since there are four series connections within the capacitor unit.

This gives us the total compression Δx of:

$$\Delta x = t \times \frac{U^2 A \varepsilon}{E d A_{profile}} = 56 \times \frac{(43.25V)^2 \times 10.032m^2 \times 2.2 \times 8.85 \times 10^{-12}}{1.5GPa \times 30.4\mu m \times 0.07m^2}$$

$$= 6.41 \times 10^{-9} m$$

The Figures 3.6, 3.7, and 3.8 show the acceleration responses of the C1 capacitor for big, thin and bottom sides respectively. Likewise the Figures 3.9, 3.10, and 3.11 show the acceleration responses of the C2 capacitor for its big, thin and bottom sides respectively. From these figures we notice that the vibration respose of the bottom side is roughly ten times higher than the other sides in both cases.

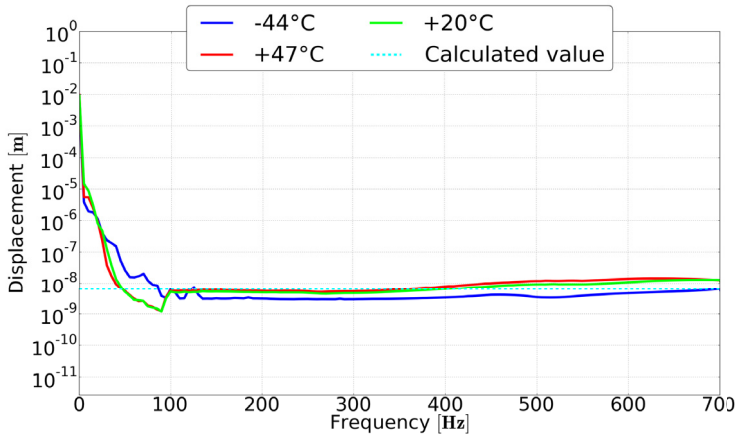

Figure 3.5. Displacement response of the bottom side of the 38.8 μF capacitor for sweep at 173 V from 50 to 350 Hz

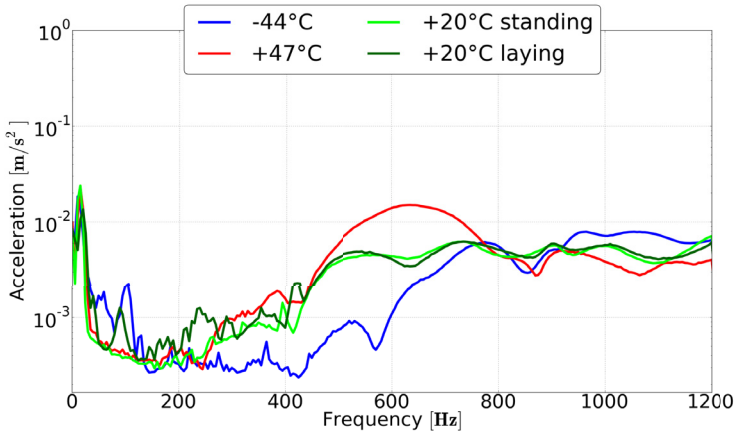

Figure 3.6. Vibration response of the big side of the 12.7 μF capacitor for sweep at 173 V from 50 to 600 Hz

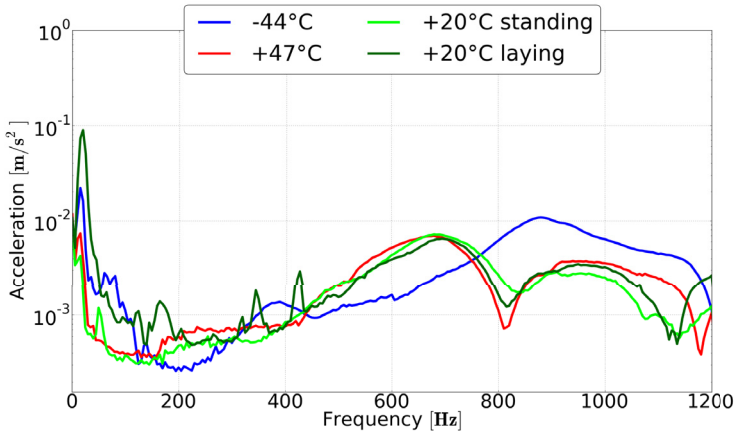

Figure 3.7. Vibration response of the thin side of the 12.7 μF capacitor for sweep at 173 V from 50 to 600 Hz

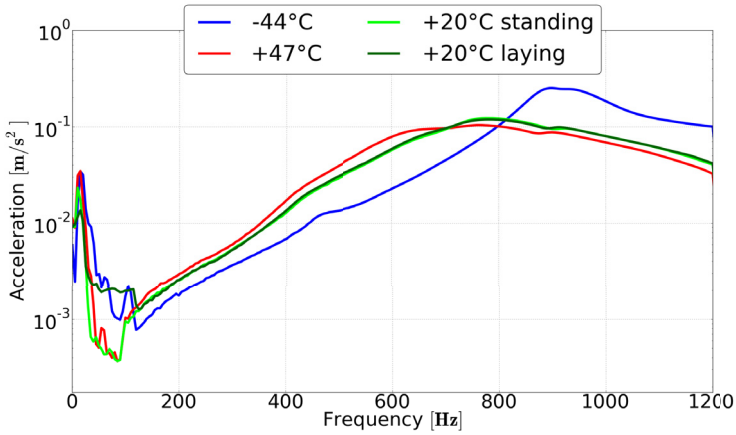

Figure 3.8. Vibration response of the bottom of the 12.7 μF capacitor for sweep at 173 V from 50 to 600 Hz

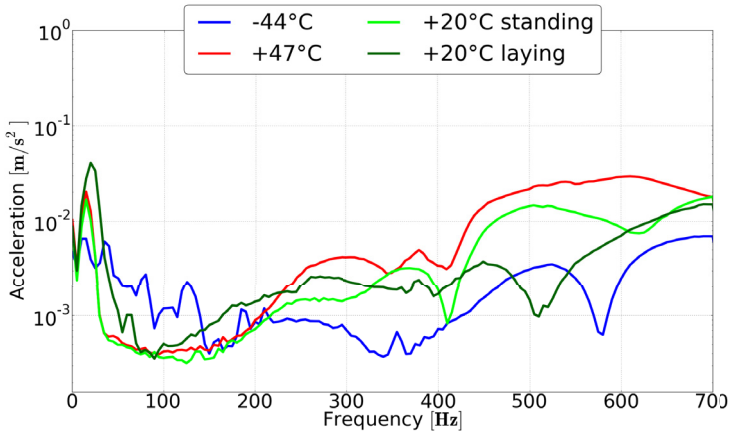

Figure 3.9. Vibration response of the big side of the 38.8 μF capacitor for sweep at 173 V from 50 to 350 Hz

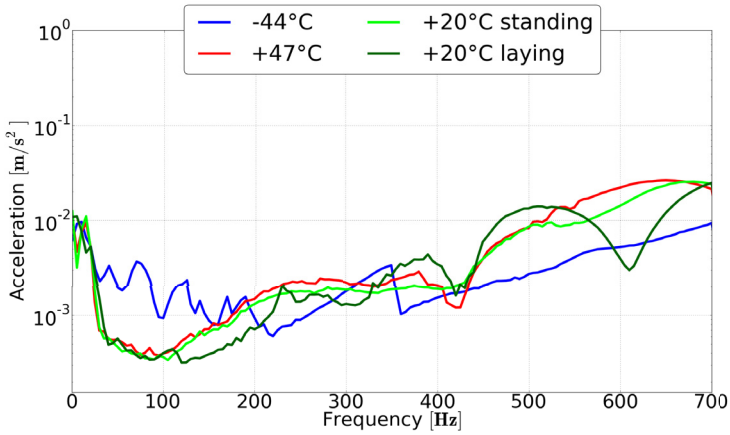

Figure 3.10. Vibration response of the thin side of the 38.8 μF capacitor for sweep at 173 V from 50 to 350 Hz

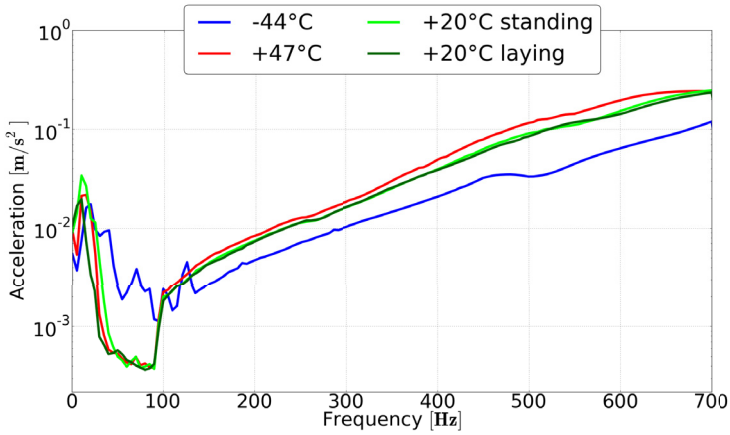

Figure 3.11. Vibration response of the bottom of the 38.8 μF capacitor for sweep at 173 V from 50 to 350 Hz

The second set of measurements was conducted using the high frequencies from 1000 to 1450 Hz every 50 Hz. These frequencies were input one at a time instead of continuous sweep as was the case in the previous results. The input voltage was 150 V for C1 and 80 V for C2. The vibration response for the high frequency inputs of the C1 capacitor's big, thin and bottom sides can be seen in the Figures 3.12, 3.13 and 3.14 respectively. Likewise, the vibration response of the C2 for the high frequency inputs of the big, thin and bottom sides can be seen in the Figures 3.15, 3.16 and 3.17.

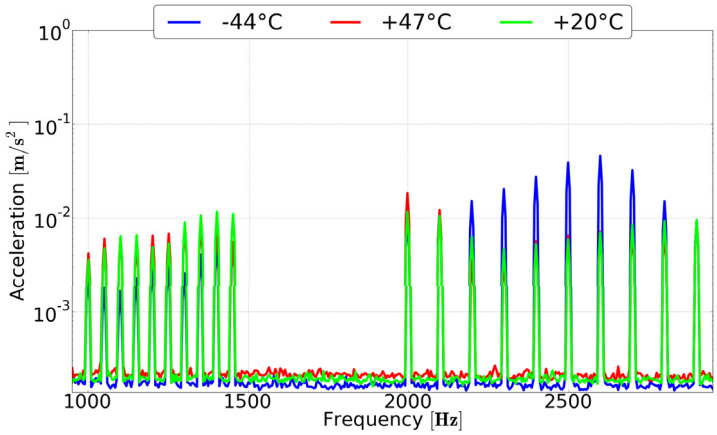

Figure 3.12. Vibration response of the big side of the 12.7 μF capacitor for high frequencies at 150 V from 1000 to 1450 Hz

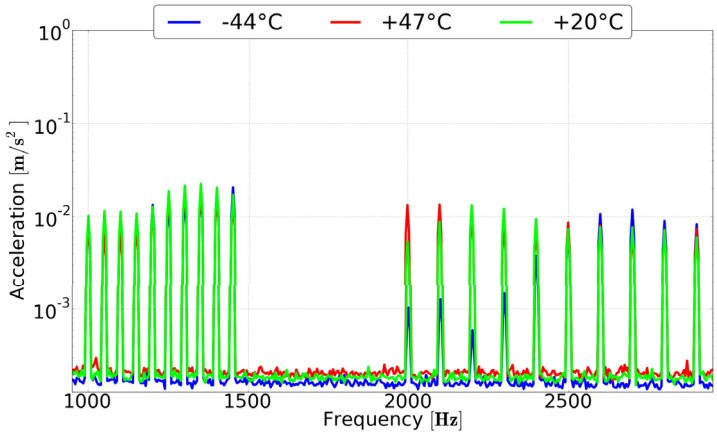

Figure 3.13. Vibration response of the thin side of the 12.7 μF capacitor for high frequencies at 150 V from 1000 to 1450 Hz

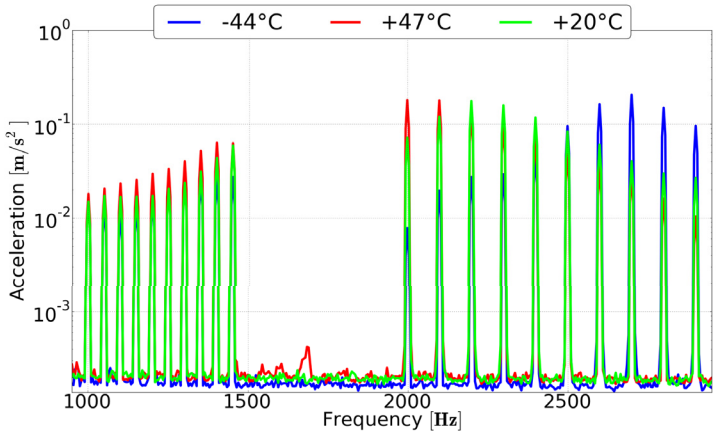

Figure 3.14. Vibration response of the bottom of the 12.7 μF capacitor for high frequencies at 150 V from 1000 to 1450 Hz

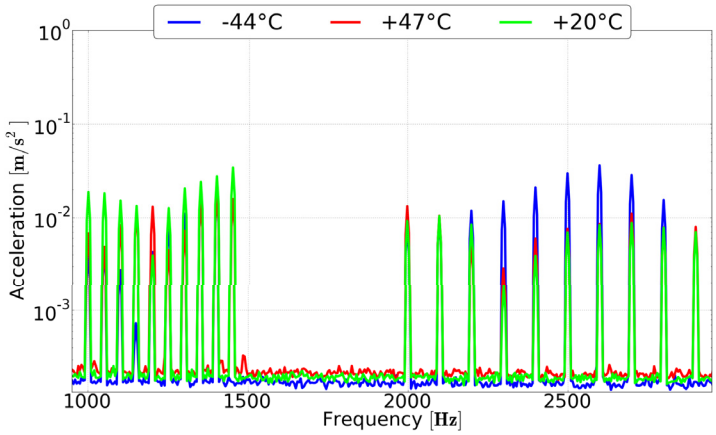

Figure 3.15. Vibration response of the big side of the 38.8 μF capacitor for high frequencies at 80 V from 1000 to 1450 Hz

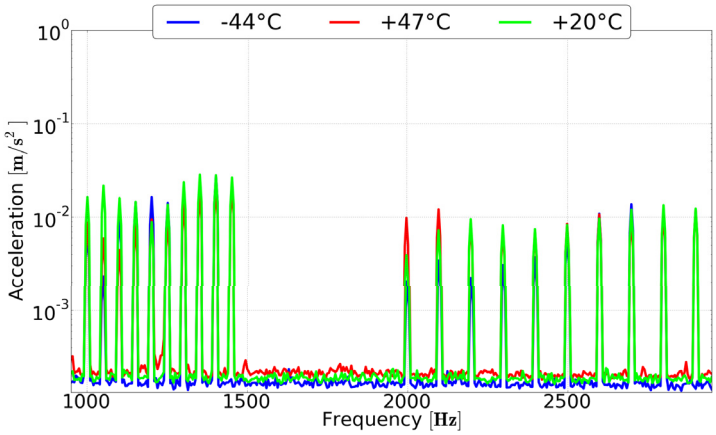

Figure 3.16. Vibration response of the thin side of the 38.8 μF capacitor for high frequencies at 80 V from 1000 to 1450 Hz

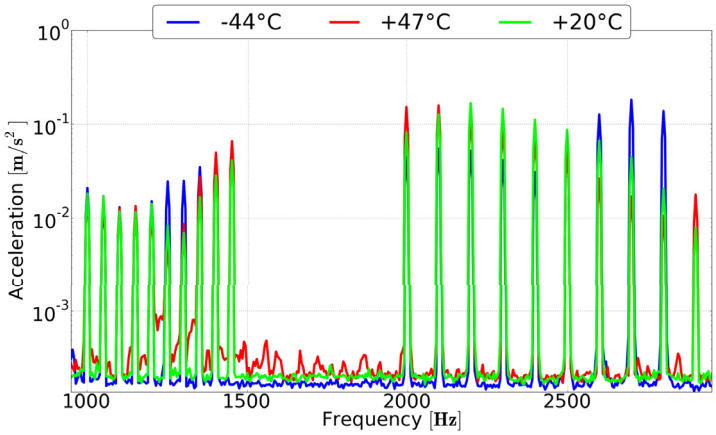

Figure 3.17. Vibration response of the bottom of the 38.8 μF capacitor for high frequencies at 80 V from 1000 to 1450 Hz

Even though the previous figures incorporate all the measurement data available, it might not be always the most easily readable format to analyze it. In order to make it easier to compare the responses at different temperatures, the Figures 3.18, 3.19, 3.20, 3.21, 3.22 and 3.23 show the same results but filter out the values not directly caused by the input voltage.

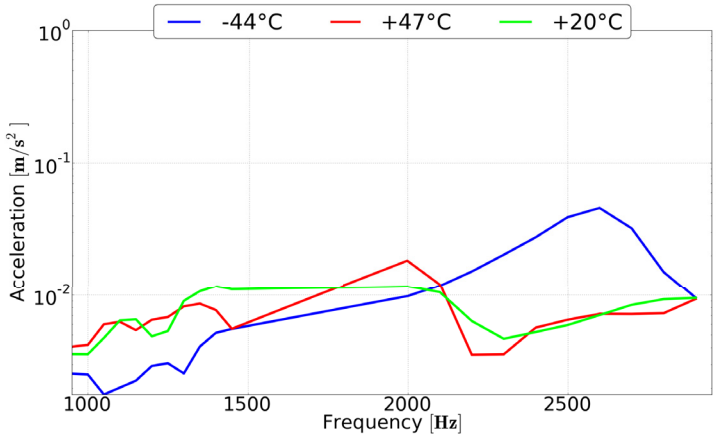

Figure 3.18. Filtered vibration response of the big side of the 12.7 μF capacitor for high frequencies at 150 V from 1000 to 1450 Hz

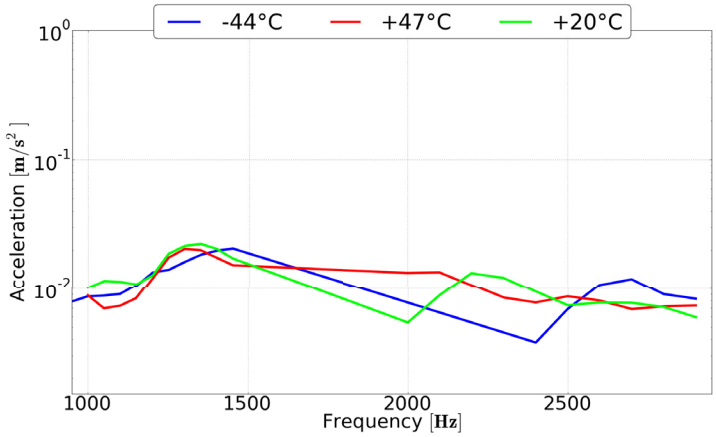

Figure 3.19. Filtered vibration response of the thin side of the 12.7 μF capacitor for high frequencies at 150 V from 1000 to 1450 Hz

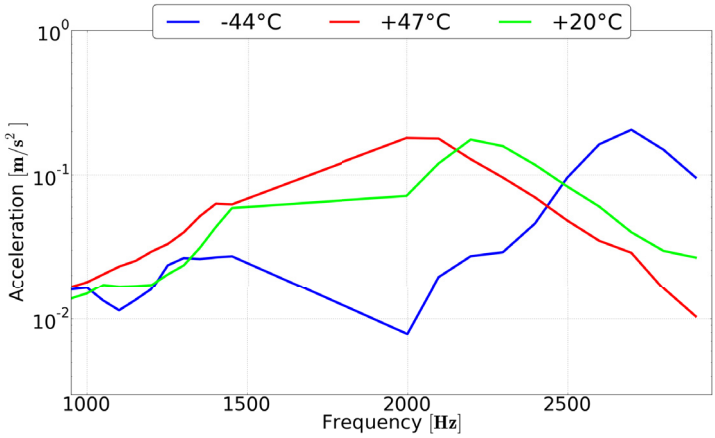

Figure 3.20. Filtered vibration response of the bottom of the 12.7 μF capacitor for high frequencies at 150 V from 1000 to 1450 Hz

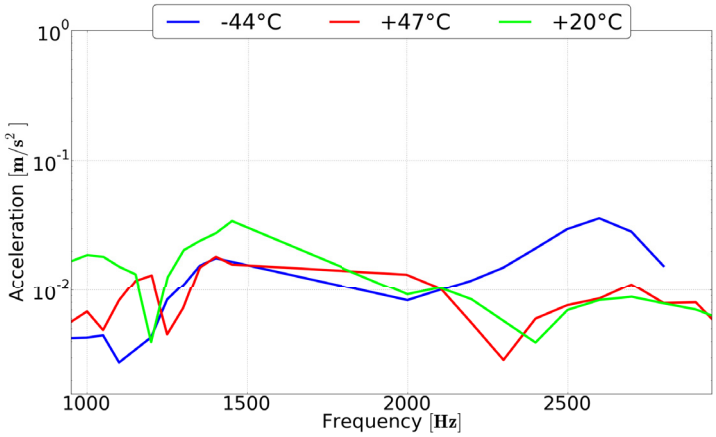

Figure 3.21. Filtered vibration response of the big side of the 38.8 μF capacitor for high frequencies at 80 V from 1000 to 1450 Hz

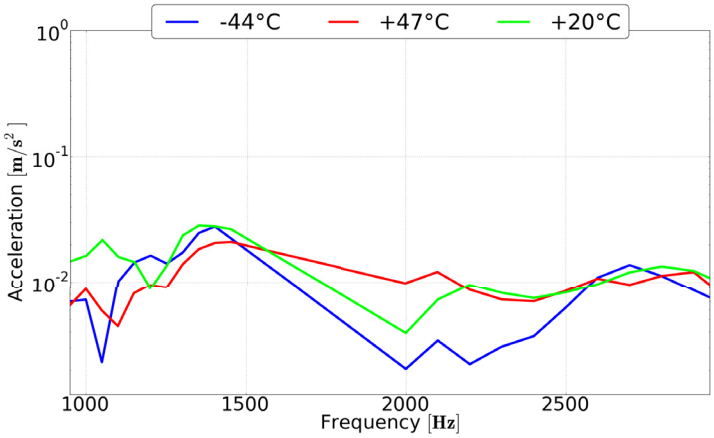

Figure 3.22. Filtered vibration response of the thin side of the 38.8 μF capacitor for high frequencies at 80 V from 1000 to 1450 Hz

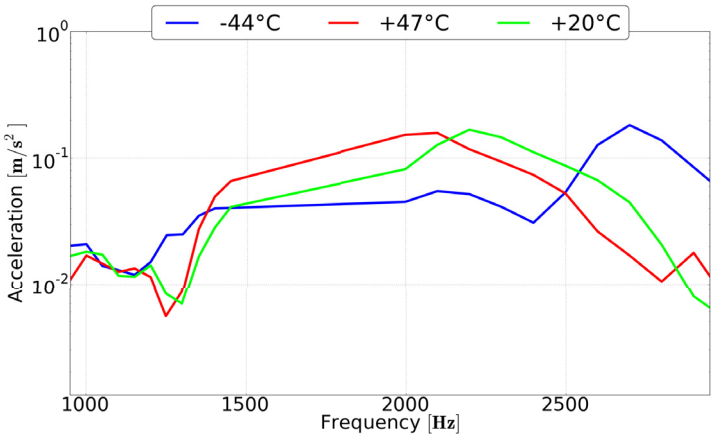

Figure 3.23. Filtered vibration response of the bottom of the 38.8 μF capacitor for high frequencies at 80 V from 1000 to 1450 Hz

3.3 Acoustic response of the capacitor sides

In the acoustic measurements there were two sets of measurements. First of them was related to the directivity of the sound at different frequencies for the two capacitor units. First was 1060 mm tall, 12.7 μF Cfo, and second was 820 mm tall 23.3 μF. In order to visualize which frequencies cause most sound and in which direction, only the frequencies which caused an average sound of at least 3 dB above the background noise were taken into account. This was done to be sure that we don't accidentally claim that there's sound in a direction where there's almost none.

There was one caveat in this approach: We wanted to get the sound pressure's directivity at different frequencies, but we couldn't quite reach the original specifications due to restrictions of the power supply, and thus had to feed less voltage in as mentioned previously in the Section 2.4.3. The input voltages that caused more than 3 dB sound compared to the background noise, as well as the original target voltages are presented in the Table 3.1. The subscript "n" refers to the nominal target voltages, and subscript "r" refers to the real input voltage.

Table 3.1. Nominal and input voltages for Cf and Cp units

Frequency [Hz]	**Cf**$_n$ **[V]**	**Cp**$_n$ **[V]**	**Cf**$_r$ **[V]**	**Cp**$_r$ **[V]**	**Cf**$_r$ **%**	**Cp**$_r$ **%**
270	690	729	469.9	401.5	68.1	55.1
300	490	519	474.4	381.8	96.8	73.6
330	290	328	289.8	327.7	99.9	99.9
360	299	356	299.0	343.4	100.0	96.5

Luckily there's a standard for measuring the noise of transformers [49], which gives us tools to handle this situation. In the standard, an Equation (3.1) can be found that can be used to calculate the reduced power level caused by the reduced current. This equation was then transformed to use voltage instead, as can be seen in the Equation 3.2 and confirmed to be working by a test measurement. The standard limits the use to cases in which the reduced load is minimum 70% of the original load, so since the 270 Hz loads are under this, the results have to be considered experimental on this part.

$$L_{WA,IN} = L_{WA,IT} + 40lg\frac{I_N}{I_T} \tag{3.1}$$

where $L_{WA,IN}$ is loudness (A-weighted sound power) at nominal current, $L_{WA,IT}$ is loudness at current I_T, I_N is the nominal current, and I_T is the current used in the measurement.

$$p_n = p_r + 40lg\frac{U_n}{U_r} \tag{3.2}$$

where p_n is the pressure at nominal voltage, p_r pressure at the reduced voltage, U_n is the nominal voltage, and U_r is the reduced voltage.

Now that we had the sound data, and the equations to make them approximately equal to the real life situations, we could easily calculate the results. The results for the capacitors are presented in the Figure 3.24 for

Cfo unit, and in the Figure 3.25 for the Cp unit. Please note that the figure is symmetrical due to the choices we made when preparing the measurement as mentioned in the Section 2.4.3. In these Figures, 0° corresponds to the side of the insulators and 180° to the bottom side of the capacitor. We notice that based on these Figures the main source of noise seems to be the bottom. Similar observations were made previously in the Section 3.2.

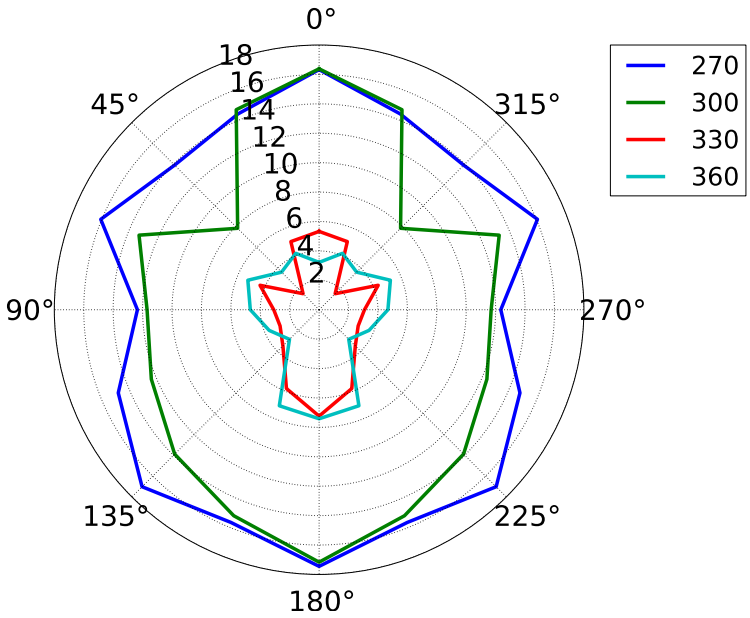

Figure 3.24. Directivity of sound at different frequencies for Cfo unit at 2 m in dB scale

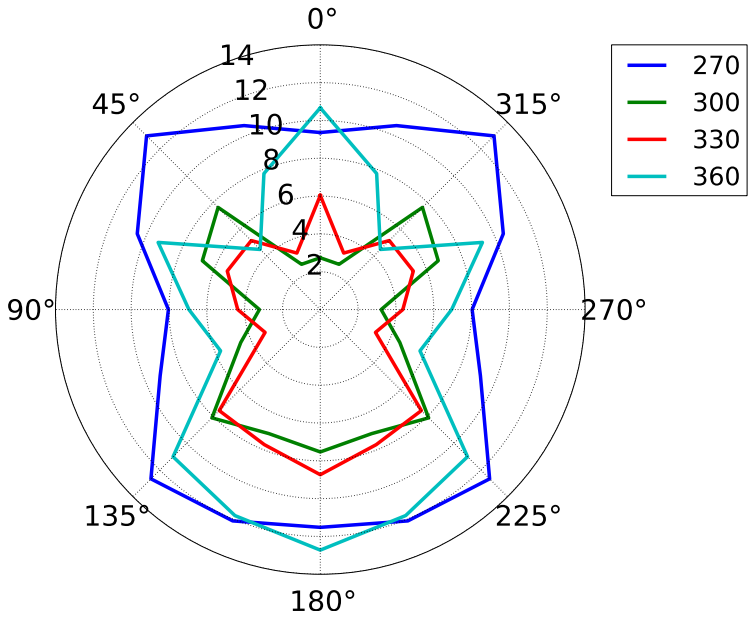

Figure 3.25. Directivity of sound at different frequencies for Cp unit at 2 m in dB scale

Since as mentioned in the Section 2.4.3 the background noise was an issue in the measurements conducted at the Alstom factory, it was necessary to verify that we can distinguish the sound of the capacitor rack from the background noise. In the case of the 125 dB band the background sound pressure was roughly 46 dB, and in the case of the other bands roughly 48 dB. As can be seen from the Figure 3.26, the 125 dB response is roughly 50 dB at the lowest point, and other responses are over 55 dB level. Thus we have 6 dB difference in almost all measuring points, which equals to double the sound pressure. This difference was deemed sufficient, as the standard used for previous measurements [49] required only 3 dB difference in order for the measurements to be counted as valid. The rack is presented here in such a position that at 0° and 180° we face the capacitors' sides, and at 90° and 270° the insulators.

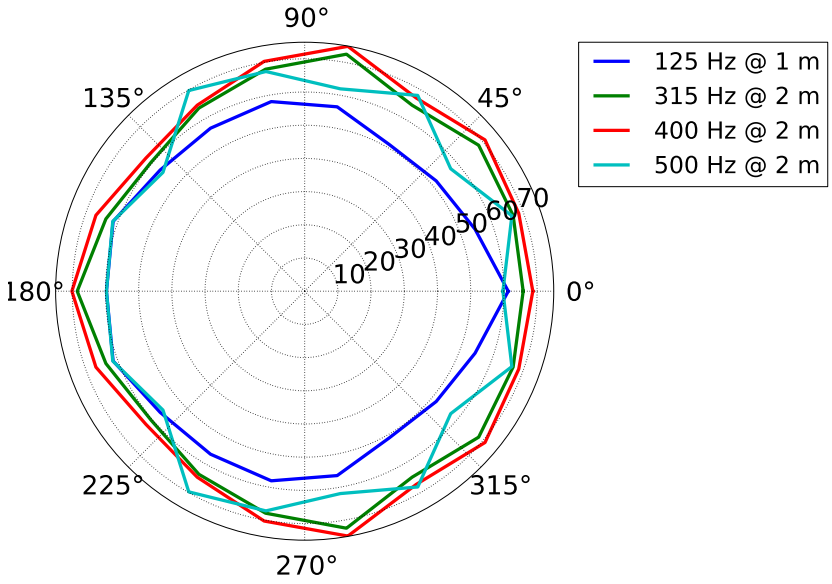

Figure 3.26. Directivity of sound at different frequency bands for rack of six Cp units in dB scale

What was more important than the amplitudes in the previously presented Figures 3.24 and 3.25 was the shape of their contours. Since the values in the Figure 3.26 are much larger, the contour cannot be easily seen. In order to counteract this issue, a second figure was produced where the amplitudes have been damped in order to get the contours to show much more clearly. In the Figure 3.27 the 125 Hz band amplitude is reduced by 50 dB, 315 Hz and 400 Hz bands by 60 dB and finally 500 Hz band is reduced by 55 dB. Now we can easily compare the directivity of different frequency responses.

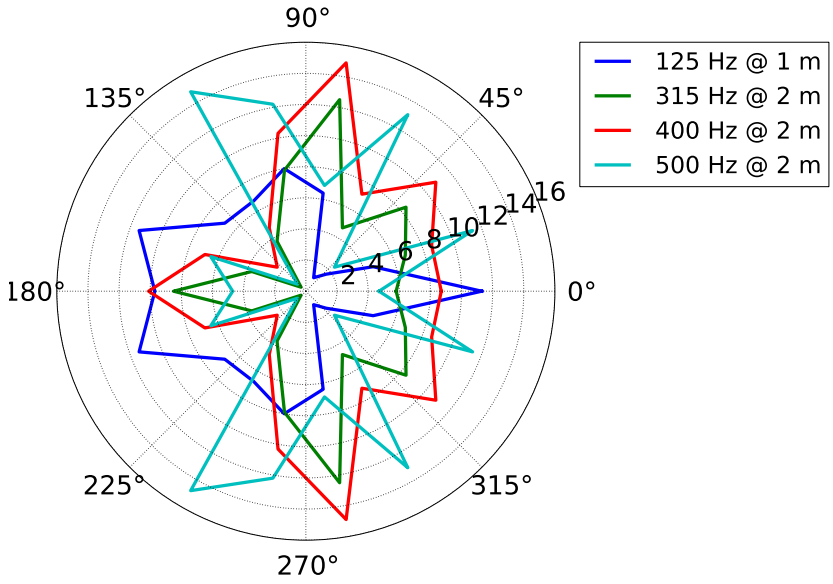

Figure 3.27. Damped directivity of sound at different frequency bands for rack of six Cp units in dB scale

Since the amplitude of both vibration and sound levels is completely related to the level of the inputs, it wasn't easy to compare the two directly. Eventually, since the goal was to compare the shapes of the responses, we decided to scale the values so that the highest point of each group of values would equal to 1.0. This allowed us to see

1. Whether the general shape of the response was the same

2. Whether the highest peak would be at the same point on the figure

3. Whether there would be surprises we didn't account for beforehand

First we get back to the 1040 mm tall, 38.8 μF capacitor, Cfb. In the Figure 3.28 we can see vibration sweep response of the bottom plate in room temperature compared to the sound data measured from 2 cm away from the same point. Both graphs were scaled so that the highest points at 700 Hz are equal to 1.0. We observe that the two graphs match each other almost perfectly, as was excpected due to posited connection of vibration and sound.

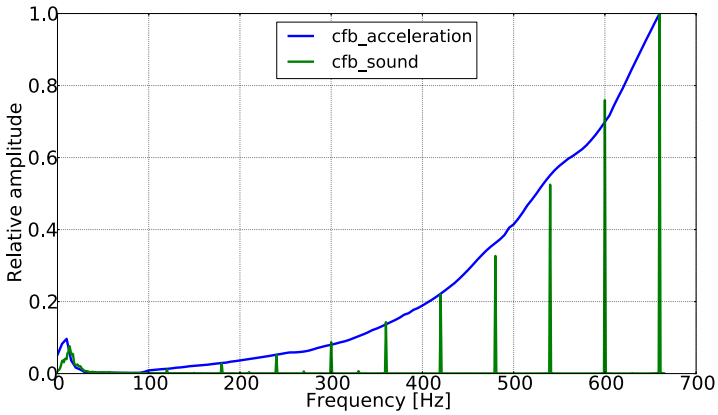

Figure 3.28. Comparison of the relative amplitudes in vibration and sound for Cfb unit at low frequencies

Next we have two comparisons of vibration and sound production responses at high frequency inputs. The inputs were between 1000 to 1450 Hz for both capacitors. The comparison for Cfb can be seen in the Figure 3.29, and for Cfo in the Figure 3.30.

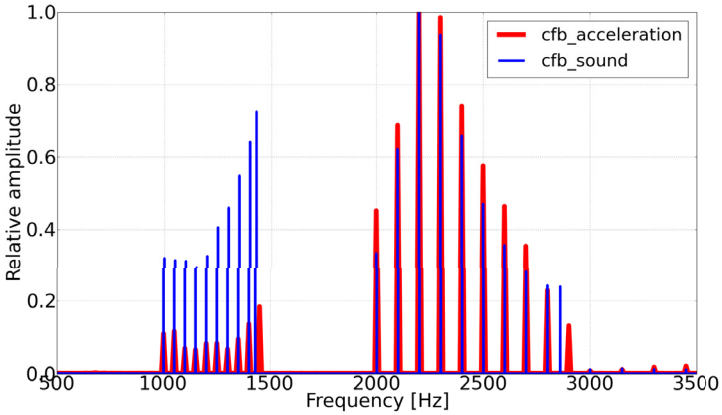

Figure 3.29. Comparison of the relative amplitudes of vibration and sound for Cfb unit at high frequencies

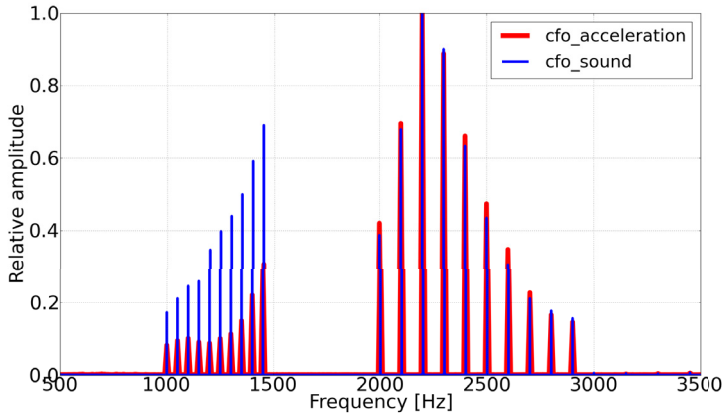

Figure 3.30. Comparison of the relative amplitudes of vibration and sound for Cfo unit at high frequencies

Lastly we wanted to compare whether there's a difference in the relative sound production at 2 cm and 1 m away from the capacitor's bottom measured from the same spot. This comparison was to see whether the distance makes any difference on the sound spectrum of the capacitor. To achieve this all the values were scaled so that the highest peak in each of the curves is scaled to be one. In Figure 3.31 we can see results of this comparison.

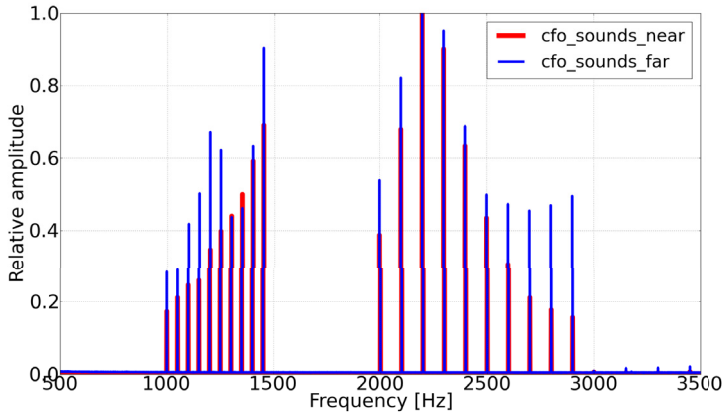

Figure 3.31. Comparison of the relative amplitudes of sound near and far for Cfo unit at high frequencies

As the Figure 3.31 doesn't show the real relations of the amplitudes between the two measurements taken from closer and further away, Figure 3.32 shows just that. In this figure the sound amplitudes obtained from the near are divided by those that are obtained from further away. This

was done so since it was assumed that all the nearer sounds would have higher amplitude than the sounds from the further away.

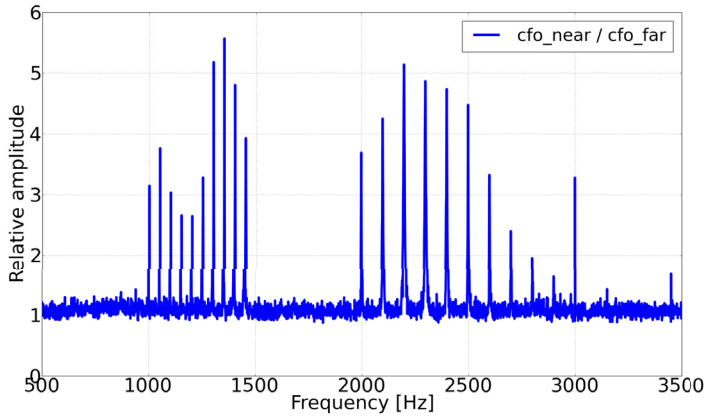

Figure 3.32. The Cfo unit acoustic amplitudes measured from the close divided by the ones measured from far

3.4 Viscosity of the capacitor oil

To explain the variations in the vibration response of the capacitor we decided to measure the viscosity of the capacitor oil in the various temperatures. We hoped that this would help us link the temperature with the reduced movement of the capacitor sides in lower temperatures. The viscosity curve with the respect to the absolute temperature can be seen in the Figure 3.33. The non-continuous point corresponding to roughly 290 K is due to the usage of two different liquids (water and glycerol) to measure the viscosity at different temperature ranges.

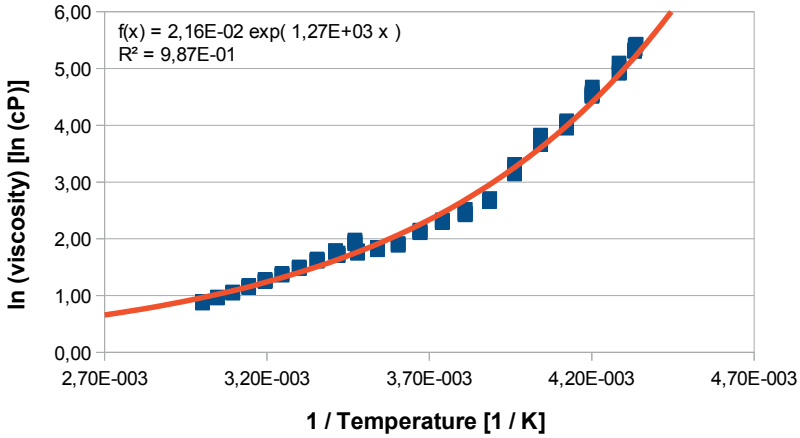

Figure 3.33. Viscosity of the capacitor oil as a function of temperature with a fitted curve

Based on the results showing that the oil's viscosity was not affected by the rate of shear (the RPM of the spindle), we posited that the oil is a Newtonian fluid, and its viscosity is dependent solely on the temperature. This includes an assumption that any other variables we didn't take into consideration have a negligent effect on the viscosity.

To obtain a suitable fit to our experimental data, we made the common[34] assumption that liquid's viscosity follows the Arrhenius equation (Equation 3.3):

$$\eta(T) = \eta_0 e^{E/RT} \tag{3.3}$$

where $\eta(T)$ is the dynamic viscosity at temperature T, η_0 is a coefficient based on the liquid, E is the activation energy, R is the universal gas constant and T is the temperature in Kelvins. This formula can be then rewritten as Equation 3.4:

$$ln\eta(T) = A + B/T \tag{3.4}$$

where $\mu(T)$ is the dynamic viscosity at temperature T, A and B are coefficients based on the liquid, and T is the temperature in Kelvins.

To get the constants for the oil in question, we plotted inversion of temperature $(1/T)$ against the natural logarithm of viscosity $(ln\eta)$, and then used spreadsheet software to find a curve that would best fit the whole range of our measuring data. In the appendix C there's full data of this measurement. The Visc_c means the corrected (by reducing the value by 10%) value of the viscosity.

After getting the constants, we could calculate the viscosity of the capacitor oil at the various temperatures we conducted our vibration measurements at. After getting these values, we tried linking the vibration results with the viscosity data. Since the results for the bottom sides were the most even, we started to work to see if we could explain the differences of specific case of 12.7 μF capacitor bottom case, which can be seen in the Figure 3.8.

We noticed empirically that the vibration seems to follow the square root of viscosity. When we used the square roots of the viscosity as a weighting coefficient for each curve, it yielded very satisfying results as can be seen in the Figures 3.34, 3.35, 3.36, 3.37, 3.38 and 3.39. Even though this finding is mostly empirical and based on this work, there are other empirical findings [36] to be found that posit that the thickness of the oil film is relative to the square root of viscosity.

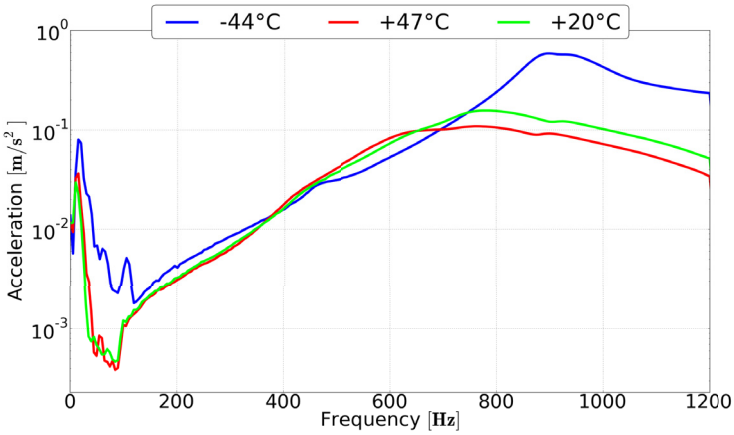

Figure 3.34. Modified vibration response of the bottom of the 12.7 μF capacitor for sweep at 173 V from 50 to 600 Hz

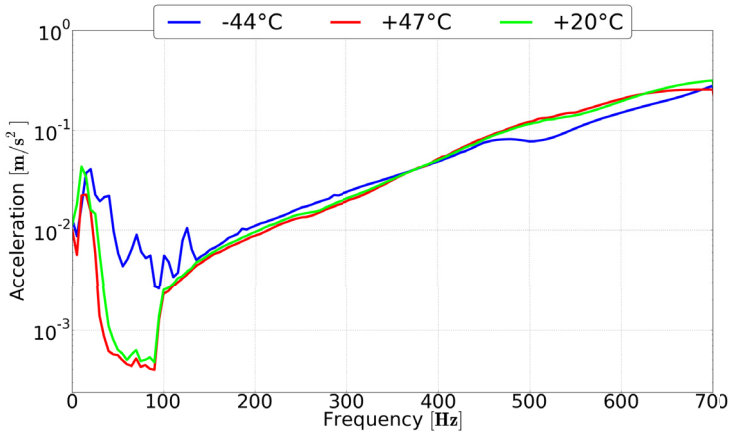

Figure 3.35. Modified vibration response of the bottom of the 38.8 μF capacitor for sweep at 173 V from 50 to 350 Hz

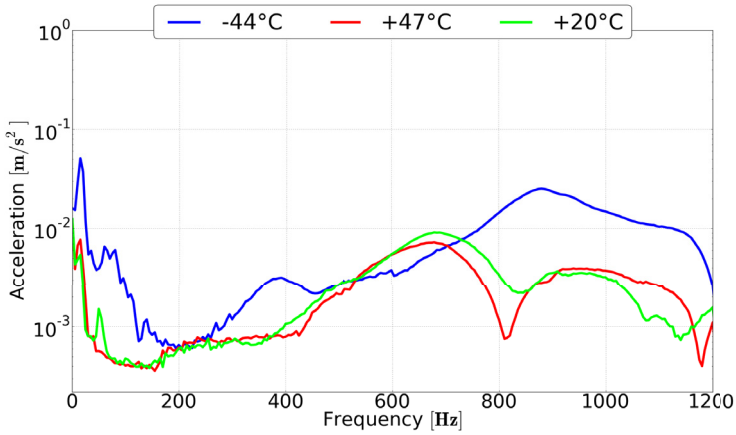

Figure 3.36. Modified vibration response of the thin side of the 12.7 μF capacitor for sweep at 173 V from 50 to 600 Hz

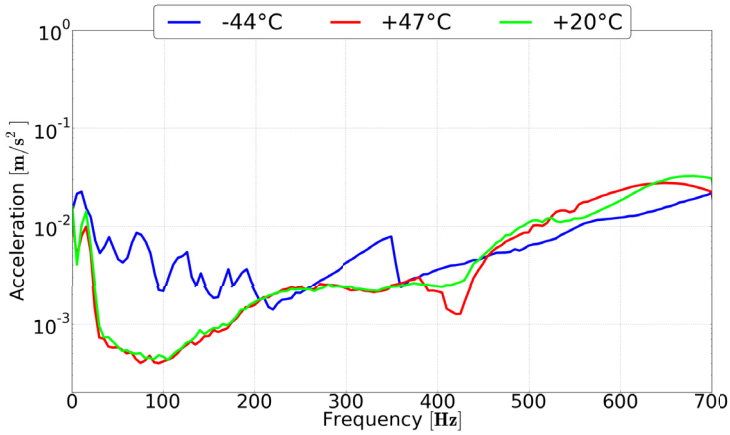

Figure 3.37. Modified vibration response of the thin side of the 38.8 μF capacitor for sweep at 173 V from 50 to 350 Hz

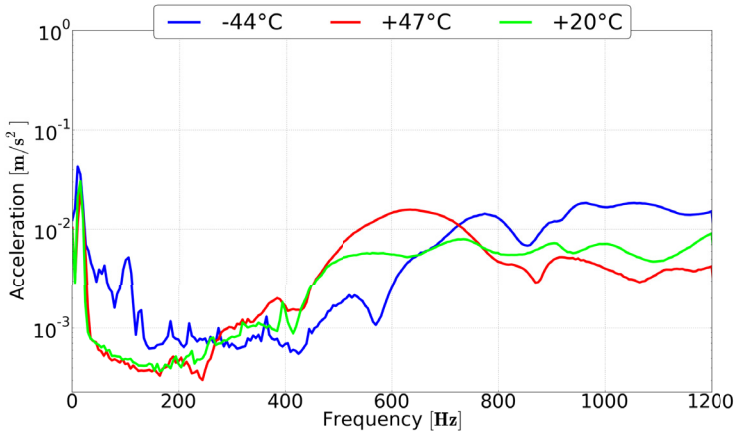

Figure 3.38. Modified vibration response of the big side of the 12.7 μF capacitor for sweep at 173 V from 50 to 600 Hz

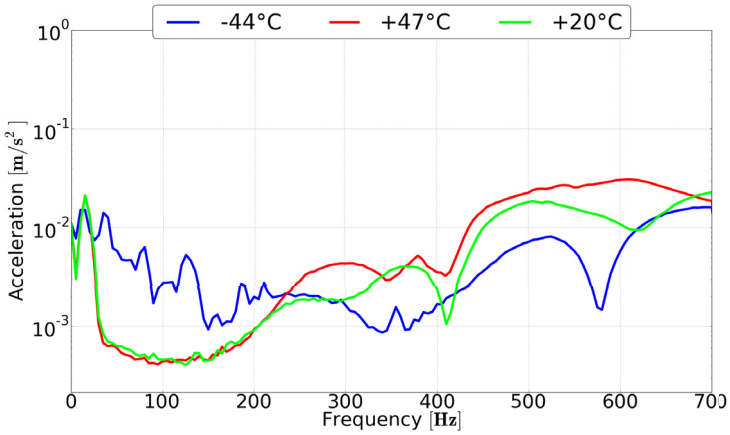

Figure 3.39. Modified vibration response of the big side of the 38.8 μF capacitor for sweep at 173 V from 50 to 350 Hz

3.5 Response of the tube extender used for measuring the reactor noise

First of all let us see what kind of spectrum our input device – a Genelec loudspeaker gives us at the different input levels. This data can be seen from the Figure 3.40.

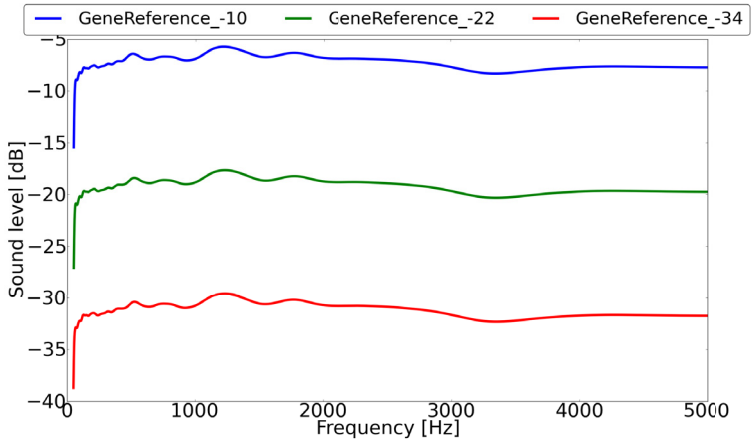

Figure 3.40. The frequency spectrum of the Genelec loudspeaker on different output levels

Then let's move on to compare how the input level changes the output spectrum of the individual tube extenders. Here one sample out of three has been taken, and only the input level has been changed. You can see how the spectra change from the Figures 3.41, 3.42, 3.43 and 3.44.

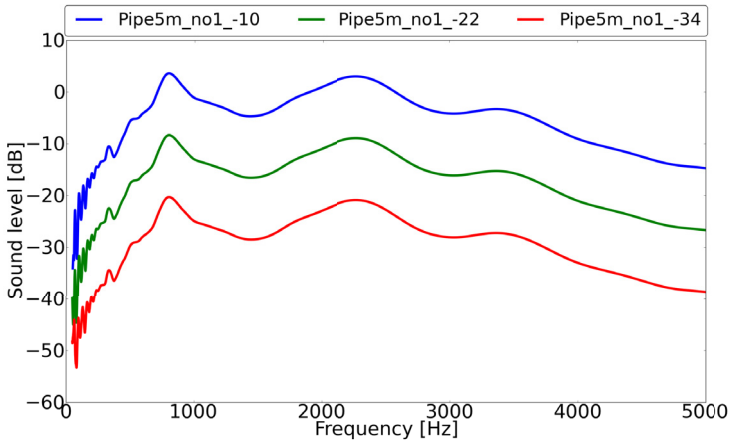

Figure 3.41. The response of one 5 m tube extender at different input levels

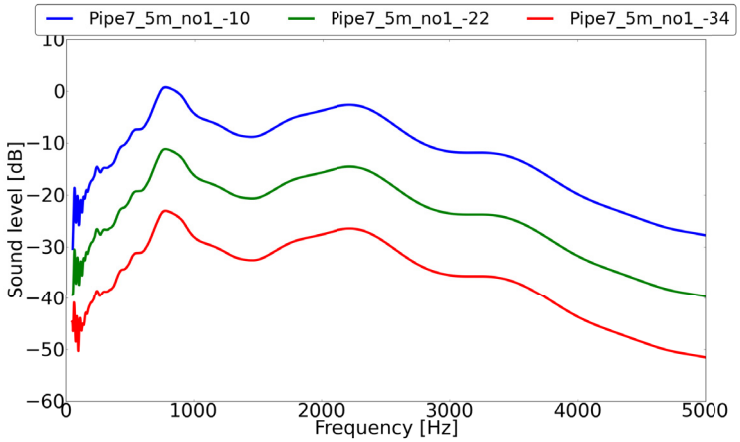

Figure 3.42. The response of one 7.5 m tube extender at different input levels

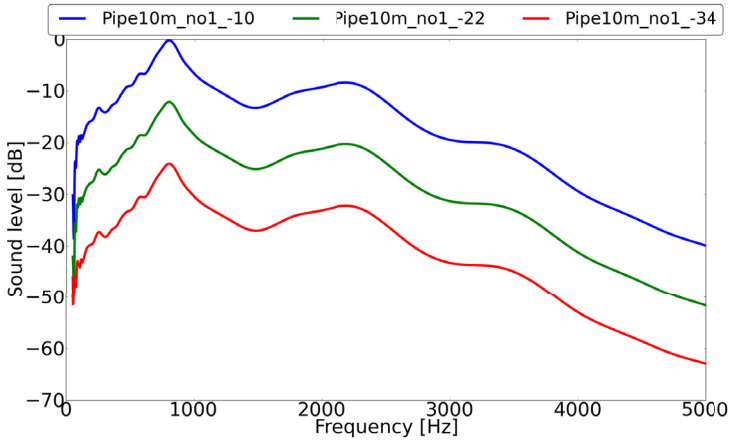

Figure 3.43. The response of one 10 m tube extender at different input levels

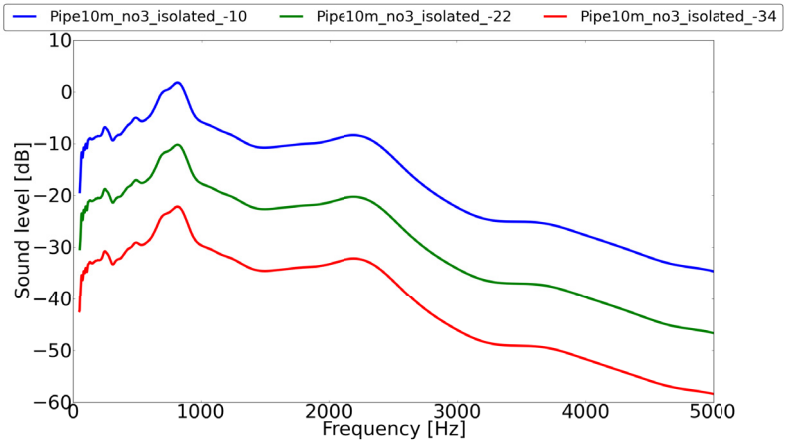

Figure 3.44. The response of 10 m insulated tube extender at different input levels

After seeing how the changes in the input level affect the response, let's compare the tube extenders which have equal length. This way we can see how much the hand-making process affects the outcome. The resulting comparison Figures are 3.45, 3.46, and 3.47.

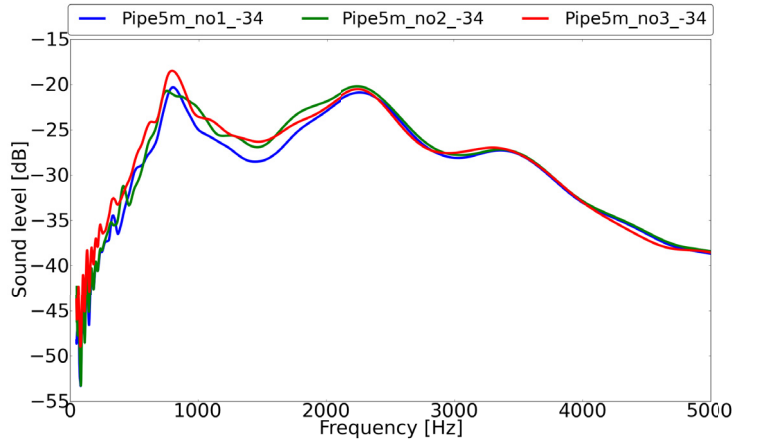

Figure 3.45. The responses of three 5 m tube extenders at -34 dB input level

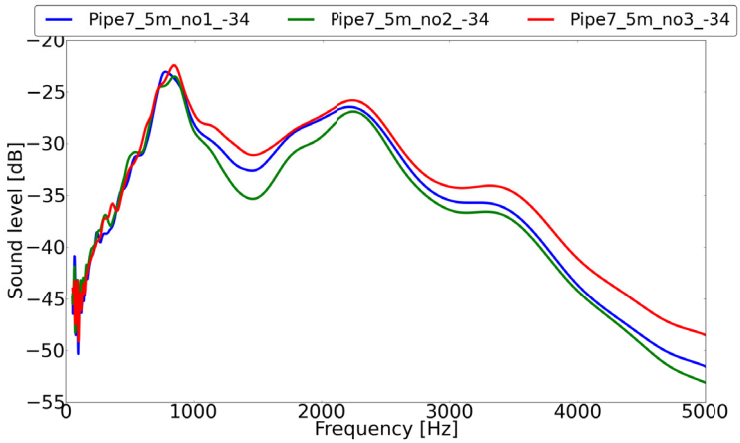

Figure 3.46. The responses of three 7.5 m tube extenders at -34 dB input level

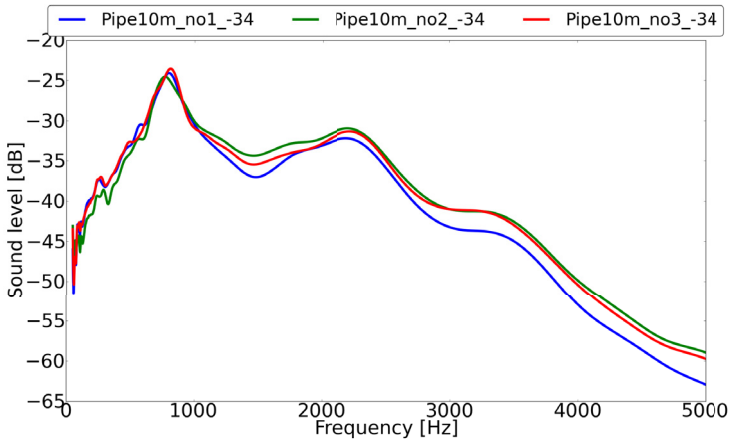

Figure 3.47. The responses of three 10 m tube extenders at -34 dB input level

Finally, let's compare the Genelec input, the 10 m long tube extender's response, and the same 10 m long tube extender's response when it's insulated in Figure 3.48.

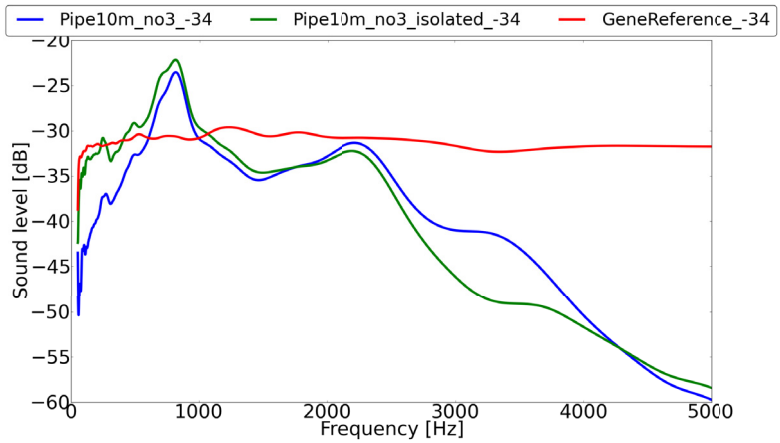

Figure 3.48. Comparison of responses of Genelec, 10 m tube extender, and insulated 10 m tube extender at -34 dB input level

3.6 Reactor noise measurement in the field using the tube extender

The measured background and operating noise spectra can be seen in the Figures 3.49, 3.50, and 3.51. In each of the figures the lighter color is the background noise, and the darker is the operating noise.

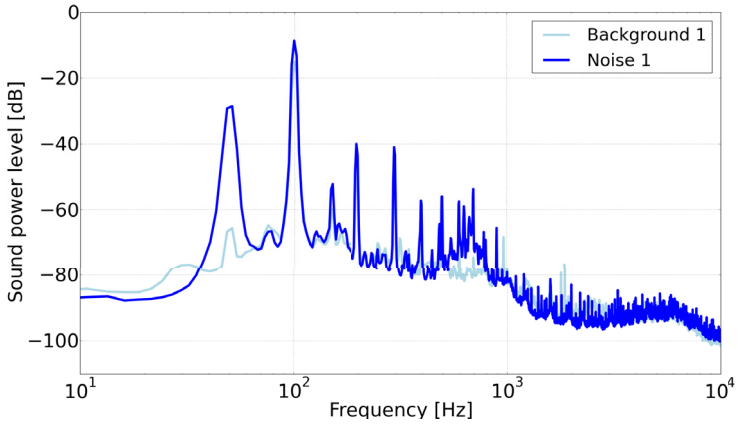

Figure 3.49. Background and operating noise under reactor #1

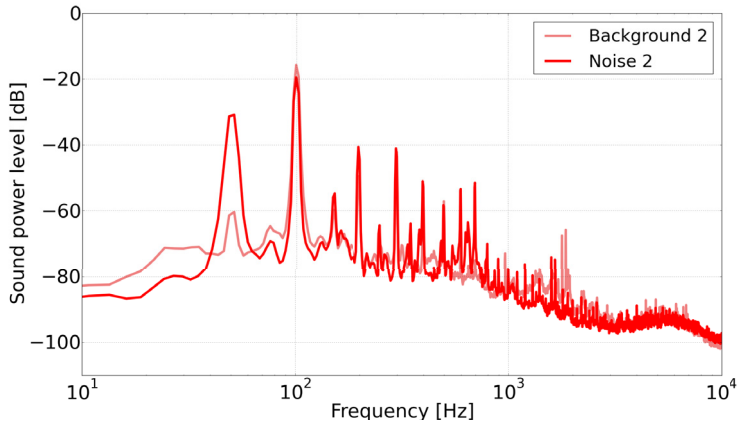

Figure 3.50. Background and operating noise under reactor #2

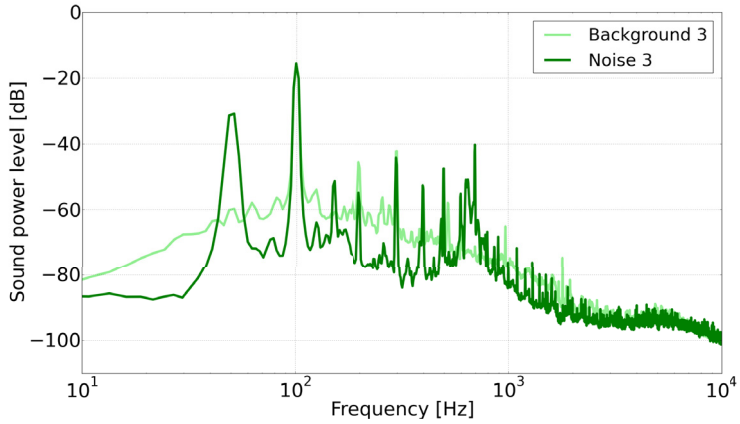

Figure 3.51. Background and operating noise under reactor #3

To easier see what changes when the reactors are turned on, in the Figure 3.52 the difference spectra between the operating and background noise are presented.

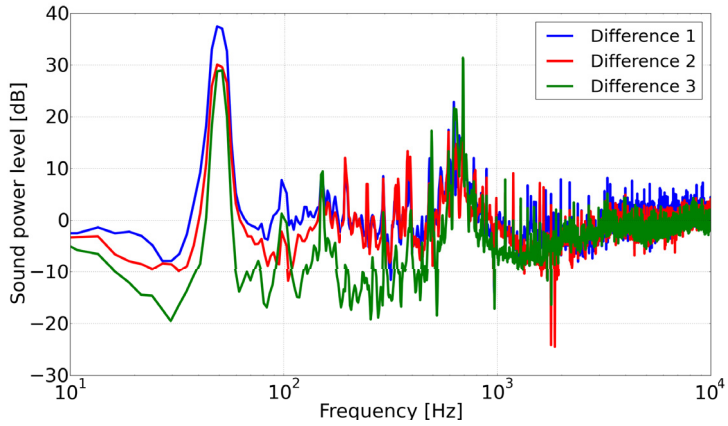

Figure 3.52. Calculated difference spectra between operating and background noise for each reactor

3.7 Reactor noise measurement in controlled environment using the tube extender

Let's first see how the results differ when we compare the background noise to the operating noise. For the case with the tube extenders downwards, please see Figure 3.53, and for the tube extenders upwards Figure 3.54. In both cases we have three measuring points underneath the reactor. The extra lines are added at 6 dB for amplitude, and 100 Hz for frequency. 6 dB raise in acoustic power means quadrupling the power, and it seemed to be a good indication of human perceivable noise level based on these measurements. The 100 Hz is the natural noise frequency for a reactor that operates in 50 Hz network.

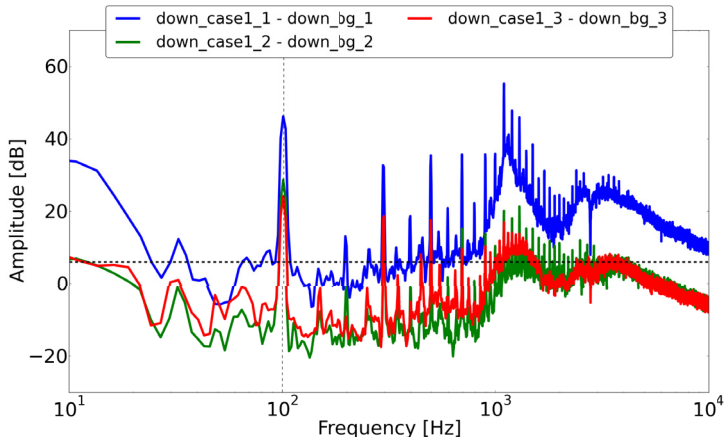

Figure 3.53. The difference in the sound spectra between the normal operating and the background noise with tube extenders downwards

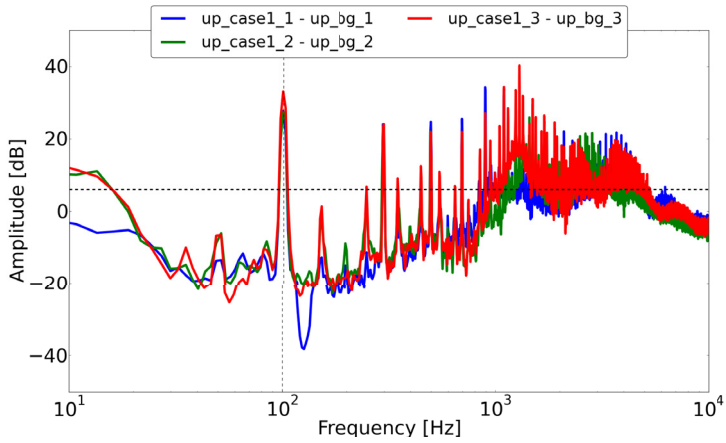

Figure 3.54. The difference in the sound spectra between the normal operating and the background noise with tube extenders upwards

Then we have the case of tube extenders installed downwards, and we have a loose isolator. In the Figure 3.55 we see the differences between the fault case noise, and normal operating noise as seen from two measuring points underneath the reactor.

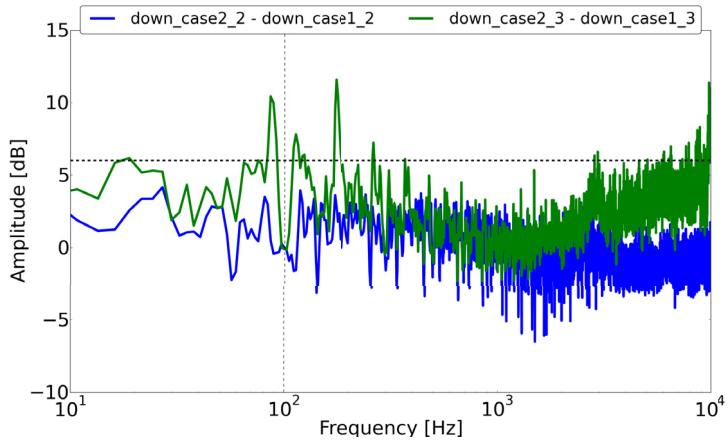

Figure 3.55. The difference in the sound spectra between the loose isolator case and normal operating noise with tube extenders downwards

In the Figure 3.56 we see how the sound spectrum changes after each change we make to the reactor. The red spectrum represents the change that was caused in the spectrum when we went from the normal operating noise to the case with loose bar. The green spectrum shows us how the spectrum changes when we go from the loose bar case to loose bar and loose middle pipe. Finally the blue spectrum represents the change in the spectrum when moving from the loose bar and middle pipe to the case where we have the previously mentioned faults, and then loose the lifting lug. Since the loose lifting lug made sound that could be heard, Figure 3.57 shows the change of spectrum between the loose lifting lug case, and normal operating noise for each of the three measuring points. In these measurements the tube extenders were in upwards position.

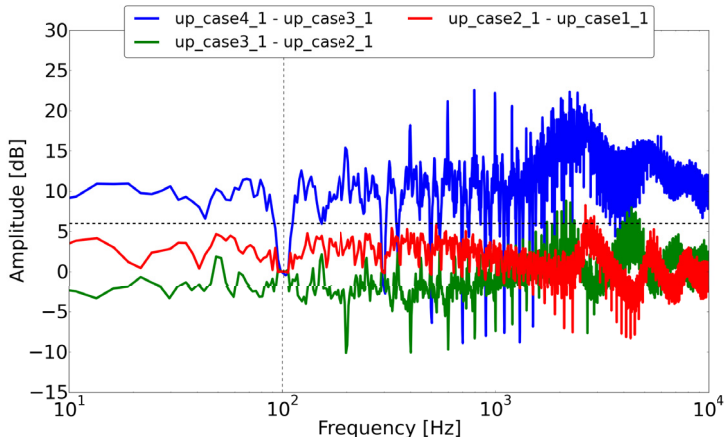

Figure 3.56. The change in the sound spectra with incremental faults up to loose lifting lug case with tube extenders upwards

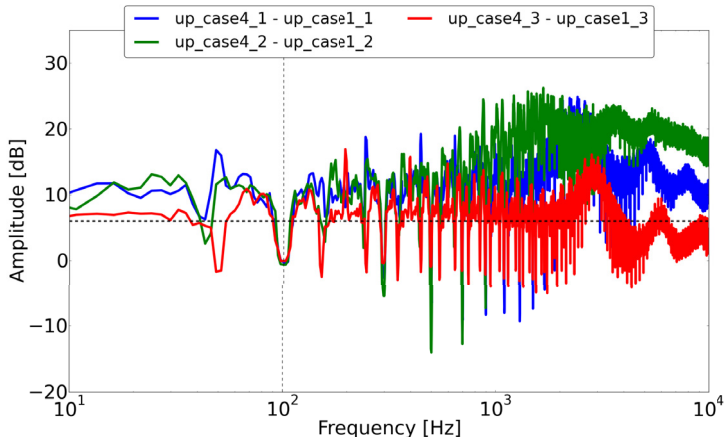

Figure 3.57. The difference in the sound spectra between the loose lifting lug case, and the normal operating noise with tube extenders upwards

Similarly as in the previous case, in the Figure 3.58 we can see how the spectrum changes when we go from the normal operating sound to first fault (green spectrum) and then from first fault to second fault (blue spectrum). Here the first fault is loosening a bolt of the input cable, and the second one is removing the cable ties and adding extra bolts near the input cables. Since in this case also the resulting noise from the extra bolt case could be heard by nearby humans, we decided to further study this case. Thus the difference in the spectra between the extra bolt case and normal operating noise in all three measuring points can be seen in the Figure 3.58. In this measurement the tube extenders were upwards as well.

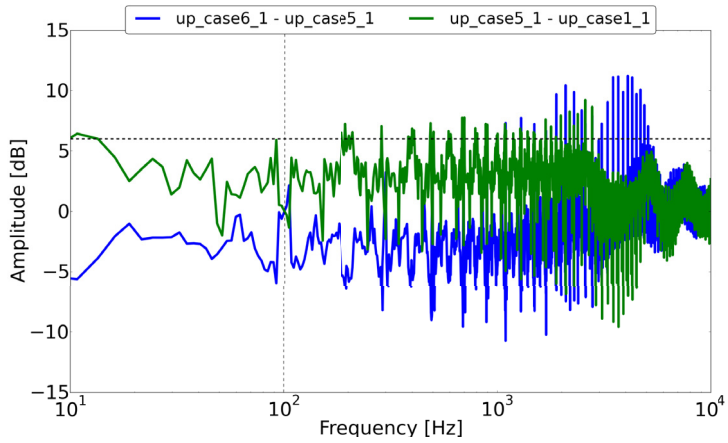

Figure 3.58. The change in the sound spectra with incremental faults up to loose extra bolts case with tube extenders upwards

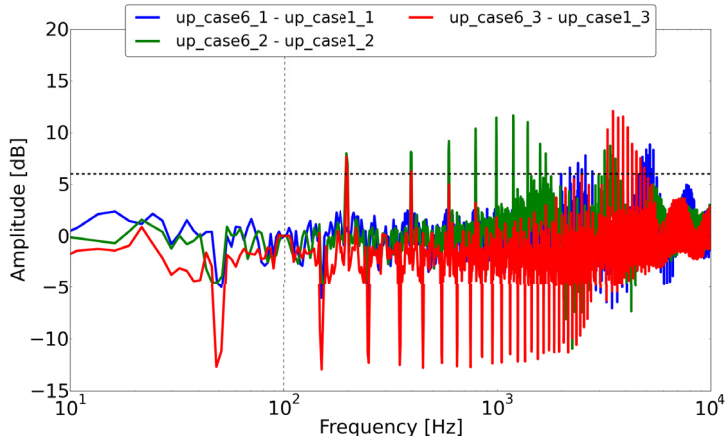

Figure 3.59. The difference in the sound spectra between the loose extra bolts case, and the normal operating noise with tube extenders upwards

4. Conclusions

4.1 DC compression of air filled capacitor element

To test the first hypothesis that the element can be divided into four symmetrical parts, the first set of measurements explained in the Section 2.4.1, and reported in Section 3.1 were carried out. From the Figure 3.1 we can see that there's a connection between the amount of compression, and the Pythagorean distance from the origin. This connection can be also seen from the high correlation (-0.77) between the two variables, and it's strong enough to eliminate the doubt cast by the relatively high spread between the singular measured points in the figures. From this we can deduce that the compression depends on the distance from the origin. This leads us to the our hypothesis in which we claimed that we can determine the compression for the whole object based on the measurements done in just one quarter of the element.

In the Figures 3.2, and 3.3 we can see similar spread as in the previous Figure 3.1. We can also see that we can as easily plot a linear estimate through the points due to high correlation as previously. When we combine these linear estimates together in Figure 3.4, we can see that the slope of the linear estimate is the steeper the higher the voltage applied is. This can be explained by assuming different Young's modulus for different parts of the element, which causes the softer parts of the element to bend more in proportion to the harder ones. In the Figure 3.4 it can also be seen that the amplitude change when moving from 2.6 kV level to 3.2 kV level is larger than when moving from 2.0 kV level to 2.6 kV level. This can be explained by Equation 2.10 which states that the force caused by the voltage is relative to the square of the voltage. Thus we see that the measurements prove this non-linearity.

In order to explain why the capacitor element's compression is smaller on the edges than in the middle we present here Figure 4.1. As we can see, the forces from the sides make the edges go up slightly, which changes the shape of the element. Then when the forces from the top and below (not picture to preserve the clarity of the figure) push the whole element equally, the middle part is being compressed comparatively more than the edges. The ends of the long sides can be explained by the fact that those ends have been soldered together, and thus are more stiff than the other parts of the capacitor element.

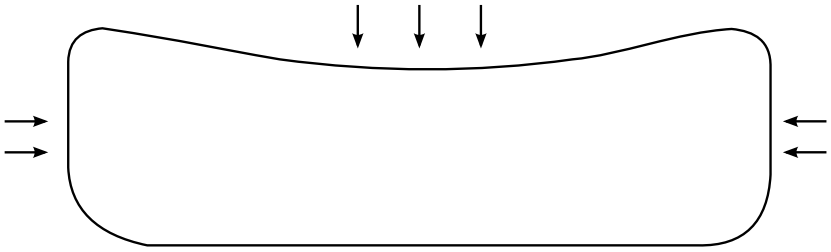

Figure 4.1. Shape of the capacitor element when subjected to voltage with forces shown.

4.2 Vibration response of the capacitor sides

When we want to compare the displacement response in the Figure 3.5 with theory, we first have to calculate the theoretical displacement using the Equation 2.14 shown in the Section 2.2. As mentioned in the Section 3.2, the capacitor unit has four elements in series, and thus we need to change the voltage to quarter of the 173 V used in our measurement. The equation tells us that the compression of a single element is roughly 1.14 $\times 10^{-10} m$ or 0.114 nm. When we take into account that the capacitor has total of 56 elements inside, the total compression equals roughly 6.41 nm Our Figure 3.5 shows displacement of 4-12 nm, so it's right were we'd supposed it would be. The differences can be mostly explained to be caused due to variation caused by temperature of the capacitor, frequency of the input, and the film/oil interaction shown in the Section 2.2.

Based on the simulation results that were discussed in the Section 2.5.2 it was expected that the vibration response of the capacitor sides would be rather flat with few spikes where the resonances were. If we compare this hypothesis to the results in Figures 3.6, 3.7, 3.8, 3.9, 3.10, and 3.11, we see that the only trend in them is that acceleration generally seems to increase as a function of frequency. There are no tall spikes in the middle

of flat plains as could be hypothesizes based on the Figures 2.50 and 2.51.

Since our other hypothesis was that the capacitor oil's viscosity changes the amplitude of vibration of the capacitor, it should be noted that in all six sweep figures the warmest capacitor has overall largest amplitude of vibrations and the coldest one has the lowest. At least until the around 700 Hz frequency, after which everything changes into more chaotic, and less predictable. The current hypotheses of why this happens are the changes in the viscosity of the oil due to change in the temperature, and the effect of the capacitor's physical size on the vibrations.

It should be also noted that the increase in temperature and hence in vibrations is *not* caused by the load current warming up the capacitor. The load current was very small compared to the rated current, and even at the rated current the capacitor doesn't warm up more than 10°C. In addition, this hypothesis was tested false with one of the sweeps by running the sweep downwards frequency wise after the primary measurement.

The sweep responses of the bottom plates (Figures 3.8 and 3.11) are both very similar up to the 700 Hz level. In the two bottom plate responses, we can see that there is little to no difference in the response between the two different capacitor positions at +20°C. The increasing amplitude level with steady voltage might have something in common with the increasing current due to the increasing frequency. This result might require some changes in the Equation 2.10 in the future.

When comparing the bottom sweep results with the thin side sweep results (Figures 3.7 and 3.10) we can see that the responses aren't as easily comprehensible. In the 12.7 μF case we see that there are two peaks near the 400 Hz level at +20°C level, but only in the laying position. We also see dip at around 800 Hz and 1150 Hz levels in all but the coldest temperature. These might be antiresonances, but they aren't very low compared to the overall amplitude levels. For the 38.8 μF capacitor, we have small dip at the 400 Hz for all temperatures, and another one at 600 Hz for +20°C only in the laying position. The cold temperature response has an expected drop at the 350 Hz, after which it seems to continue upwards as linearly as it did at 200-350 Hz before the drop.

The big side sweep results differ wildly between the two capacitors as can be seen from the Figures 3.6 and 3.9. Whereas 12.7 μF capacitor's +20°C responses are almost identical, the 38.8 μF capacitor's responses vary. In addition to this, the 12.7 μF capacitor doesn't seem to have dips outside of the 600 Hz one in the cold temperature, but the 38.8 μF one has

one at 400 Hz (standing room temperature), 500 Hz (laying room temperature) and 600 Hz (cold temperature).

Summarizing the sweep results it seems that the hypothesized spikes in the amplitudes are nowhere to be found, temperature seems to have direct effect on the amplitudes, but so does the position in the case of the thin and big sides. Since the position does matter, and the spikes are absent, the assumption that the capacitors' sides can be approximated by clamped plates cannot be fully correct.

The other major obervation was that the bottom plate vibrates roughly ten times as much as the other sides. Thus we can safely assume that it is the most important constituent in the noise produced by the capacitor. Accordingly, we can assume that changing the construction of the capacitor bottom will have the biggest effect on the noise produced by the capacitor.

Moving on to the high frequency results, we see that the same axioms we saw hold in the sweep results do not apply any more. No longer can we see that the temperature has direct result on the amplitudes. Also, the response isn't just the double of the input frequency. Now the capacitors also respond with the same frequency we excite them with. This said there's no clear logic between the bottom, thin, and big side results of one capacitor. There is a sliver of hope though, as if we juxtapose the capacitors' individual sides, we see that Figures 3.12 and 3.15, 3.13 and 3.16, and finally 3.14 and 3.17 are very similar. This is a good sign, as we can assume that whilst the high frequency response is much more complicated than the low frequency one, it's not completely random.

4.3 Acoustic response of the capacitor sides

With the directivity acoustic response measurement we aimed to study whether we could get any link between the capacitor's directivity and the input frequency. If we start our analysis with Figure 3.24, we clearly see, that even by comparing the two lowest frequencies (270 and 300 Hz), the directivity figure is completely different. Whereas at 0° (the bushing's side) and 180° (the bottom) the amplitude is almost identical, at 67.5°, 135° and especially at 45° the amplitudes are completely different. The situation gets even more complicated if we compare the Figures 3.24 and 3.25. At 270 Hz, even though the capacitors' bushings and bottoms are identical, and the input frequency is the same, the directivity pattern is completely different. Whereas for Cfo unit the directivity figure is roughly

round, it's roughly square for Cp. The situation is similar for other frequencies, and few similarities can be seen between the two capacitors' figures.

In the rack's case we can see that it doesn't produce the same sound from its both sides. The most probable reason for this would probably be that as per Figure 2.24, the capacitors weren't bolted symmetrically to the rack. As we compare the different contours with each other, we see that 315 Hz and 400 Hz contours match very closely shape wise. Since they're both measuring the same sound, this is expected and welcome result. As previously in the case of single capacitors, we also notice that the other bands have little in common with each other. This further suggests that the directivity of the noise produced by the capacitors is a subject in need of further research. It is worth noting that these measurements are similar to the ones conducted by Smede et al.[88], but are more detailed.

When comparing the relative amplitudes of sound and vibration in the Figure 3.28, we see that the sweep matches the individual spikes from the sound almost perfectly. As this close (2 cm) to the bottom of the capacitor, the sound wave shouldn't be a plane wave yet at this low frequencies, thus this result is expected. When we move to higher frequencies as can be seen in the Figures 3.29 and 3.30, we see that response of the frequencies that are double of the input frequencies still match with acceleration, but the ones that are equal to the input frequencies do not match. As we move further away from the bottom (from 2 cm to 1 m) in the Figure 3.31, we see that the two figures now little in common. This is because as we move further from the target, the pressure waves caused by the vibrations in individual spots mix up, and thus are much different than if we'd listen to just one spot as we did when the microphone was in the close position.

4.4 Viscosity of the capacitor oil

To link the temperature to the vibration we had to find out how the viscosity of the capacitor oil changes in the respect to the temperature. After few days of measuring, we ended up with the curve seen in the Figure 3.33. As can be seen, the lowest temperatures do not fit the measuring points ideally, but overall it's a good fit with 98.7% correlation. There's a non-continuous point at around 290K due to the fact we had to use both water and glycerol in order to measure the full range of temperatures.

After some experimentation with how to possibly use the viscosity to

explain the changes in vibrations, we came up with the use of multiplying the amplitudes by the square root of the viscosity ($\sqrt{viscosity}$). This method is in use in the field of tribology, where it is known that the thickness of the oil film is relative to the square root of viscosity. The multiplied results for the bottom side can be seen in the Figures 3.34 and 3.35. As one can see, up to the 700 Hz the modified vibration responses are almost identical for each temperature. Moving on to the thin sides in the Figures 3.36 and 3.37, we can see that while there's some relative increase in the 350 Hz area in the coldest response, otherwise the responses are again very similar in the under 700 Hz range. Unfortunately since this technique is very simple, it cannot explain the complicated curve shapes of the big sides. Nevertheless, as can be seen in the Figures 3.38 and 3.39, the results aren't worse than the original unmodified responses, although not as good as the bottom and thin side ones.

4.5 Response of the tube extender used for measuring the reactor noise

At the start of the measurement we had to define a baseline for comparison of the responses of the tube extenders. This was acquired by measuring the response of the Genelec loudspeaker directly as it was the source of sound in our measurements. As we can see in the Figure 3.40, the response of the loudspeaker is very flat over the whole frequency range at each input level. This makes the later comparisons very easy, as any swings in the amplitude are caused by the response of the tube extender itself.

Next we wanted to examine whether the response spectra of the tube extenders would change only amplitude wise when the input amplitude would change, or would the input amplitude affect also the spectrum. As can be seen in the Figures 3.41, 3.42, 3.43 and 3.44, each tube extender is completely linear over the whole measuring frequency range. Thus the changes in the input amplitude do not change the output spectrum. This is a very good result, as this means we do not have to be concerned about what levels of input we measure using this tube extender.

Since the tube extenders were hand-made, we wanted to also measure how big of a difference the hand-making process causes on the responses of the tube extenders. We have three pieces of each tube extender length, and we measured their response at -34 dB and then compared them against

each other. As can be seen in the Figures 3.45, 3.46 and 3.47, the response curves are very similar. There are some small differences in amplitudes, especially in 7.5 m tube extenders, but the general shape is still intact, and thus each of the tube extenders should be acceptable to use in normal measurements. That said, the hand-made nature of the tube extenders did not have excessive negative effect on their response.

Finally in the Figure 3.48 we see how the 10 m tube extender compares to its insulated variation and the Genelec loudspeaker. The biggest difference is in the low frequency band under 500 Hz, where the insulated tube extender almost matches the Genelec loudspeaker's response. Unfortunately here the uninsulated tube extender's response drops sharply. When we move to higher frequencies, both tube extenders have very similar response, and match the Genelec's response fairly closely up to around 2300 Hz. After this the tube extender's response drops almost linearly as a function of frequency. It should be also noted, that near the 1000 Hz level the tube extender *amplifies* the input instead of dampening it. The response of the tube extenders is very good for the measurement of the reactors, since the effective bandwidth is at its best where the human ears are also the most sensitive.

4.6 Reactor noise measurement in the field using the tube extender

The Figures 3.49, 3.50 and 3.51 we can see the spectra of sound underneath the three reactors when they're turned off (background noise) and on (normal operating noise). The most interesting points in each spectrum are 50 Hz, 100 Hz, and the multiples of these frequencies. 100 Hz should be the natural sound frequency of a reactor that is fed with 50 Hz, and it's the most prominent peak in each of the three figures. What should be noted though that the peak is almost identical in both background and operating noise spectra. This is due to the fact that these measurements were conducted at a power plant, where the surroundings were full of active power system components. All these components produce sound, and since mechanical noise is generally produced at double of the input frequency, the general noise frequency is 100 Hz. The 50 Hz component seem to rise in each figure when the reactors are turned on. This brings upon again, as we saw in Section 4.2, a need to study more the situations in which the components of the power system respond with the same frequency they're excited with instead of double the frequency. In addition to

these frequencies we can observe a plethora of resonance frequencies over the whole measuring range. As the frequency increases, the overall level of response decreases, which agrees with the response measurements in Section 4.5 according to which the response of the tube extender drops as the frequency increases.

For easier comparison of the background and actual operating noise please see Figure 3.52. Here we can see clearly that the 50 Hz component rises when the reactors are turned on. We can also see that the 100 Hz component's change is pretty close to zero due to reasons explained previously. What we can see here the best is that the various resonance frequencies are quite different in different reactors. Also, we see very clearly that as the frequency increases, the difference spectra converge towards zero further proving the nature of the tube extenders' response.

4.7 Reactor noise measurement in controlled environment using the tube extender

When we did the controlled measurements, we wanted to see what kind of difference would it make if we'd have the tube extenders downwards instead of the previously used upwards. In the Figure 3.53 we see the spectra of how the operating noise spectra differ from the background noise spectra, and in Figure 3.54 we see the same figure based on the data when the tube extenders were upwards. In both figures we see that the 100 Hz component clearly stands out as expected, since the measuring location didn't have any other power systems components powered nearby. We also see, that when the tube extenders were upwards, there's a slight increase in the 50 Hz component that is not seen in the case of downwards tube extenders. In addition to these two we once again see a wide range of resonance frequencies. It should be noted that some of these frequencies seem to have a higher amplitude than the 100 Hz component. It might be true or it might be related to the fact that background noise is usually consisted of low frequency band, which would dampen the relative height of the 100 Hz peak. Nevertheless, this means that we should consider the normal operating noise as the baseline to compare other cases to instead of the background noise, to get good results when trying to locate faults in the reactors. The extra lines drawn in all the figures are located at 100 Hz, and at 6 dB. The 6 dB level means quadrupling the sound power, which will be shown to be surpassed in the cases where an audible sound

was heard later in this chapter.

We did one test case which is picture in the Figure 3.55 in which one isolator was loosened, and then two tube extenders were listened to to see if there's any change in the sound produced. As we can see from the figure, unsurprisingly, the 100 Hz is exactly the same as in the normal operating conditions. Other than that we see little change in channel two (the blue curve), and some small changes in channel three (the green curve) especially at very high frequencies. We see only singular frequency rising over 6 dB level in channel three, which might indicate some faint change in the noise produced by the reactor, but it can't be further verified by this singular measurement.

Next we caused incrementally worse faults to see when the reactor would produce audible noise. In this measurement the tube extenders were upwards. First we loosened supporting bar, then loosened middle pipe and finally we loosened the lifting lug. The differences in spectra when going from normal operating noise to more and more severe fault condition one by one can be seen in the Figure 3.56. Here we can see that the loosening of the bar (the red curve) caused some small changes in the sound, especially there was a small hill at around 2 kHz. Change from this situation to having an additional loose middle bar (the green curve) has even lower overall amplitude, but has also two hills at around 1 kHz and 3 kHz. Finally the blue curve shows the situation when moved from the situation shown at the green curve to loose lifting lug case. This one's around 10 dB higher than the previous case at almost the whole frequency band. This one was clearly heard by the measurers, and the pure amplitude difference seen from the figure explains the sensory reception well. We can also note that in all three cases the difference at the 100 Hz is close to zero again. When comparing the loose lifting lug case to normal operating noise in the Figure 3.57 in all three channels, we see that each and every channel is over the 6 dB amplitude difference. Still, there's quite big variation in the amplitude differences, as channel three (red) has mostly barely over 6 dB amplitude difference, whereas channel two's (green) difference reaches over 24 dB. This noise would've been noticed with all three channels, but in order to measure this kind of faults precisely it's important to remember that the absolute amplitudes do not matter, but the differences, and that 6 dB difference means already that the sound power has quadrupled, so it's a very meaningful difference.

Our final measurement was also an incremental fault case with the tube

extenders in the upwards position. We compared the normal operating noise to the case where an input bolt was loose, and then we compared that case to the case where in addition we added extra loose bolts to the input. The differences can be seen in the Figure 3.58. Here the first case (green curve) wasn't audible, but the second (blue curve) was. When looking at the Figure 3.58 this might be bit counter-intuitive as the overall amplitude level of the first difference spectrum (green) is higher than the second one (blue). According to my understanding this is mostly due to the fact that ears are quite good at hearing singular loud high frequencies better than wide bandwidth low frequency din. Luckily microphones can be perhaps used to hear these sounds which human ear can't. The Figure 3.59 shows the difference between the loose bolts case, and the normal background sound as heard in all three channels. In this figure we see that all three tube extenders hear the high frequency sound increase, but in addition to that channel two (green) hears additional peaks, which look like resonance frequencies. Overall, as in the previous case, any of the three channels would be enough to figure out that there's some fault going on in this case.

5. Recommendations for future research

Since the measurement for the compression was done using a DC voltage due to the difficulties in measuring quickly changing compression when using AC voltage, it would be recommended to try and measure the compression using AC voltage. This could be perhaps achieved by using a laser measuring technology. Of course since the real life element is impregnated with oil, it would be best to measure it directly, but this researcher has no good method to offer in order to perform such a measurement.

A replacement or complement to the measurement would be a model of the singular element that could be used in simulations. Since the element's layers are extremely thin compared to its other dimensions, a direct simulation was deemed impossible as this work was being written. Some insight in what kind of simplifications could be done to facilitate the simulations would be a good next step to start with.

Since the sides of the capacitors do not seem to follow exactly the rules and formulas for the clamped plates, a new way of modeling them would be also needed. After there's a new theory for both individual elements, and capacitor sides, the simulation results could be tested by comparing them to the direct vibration measurements. For more thorough testing, and getting a better overview of the situation it could be a good idea to conduct a more thorough vibration testing as was done by Cox and Guan [19]. If a simulation model can be created that gives us a realistic vibration response, it could be then most probably used to calculate sound response as well.

The changes that occur in the capacitor's vibration response when the temperature changes were quite adequately explained through the use of viscosity in this work. Further work in this section could entail a more complex formula. This could yield a more agreeable result when we move

to higher frequency range. A completely new type of formula would be also needed to explain the differences in the vibration response at high frequencies.

Since the tube extenders were recognized as a good solution for transferring the sound away from the reactor, it would be recommended to research what kind of difference it makes to the response when other variables than length changes. These kind of variables would be for example the diameter of the tube, the thickness of the wall of the tube or change of material of the tube. For further field use it would be also highly recommended to research ways of installation that would best withstand the wear and tear of the weather.

To best use these tube extenders to save money through fault identification there's plenty of work to be done in order to combine the sound of the individual faults to the spectra that can be measured. This is dependent on the response of the tube extenders, and thus it might be best to move to this part only after further researching the various options in the tube extenders.

Finally, the future research should take into consideration the option of placing the capacitors or reactors in sound-proof rooms of buildings or dampening the connection between the components and their supporting structures to lessen the vibrations as a means of sound reduction. This path of research may provide an alternative method to lessening the noise of these components without making changes to the components themselves.

6. Summary

In order to place power stations closer to the living quarters, we need to know how much sound they produce so we can estimate the noise pollution caused. Secondly, the users of the compensation equipment, namely capacitors and reactors, have noticed that reactors often produce extra sound before they break down.

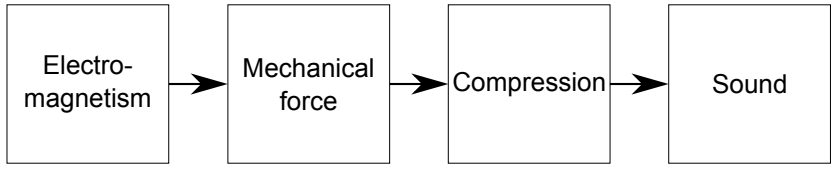

Figure 6.1. Flowchart showing how electromagnetism causes sound.

In order to understand how the compensation equipment produces noise we present here Figure 6.1. As we can see, the electromagnetism causes mechanical force to the equipment, which then causes compression. Compression causes fluctuation in pressure which is the very definition of sound.

The research started by trying to model a single capacitor element using finite element method (FEM). The same method was also applied in order to model the capacitor's sides as individual clamped plates. After modeling it was noticed that the capacitor element is too complicated to model directly with FEM, but the capacitor's sides were successfully modeled.

When the work moved to the domain of measurements, vibration measurements for each side were done to obtain the response of each side in respect to frequency and voltage pairs in three different temperatures. The measurements were done in cold, room, and warm temperature. In addition in the room temperature the measurements were done in two positions: the normal operating position where the capacitor is on its side, and standing up in order to fit the capacitor in the freezer that was used

to do the cold measurements. The results of these measurements were that the vibration response was increasing linearly as the function of frequency even though the voltage stayed the same. The power increase was deemed insignificant compared to the rating of the capacitor, and thus the current value itself might have an effect on the vibration. The temperature seemed to affect the vibration and this was seen best at the bottom plate responses at 50-700 Hz response range. With these parameters the cold plate vibrated the least, the warm the most, and the room temperature one was in between the two. The responses of the other two sides were more complicated, but the effect of temperature and frequency could be seen there as well. The variations in the vibration response due to the temperature were partially explained by the variation in the capacitor oil viscosity that was measured as a part of this work.

After the vibration measurements the work moved to measure the sound of the capacitor directly. This was done in the anechoic chamber, and yielded data, that could be compared to the vibration results. The comparison of the two was inconclusive at the first sight, but in the end it was seen that the lower the frequency, the more the vibration is comparable to the sound measured from close range. When we move to further distance or raise the frequency, the comparison is no longer valid. In these measurements a contour of the sound directivity was obtained. This allowed us to see that the two capacitors measured had completely different contours even though they were operated with the same frequency, and had partially the same physical dimensions.

With the respect to the capacitor noise we also observed that the capacitor noise is primarily caused by the bottom side. The bottom side vibrates roughly ten times as much as the larger sides of the capacitor, and thus changing the construction of that part would most probably significantly alter the spectrum of sound produced by the capacitor. The theoretical amplitude of the displacement of the capacitor's bottom side was also calculated based on the theoretical compression of the capacitor element, and matched with the empirical measurements.

Further work recommended to be done on capacitor includes examining the possibilities of making a simplified FEM model of a single element, and more complicated one of capacitor side or sides, as the clamped plate method was found not agreeing with the reality. Further, more thorough, vibration measurements could help in bringing more data to verify the simulation models against.

With the reactors the major issue was the method of measuring the sound. Since the high magnetic field precludes the use of normal microphones directly, a plastic tube extender was devised. This simple tool allowed for the noise to be moved farther from the reactor, and this in turn allowed for the use of a regular microphone to measure the noise.

The tube extender was installed in field conditions, and it was verified that the resulting noise measurements were reasonable. Further measurements in controlled environment allowed to posit that using the tube extender it was possible to "hear" the difference in the noise produced by the reactor when a fault is introduced to the system. The tube extenders' response was measured in anechoic chamber. There the effect of tube extender's length, isolation at its end, and variation due to hand-made nature was examined.

For the next step it would be recommended to further examine the various possibilities of materials that can be used in making of the tube extender. The changes in the tube extender probably change its frequency response, and thus might make it even better for the reactor measurements. Also, it could be possible to combine the different faults with the different spectra changes in the noise they cause. If these changes could be observed before the breakdown occurs, money could be saved with replacing the forced interruption with a controlled one.

Short summary of the scientific findings in this work:

- Compression of a single capacitor element depends linearly on the distance from its centre.

- Capacitor sides' natural frequencies have little effect on the vibration produced by the capacitor.

- Viscosity of the capacitor oil has a very clear effect on the vibration of the capacitor.

- Noise of a reactor can be measured using an inexpensive tube extender.

- Faults of a reactor can be "heard" using a microphone and spectrum analysis.

A. Air filled capacitor element DC measurement data

Point = location of a point (e.g. N5)
measured = measured average compression [µm]
x-distance = x-distance of the furthest edge from origo [mm]
y-distance = y-distance of the furthest edge from origo [mm]
xy-distance = distance of the furthest vertice from origo [mm]
xy-linest = linearly estimated value of the compression [µm]
U = 2.0±0.1kV C=9.69µF d=2*15.2µm Dry element

Table A.1 – Compression of 9.69µF element at 2.0 kV DC

Point	x-distance	y-distance	xy-distance	measured	xy-Linest
H5	20	20	28,28	93,3	91,32
I6	40	40	56,57	85	84,55
H7	20	60	63,25	83,8	82,95
J5	60	20	63,25	85,1	82,95
J7	60	60	84,85	81,7	77,77
I8	40	80	89,44	62,1	76,67
K6	80	40	89,44	79,7	76,67
L5	100	20	101,98	70	73,66
K8	80	80	113,14	65	70,99
L7	100	60	116,62	80	70,15
M6	120	40	126,49	69	67,79
N5	140	20	141,42	60	64,21
M8	120	80	144,22	61,7	63,54
N7	140	60	152,32	68,4	61,6

x-distance	Correlation:	-0,68
y-distance	Correlation:	-0,4
xy-distance	Correlation:	-0,83

xy-linest:

-0,24	98,1
0,05	4,86
0,69	6,2
26,42	12
1015,86	461,39

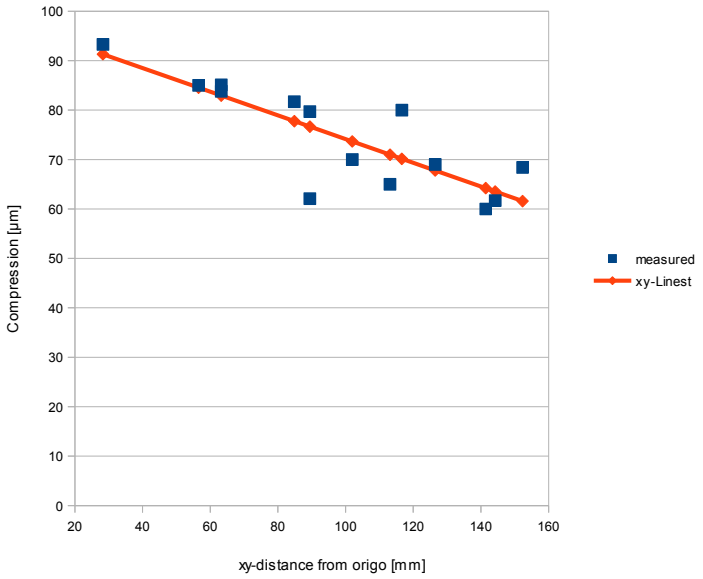

Figure A.1 – Compression of 9.69µF element at 2.0 kV

Point = location of a point (e.g. N5)
measured = measured average compression [µm]
x-distance = x-distance of the furthest edge from origo [mm]
y-distance = y-distance of the furthest edge from origo [mm]
xy-distance = distance of the furthest vertice from origo [mm]
xy-linest = linearly estimated value of the compression [µm]
U = 2.6±0.1kV C=9.69µF d=2*15.2µm Dry element

Table A.2 – Compression of 9.69µF element at 2.6 kV DC

Point	x-distance	y-distance	xy-distance	measured	xy-Linest
H5	20	20	28,28	136,7	133,26
I6	40	40	56,57	130	123,6
J5	60	20	63,25	120	121,32
H7	20	60	63,25	126,7	121,32
J7	60	60	84,85	113,3	113,94
K6	80	40	89,44	113,3	112,37
I8	40	80	89,44	90	112,37
L5	100	20	101,98	106,7	108,09
K8	80	80	113,14	90	104,28
L7	100	60	116,62	123,3	103,09
M6	120	40	126,49	96,7	99,72
N5	140	20	141,42	92,5	94,62
M8	120	80	144,22	93,3	93,66
N7	140	60	152,32	100	90,9

x-distance	Correlation:	-0,64
y-distance	Correlation:	-0,42
xy-distance	Correlation:	-0,78

xy-linest:

-0,34	142,92
0,08	8,14
0,61	10,39
19,1	12
2063,25	1296,11

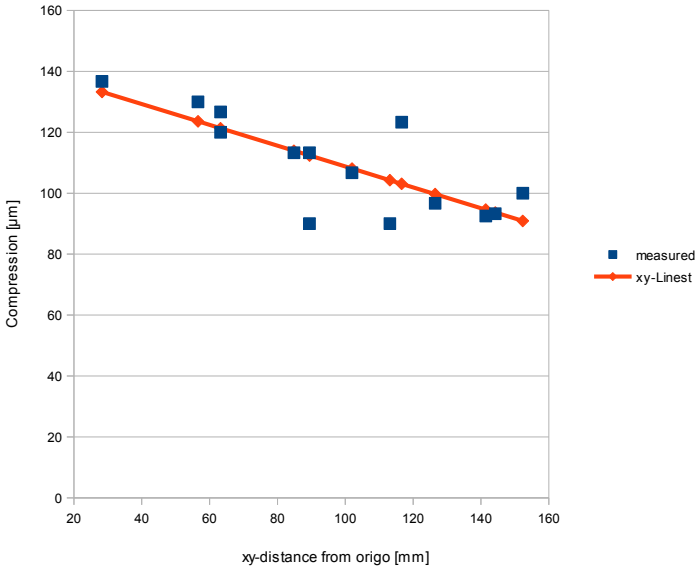

Figure A.2 – Compression of 9.69µF element at 2.6 kV

Point = location of a point (e.g. N5)
measured = measured average compression [µm]
x-distance = x-distance of the furthest edge from origo [mm]
y-distance = y-distance of the furthest edge from origo [mm]
xy-distance = distance of the furthest vertice from origo [mm]
xy-linest = linearly estimated value of the compression [µm]
U = 3.2±0.1kV C=9.69µF d=2*15.2µm Dry element

Table A.3 – Compression of 9.69µF element at 3.2 kV DC

Point	x-distance	y-distance	xy-distance	measured	xy-Linest
A4	140	20	141,42	126,7	144,47
A5	140	20	141,42	146,7	144,47
C4	100	20	101,98	145	162,62
C5	100	20	101,98	195	162,62
E4	60	20	63,25	170	180,45
E5	60	20	63,25	206,7	180,45
G4	20	20	28,28	166,7	196,54
G5	20	20	28,28	206,7	196,54
H4	20	20	28,28	176,7	196,54
H5	20	20	28,28	210,7	196,54
H7	20	60	63,25	191,1	180,45
I5	40	20	44,72	213,4	188,97
I6	40	40	56,57	187,1	183,52
I8	40	80	89,44	143,4	168,39
J4	60	20	63,25	166,7	180,45
J5	60	20	63,25	182,5	180,45
J7	60	60	84,85	172,7	170,5
K5	80	20	82,46	173,3	171,6
K6	80	40	89,44	176,7	168,39
K8	80	80	113,14	140	157,48
L4	100	20	101,98	153,3	162,62
L5	100	20	101,98	155,9	162,62
L7	100	60	116,62	173,3	155,88
M5	120	20	121,66	153,3	153,56
M6	120	40	126,49	151,7	151,34
M8	120	80	144,22	127,9	143,18
N4	140	20	141,42	143,3	144,47
N5	140	20	141,42	140	144,47
N6	140	40	145,6	160	142,54
N7	140	60	152,32	155	139,45

x-distance	Correlation:	-0,69
y-distance	Correlation:	-0,29
xy-distance	Correlation:	-0,76

xy-linest:	
-0,46	209,55
0,07	7,48
0,58	16,06
38,2	28
9858.8	7225.58

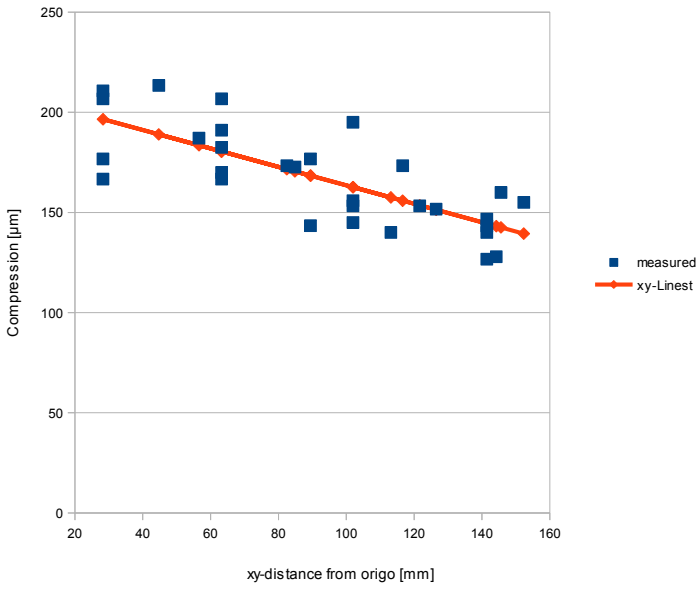

Figure A.3 – Compression of 9.69µF element at 3.2 kV

Point = location of a point (e.g. N5) C=9.69µF d=2*15.2µm Dry element
Compression = measured average compression [µm]
xy-distance = distance of the furthest vertice from origo [mm]
xy-linest = linearly estimated value of the compression [µm]

Table A.4 – Summary of compression of 9.69µF element

Point	xy-distance	3.2 xy-linest	2.6 xy-linest	2.0 xy-linest
H5	28,28	196,54	133,3	91,3
I6	56,57	183,52	123,6	84,5
H7	63,25	180,45	121,3	82,9
J5	63,25	180,45	121,3	82,9
J7	84,85	170,5	113,9	77,8
I8	89,44	168,39	112,4	76,7
K6	89,44	168,39	112,4	76,7
L5	101,98	162,62	108,1	73,7
K8	113,14	157,48	104,3	71
L7	116,62	155,88	103,1	70,2
M6	126,49	151,34	99,7	67,8
N5	141,42	144,47	94,6	64,2
M8	144,22	143,18	93,7	63,5
N7	152,32	139,45	90,9	61,6

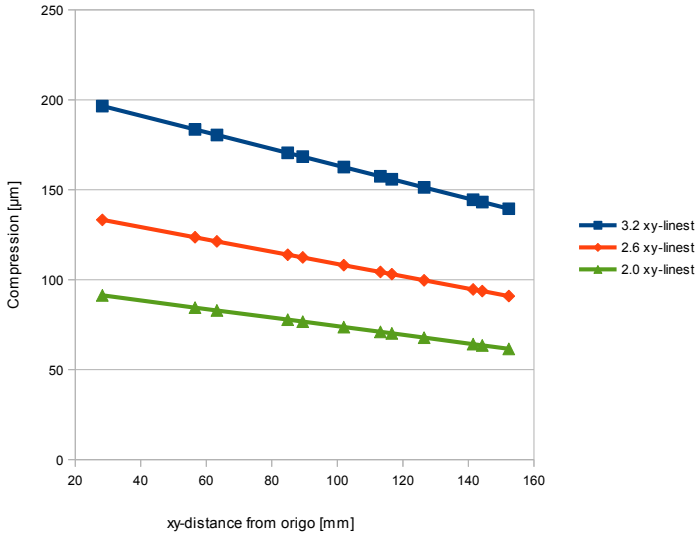

Figure A.4 – Compression of 9.69µF element at different voltages

B. Simulated amplitudes at different frequencies

Displacement field
abs(z-component)

1e6*sin(2*pi*f) [Pa] load

f	Amp	Amp*1e16	Log (Amp*1e16)
311,4	206,42	2,06E+018	18,31
434,7	0,04	3,5300E+014	14,55
649,7	59,69	5,97E+017	17,78
791,9	0,01	5,3134E+013	13,73
909,1	0,00	3,6055E+013	13,56
952,2	0,01	5,1205E+013	13,71
1110,3	0,00	4,4121E+013	13,64
1338,1	3,71	3,71E+016	16,57
1397,5	0,00	75,69	1,88
1531,5	0,00	73,93	1,87

f	Amp	Amp*1e16	Log (Amp*1e16)
50	5,65E-017	0,57	-0,25
60	1,26E-015	12,57	1,10
100	1,24E-016	1,24	0,09
120	2,87E-015	28,66	1,46
150	1,89E-015	18,9	1,28
180	6,76E-016	6,76	0,83
200	3,87E-016	3,87	0,59
240	1,25E-014	124,85	2,10
250	1,34E-014	133,51	2,13
300	4,31E-014	431,27	2,63
350	3,25E-014	324,51	2,51
360	2,97E-015	29,69	1,47
400	8,07E-016	8,07	0,91
420	1,64E-015	16,43	1,22
450	5,07E-015	50,7	1,70
480	9,66E-015	96,61	1,99
500	8,29E-015	82,95	1,92
540	6,50E-015	64,99	1,81
550	8,33E-016	8,33	0,92
600	5,90E-015	59	1,77
650	1,14E-012	11446	4,06
660	5,23E-014	523,27	2,72
700	1,13E-014	112,63	2,05
720	9,85E-016	9,85	0,99
750	3,01E-015	30,1	1,48
780	4,31E-015	43,12	1,63
800	2,73E-016	2,73	0,44
840	5,73E-016	5,73	0,76
850	4,17E-015	41,67	1,62
900	1,85E-015	18,5	1,27
950	1,06E-016	1,06	0,02
960	3,66E-015	36,61	1,56
1000	3,20E-015	32,03	1,51
1020	8,00E-016	8	0,90
1050	1,69E-015	16,88	1,23
1080	2,56E-015	25,56	1,41

1100	3,27E-016	3,27	0,51
1140	1,10E-016	1,1	0,04
1150	3,28E-015	32,85	1,52
1200	2,08E-015	20,84	1,32
1250	7,46E-016	7,46	0,87
1260	7,68E-016	7,68	0,89
1300	7,50E-015	74,98	1,87
1320	2,07E-014	207,18	2,32
1350	1,12E-014	112,02	2,05
1380	2,52E-015	25,16	1,40
1400	8,84E-015	88,35	1,95
1440	1,02E-015	10,25	1,01
1450	6,92E-015	69,15	1,84
1500	1,37E-014	136,62	2,14
1550	2,82E-015	28,23	1,45
1560	9,01E-015	90,07	1,95

1e6*sin(2*pi*f) [Pa] load

f	Amp	Amp*1e16	Log (Amp*1e16)
280	1,97E-014	196,61	2,29
290	2,59E-014	258,7	2,41
300	4,31E-014	431,27	2,63
305	1,33E-014	132,68	2,12
310	3,10E-014	310,3	2,49
311	1,38E-012	13788	4,14
311,2	24,33	2,43E+017	17,39
311,3	52,48	5,25E+017	17,72
311,4	206,42	2,06E+018	18,31
311,5	3,69E-013	3691,6	3,57
311,6	13,12	1,31E+017	17,12
311,8	10,96	1,10E+017	17,04
312	1,04E-012	10351	4,01
313	4,57E-013	4568,7	3,66
315	3,87E-014	387,1	2,59
320	4,31E-014	430,69	2,63
325	6,45E-014	644,71	2,81
330	7,42E-014	741,69	2,87
340	8,94E-014	893,85	2,95
370	1,93E-014	193,21	2,29
400	8,07E-016	8,07	0,91
410	9,22E-015	92,15	1,96
420	1,64E-015	16,43	1,22
430	6,78E-015	67,78	1,83
432	8,30E-015	83	1,92
433	5,13E-016	5,13	0,71
434	9,77E-015	97,75	1,99
434,4	0,02	2,1800E+014	14,34
434,5	2,51E-015	25,09	1,40
434,6	0,02	2,1800E+014	14,34
434,7	0,04	3,5300E+014	14,55
434,8	0,04	3,5200E+014	14,55
434,9	0,02	2,1700E+014	14,34
435	2,10E-015	20,98	1,32

435,5	6,67E-015	66,69	1,82
436	1,12E-014	112,05	2,05
437	3,63E-015	36,34	1,56
438	3,82E-015	38,22	1,58
440	2,23E-015	22,32	1,35
445	9,35E-015	93,48	1,97
450	5,07E-015	50,7	1,70
460	2,69E-015	26,88	1,43
470	3,81E-015	38,08	1,58
480	9,66E-015	96,61	1,99
500	8,29E-015	82,95	1,92
550	8,33E-016	8,33	0,92
600	5,90E-015	59	1,77
620	7,10E-015	71	1,85
630	3,14E-015	31,39	1,50
640	1,52E-014	151,93	2,18
645	7,02E-015	70,18	1,85
647	2,57E-014	257,29	2,41
648	1,67E-013	1674,5	3,22
649	1,51E-013	1513,5	3,18
649,5	1,02E-012	10163	4,01
649,6	4,53	4,53E+016	16,66
649,7	59,69	5,97E+017	17,78
649,8	9,71	9,71E+016	16,99
649,9	2,78	2,78E+016	16,44
650	1,14E-012	11446	4,06
651	1,14E-013	1143,4	3,06
652	1,61E-013	1611,4	3,21
653	6,64E-014	663,97	2,82
655	4,29E-014	429,27	2,63
660	5,23E-014	523,27	2,72
670	1,63E-014	163,4	2,21
680	3,56E-015	35,63	1,55

C. Viscosity measurement data

T [ºC]	RPM	Torque %	Visc. [cP]	Visc_c [cP]	T [K]	1 / T [1 / K]	ln Visc_c
-42,56	0,5	21,1	253	227,7	230,59	0,0043367015	5,43
-42,4	0,6	24,9	249	224,1	230,75	0,0043336945	5,41
-42,4	1	38,9	233,4	210,06	230,75	0,0043336945	5,35
-42,3	1,5	57,1	228,4	205,56	230,85	0,0043318172	5,33
-42,3	2	74,6	223,8	201,42	230,85	0,0043318172	5,31
-42,3	2,5	93,1	223,4	201,06	230,85	0,0043318172	5,30
-39,74	0,5	15,2	182	163,8	233,41	0,0042843066	5,10
-39,75	0,6	17	170	153	233,4	0,0042844901	5,03
-39,75	1	26,1	156,6	140,94	233,4	0,0042844901	4,95
-39,76	1,5	38,6	154,4	138,96	233,39	0,0042846737	4,93
-39,75	2	51,1	153,3	137,97	233,4	0,0042844901	4,93
-39,76	2,5	63,5	152,4	137,16	233,39	0,0042846737	4,92
-39,76	3	75,9	151,8	136,62	233,39	0,0042846737	4,92
-35,14	1	19,8	118,8	106,92	238,01	0,0042015041	4,67
-35,13	1,5	27,4	109,6	98,64	238,02	0,0042013276	4,59
-35,13	2	35,5	106,5	95,85	238,02	0,0042013276	4,56
-35,13	2,5	43,8	105,1	94,59	238,02	0,0042013276	4,55
-35,12	3	51,9	103,8	93,42	238,03	0,0042011511	4,54
-35,12	4	68,2	102,3	92,07	238,03	0,0042011511	4,52
-35,1	5	84,2	101	90,9	238,05	0,0042007982	4,51
-30,59	1,5	16,4	65,6	59,04	242,56	0,0041226913	4,08
-30,59	2	21,3	63,9	57,51	242,56	0,0041226913	4,05
-30,58	2,5	25,9	62,2	55,98	242,57	0,0041225213	4,02
-30,59	3	30,6	61,2	55,08	242,56	0,0041226913	4,01
-30,58	4	39,9	59,9	53,91	242,57	0,0041225213	3,99
-30,58	5	49,1	58,9	53,01	242,57	0,0041225213	3,97
-30,59	6	58,2	58,2	52,38	242,56	0,0041226913	3,96
-30,58	10	96,2	57,72	51,948	242,57	0,0041225213	3,95
-25,78	2	17	51	45,9	247,37	0,0040425274	3,83
-25,77	2,5	20,4	49	44,1	247,38	0,004042364	3,79
-25,76	3	23,7	47,4	42,66	247,39	0,0040422006	3,75
-25,78	4	30,5	45,8	41,22	247,37	0,0040425274	3,72
-25,77	5	37,3	44,8	40,32	247,38	0,004042364	3,70
-25,76	6	44,3	44,3	39,87	247,39	0,0040422006	3,69
-25,76	10	72,6	43,56	39,204	247,39	0,0040422006	3,67
-25,77	12	86,4	43,2	38,88	247,38	0,004042364	3,66
-20,79	2,5	12,7	30,5	27,45	252,36	0,0039625931	3,31
-20,78	3	14,4	28,8	25,92	252,37	0,0039624361	3,26
-20,78	4	18,5	27,7	24,93	252,37	0,0039624361	3,22
-20,78	5	22,5	27	24,3	252,37	0,0039624361	3,19
-20,79	6	26,7	26,7	24,03	252,36	0,0039625931	3,18
-20,76	10	43,3	25,98	23,382	252,39	0,0039621221	3,15
-20,77	12	51,7	25,85	23,265	252,38	0,0039622791	3,15
-20,78	20	85,9	25,77	23,193	252,37	0,0039624361	3,14
-15,8	6	16,7	16,7	15,03	257,35	0,0038857587	2,71
-15,75	10	26,7	16,02	14,418	257,4	0,0038850039	2,67
-15,78	12	33	16	14,4	257,37	0,0038854567	2,67
-15,76	20	53	15,9	14,31	257,39	0,0038851548	2,66
-15,75	30	79,1	15,82	14,238	257,4	0,0038850039	2,66
-10,73	6	13,8	13,8	12,42	262,42	0,0038106852	2,52
-10,67	10	21,6	12,96	11,664	262,48	0,0038098141	2,46
-10,73	12	25,5	12,75	11,475	262,42	0,0038106852	2,44

-10,66	20	42,2	12,66	11,394	262,49	0,0038096689	2,43
-10,72	30	62,6	12,52	11,268	262,43	0,00381054	2,42
-5,78	10	19,1	11,46	10,314	267,37	0,0037401354	2,33
-5,73	12	22,6	11,3	10,17	267,42	0,0037394361	2,32
-5,77	20	37,2	11,16	10,044	267,38	0,0037399955	2,31
-5,74	30	55,1	11,02	9,918	267,41	0,0037395759	2,29
-5,77	50	91	10,92	9,828	267,38	0,0037399955	2,29
-0,74	12	19,1	9,55	8,595	272,41	0,0036709372	2,15
-0,74	20	31,3	9,39	8,451	272,41	0,0036709372	2,13
-0,74	30	46,2	9,24	8,316	272,41	0,0036709372	2,12
-0,78	60	91,6	9,16	8,244	272,37	0,0036714763	2,11
-0,76	50	76,3	9,16	8,244	272,39	0,0036712067	2,11
14,97	12	16,1	8,05	7,245	288,12	0,0034707761	1,98
14,97	20	26,2	7,86	7,074	288,12	0,0034707761	1,96
14,97	30	38,8	7,76	6,984	288,12	0,0034707761	1,94
4,33	20	25,2	7,56	6,804	277,48	0,0036038633	1,92
14,97	50	62,8	7,54	6,786	288,12	0,0034707761	1,91
14,97	60	75,2	7,52	6,768	288,12	0,0034707761	1,91
4,33	30	37,1	7,42	6,678	277,48	0,0036038633	1,90
4,33	50	61,1	7,33	6,597	277,48	0,0036038633	1,89
4,33	60	73,2	7,32	6,588	277,48	0,0036038633	1,89
9,33	20	23,5	7,05	6,345	282,48	0,0035400736	1,85
9,32	30	34,4	6,88	6,192	282,47	0,003540199	1,82
9,31	50	56,6	6,79	6,111	282,46	0,0035403243	1,81
9,33	60	67,7	6,77	6,093	282,48	0,0035400736	1,81
19,98	20	22,3	6,69	6,021	293,13	0,0034114557	1,80
14,3	20	22,2	6,66	5,994	287,45	0,0034788659	1,79
19,98	30	33	6,6	5,94	293,13	0,0034114557	1,78
19,98	50	54,2	6,5	5,85	293,13	0,0034114557	1,77
14,28	30	32,5	6,5	5,85	287,43	0,003479108	1,77
19,98	60	64,6	6,46	5,814	293,13	0,0034114557	1,76
14,31	50	53,5	6,42	5,778	287,46	0,0034787449	1,75
19,35	20	21,3	6,39	5,751	292,5	0,0034188034	1,75
14,3	60	63,8	6,38	5,742	287,45	0,0034788659	1,75
19,38	30	31,1	6,22	5,598	292,53	0,0034184528	1,72
19,36	50	51,1	6,13	5,517	292,51	0,0034186865	1,71
19,36	60	61,2	6,12	5,508	292,51	0,0034186865	1,71
24,95	20	19,2	5,76	5,184	298,1	0,003354579	1,65
24,95	30	28,4	5,68	5,112	298,1	0,003354579	1,63
24,95	50	46,6	5,59	5,031	298,1	0,003354579	1,62
24,95	100	92,8	5,568	5,0112	298,1	0,003354579	1,61
24,95	60	55,5	5,55	4,995	298,1	0,003354579	1,61
29,92	30	25	5	4,5	303,07	0,0032995678	1,50
29,92	50	41	4,92	4,428	303,07	0,0032995678	1,49
29,92	100	71,4	4,884	4,3956	303,07	0,0032995678	1,48
29,92	60	48,8	4,88	4,392	303,07	0,0032995678	1,48
34,9	30	22,3	4,46	4,014	308,05	0,0032462263	1,39
34,9	50	36,4	4,37	3,933	308,05	0,0032462263	1,37
34,9	60	43,3	4,33	3,897	308,05	0,0032462263	1,36
34,9	100	72,1	4,326	3,8934	308,05	0,0032462263	1,36
39,92	30	20,1	4,02	3,618	313,07	0,0031941738	1,29
39,92	50	32,7	3,92	3,528	313,07	0,0031941738	1,26
39,92	60	39	3,9	3,51	313,07	0,0031941738	1,26

39,92	100	64,5	3,87	3,483	313,07	0,0031941738	1,25
44,93	30	18,1	3,62	3,258	318,08	0,0031438632	1,18
44,93	50	29,4	3,53	3,177	318,08	0,0031438632	1,16
44,93	60	35	3,5	3,15	318,08	0,0031438632	1,15
44,93	100	58	3,48	3,132	318,08	0,0031438632	1,14
49,99	50	26,8	3,22	2,898	323,14	0,0030946339	1,06
49,99	60	31,8	3,18	2,862	323,14	0,0030946339	1,05
49,99	100	52,6	3,156	2,8404	323,14	0,0030946339	1,04
54,98	50	24,6	2,95	2,655	328,13	0,0030475726	0,98
54,98	60	29,2	2,92	2,628	328,13	0,0030475726	0,97
54,98	100	48,2	2,892	2,6028	328,13	0,0030475726	0,96
60	50	22,7	2,72	2,448	333,15	0,0030016509	0,90
60	60	26,7	2,67	2,403	333,15	0,0030016509	0,88
60	100	44,2	2,652	2,3868	333,15	0,0030016509	0,87

Bibliography

[1] E. J. Abbott. Quieting Substation Equipment. *Transactions of the American Institute of Electrical Engineers,*, 54(1):20 – 26, 1935.

[2] B. Abedian and K. N. Baker. Temperature effects on the electrical conductivity of dielectric liquids. *IEEE Transactions on Dielectrics and Electrical Insulation*, 15(3):888–892, 2008.

[3] M. Abramowitz and W. F. Cahill. On the vibration of a square clamped plate. *Journal of the ACM*, (1):162–168, 1955.

[4] P. N. Adkins. Transformer Noise Reduction witk a Close-Fitting Mass-Law Enclosure. *IEEE Transactions on Power Apparatus and Systems*, 82(66):302 – 308, 1963.

[5] AIEE Committee. Bibliography on Transformer Noise - AIEE Committee Report. *Power Apparatus and Systems, Part III. Transactions of the American Institute of Electrical Engineers*, 79(3):735–740, 1960.

[6] AIEE Committee. Suggestions for Improving the Accuracy of Transformer Noise Tests in Tde Field AIEE Committee Report. *Power Apparatus and Systems, Part III. Transactions of the American Institute of Electrical Engineers*, 80(3):1–3, 1961.

[7] J. P. Arenas. On the vibration analysis of rectangular clamped plates using the virtual work principle. *Journal of Sound and Vibration*, 266(4):912–918, September 2003.

[8] J. Aubin and Y. Langhame. Effect of oil viscosity on transformer loading capability at low ambient temperatures. *IEEE Transactions on Power Delivery*, 7(2):516–524, 1992.

[9] D. W. Auckland, K. Chandraker, M. A. Golra, and B. R. Varlow. Water treeing in insulating liquids. *IEE Proceedings Science, Measurement and Technology*, 142(2):157–161, 1995.

[10] N. S. Bardell, R. S. Langley, and J. M. Dunsdon. On the free in-plane vibration of isotropic rectangular plates. *Journal of Sound and Vibration*, 191(3):459–467, 1996.

[11] R. Bartnikas. Electrical Conduction in Medium Viscosity Oil-Paper Films-Part II. *IEEE Transactions on Electrical Insulation*, EI-9(3):85–91, September 1974.

[12] C. E. Baugh. Audio noise of power transformers in residential and commercial areas. *Transactions of the American Institute of Electrical Engineers*, 69(1):121–128, 1950.

[13] B. N. W. Bazley, D. W. Fox, and J. T. Stadter. Upper and Lower Bounds for the Frequencies of Rectangular Clamped Plates. *Journal of Applied Mathematics and Mechanics*, (3):191–198, 1967.

[14] A. W. Benoit, R. T. Hemmes, and M. W. Schulz. An Anechoic Chamber for Noise Tests on Large Power Transformers. *Power Apparatus and Systems, Part III. Transactions of the American Institute of Electrical Engineers*, 74(3):50–56, 1955.

[15] L. L. Beranek. *Acoustics*. McGraw-Hill Book Company, Inc., 1954.

[16] J. Borenius, E. Lampio, K. Pesonen, T. Jauhiainen, J. Nuotio, I. Pyykkö, and Insinööritieto Oy. *Akustiikan perusteet*. Insinööritieto Oy, Espoo, Finland, 1981.

[17] Y Champoux. Application of the intensity technique to the characterization of transformer noise. *IEEE Transactions on Power Delivery*, 3(4), 1988.

[18] W. B. Conover and R. J. Ringlee. Recent contributions to transformer audible noise control. *Power Apparatus and Systems, Part III. Transactions of the American Institute of Electrical Engineers*, 74(3):77–90, 1955.

[19] M. D. Cox and H. H. Guan. Vibration and audible noise of capacitors subjected to nonsinusoidal waveforms. *IEEE Transactions on Power Delivery*, 9(2):856–862, 1994.

[20] J. Dai and Z. Wang. A Comparison of the Impregnation of Cellulose Insulation by Ester and Mineral oil. *IEEE Transactions on Dielectrics and Electrical Insulation*, 15(2):374–381, April 2008.

[21] Z. Ding. Natural frequencies of rectangular plates using a set of static beam functions in Rayleigh-Ritz method. *Journal of Sound and Vibration*, 189:81–87, 1996.

[22] A. T. Edwards. Transformer Noise Problem-Performance of Acoustic Treatments and Vibration Isolators. *Power Apparatus and Systems, Part III. Transactions of the American Institute of Electrical Engineers*, 76(3):1185 – 1191, 1957.

[23] J. W. Erven and C. S. Fiske. Location and design of distribution substations in residential areas. *Electrical Engineering*, 75(2):148 – 153, 1956.

[24] H. Fahnoe. A study of sound levels of transformers. *Electrical Engineering*, 60(June):277–283, 1941.

[25] F. Fahy. *Foundations of Engineering Acoustics*. Academic Press, 2007.

[26] I. Fofana, V. Wasserberg, H. Borsi, and E. Gockenbach. Challenge of Mixed Insulating Liquids for Use in High-Voltage Transformers , Part 1 : Investigation. *IEEE Electrical Insulation Magazine*, pages 18–31, 2002.

[27] S. L. Foster and E. Reiplinger. Charcteristics and Control of Transformer Sound. *IEEE Transactions on Power Apparatus and Systems*, PAS-100(3):1072–1077, 1981.

[28] E. E. Franco, J. C. Adamowski, R. T. Higuti, and F. Buiochi. Viscosity measurement of Newtonian liquids using the complex reflection coefficient. *IEEE transactions on ultrasonics, ferroelectrics, and frequency control*, 55(10):2247–53, October 2008.

[29] A. P. Fugill. Measurement of Noise From Power Transformers. *Transactions of the American Institute of Electrical Engineers*, 53(12):1603–1608, 1934.

[30] Y. Gao, K. Muramatsu, K. Fujiwara, Y. Ishihara, S. Fukuchi, and T. Takahata. Vibration Analysis of a Reactor Driven by an Inverter Power Supply Considering Electromagnetism and Magnetostriction. *IEEE Transactions on Magnetics*, 45(10):4789–4792, October 2009.

[31] Y. Gao, M. Nagata, K. Muramatsu, K. Fujiwara, Y. Ishihara, and S. Fukuchi. Noise Reduction of a Three-Phase Reactor by Optimization of Gaps Between Cores Considering Electromagnetism and Magnetostriction. *IEEE Transactions on Magnetics*, 47(10):2772–2775, October 2011.

[32] R. B. George. Power Transformer Noise Its Characteristics and Reduction. *Transactions of the American Institute of Electrical Engineers*, 50(1):347–352, 1931.

[33] B. Gettys and W. B. Conover. Acoustic Models of Transformer Installations. *Transactions of the American Institute of Electrical Engineers*, 70(1):333–338, 1951.

[34] S. G. E. Giap. The Hidden Property of Arrhenius-type Relationship: Viscosity as a Function of Temperature. *Journal of Physical Science*, 21(1), 2010.

[35] R. Girgis, M. Bernesjo, and S. Thomas. Development of ultra—Low noise transformer technology. *IEEE Transactions on Power Delivery*, 26(1):228–234, 2011.

[36] W. A. Glaeser. *Tribology, the Science of Combatting Wear*. 1981.

[37] C. G. Gordon. A method for predicting the audible noise emissions from large outdoors power transformers. *IEEE Transactions on Power Apparatus and Systems*, PAS-98(3):1109–1112, 1979.

[38] T. D. Gordy. Audible noise of power transformers. *Transactions of the American Institute of Electrical Engineers*, 69(1):45–53, 1950.

[39] D. J. Gorman. Accurate analytical type solutions for the free in-plane vibration of clamped and simply supported rectangular plates. *Journal of Sound and Vibration*, 276(1-2):311–333, September 2004.

[40] R. L. Grubb, M. Hudis, and A. R. Traut. A transformer thermal duct study of various insulating fluids. *IEEE Transactions on Power Apparatus and Systems*, 100(2):466–473, 1981.

[41] S. Hagiwara, Y. Hori, Y. Suzuki, and T. Obata. Vibration Analysis of a Large Capacity Shunt Reactor. *IEEE Transactions on Power Apparatus and Systems*, PER-2(3):737–745, 1982.

[42] R. M. Hakim. The Properties of an Insulating Oil and Its Fractions at Low Temperatures. *IEEE Transactions on Electrical Insulation*, 16(4):124–134, 1975.

[43] D. E. Hall. *Basic acoustics*. John Wiley & Sons, Inc., 1987.

[44] M. Hamada. A method for solving problems of vibration, deflection and buckling of rectangular plates with clamped or supported edges. *Bulletin of The Japan Society of Mechanical Engineers*, 1959.

[45] C. M. Harris, editor. *Handbook of noise control*. McGraw-Hill Book Company, Inc., 1957.

[46] R. T. Hemmes and D. G. Graham. Measurement of self cooled transformer sound levels in relatively high ambients. *IEEE Transactions on Power Apparatus and Systems*, PAS-89(7):1657 – 1662, 1970.

[47] R. D. Henshell, P. J. Bennett, H. McCallion, and M. Milner. Natural frequencies and mode shapes of vibration of transformer cores. *Proceedings of the Institution of Electrical Engineers*, 112(11):2133–2139, 1965.

[48] Y. Huang and K. Boyle. *Antennas: From Theory to Practice*. John Wiley & Sons Inc, 2008.

[49] IEC 60076-10. Power transformers – Part 10: Determination of sound levels, 2001.

[50] IEEE Committee. Bibliography on Transformer Noise. *IEEE Transactions on Power Apparatus and Systems*, PAS-87(2):372 – 387, 1968.

[51] ISO 226:2003. Acoustics – Normal equal-loudness-level contours, 2008.

[52] B. Jakoby and M. Scherer. An automotive engine oil viscosity sensor. *IEEE Sensors Journal*, 3(5):562–568, 2003.

[53] H. Ju and E. J. Gottlieb. An empirical method to estimate the viscosity of mineral oil by means of ultrasonic attenuation. *IEEE Transactions on Ultrasonics, Ferroelectrics and Frequency Control*, 57(7):1612–1620, 2010.

[54] B. P. Kang. Thermal Dependency of Viscosity, Power Factor, and Ion Content of Electrical Insulating Oils. *IEEE Transactions on Power Apparatus and Systems*, 84(9):756 – 761, 1965.

[55] M. Kanoi, Y. Hori, M. Maejima, and T. Obata. Transformer noise reduction with new sound insulation panel. *IEEE Transactions on Power Apparatus and Systems*, PAS-102(9):2817 – 2825, 1983.

[56] R. P. Kendig. Sound intensity of the Comerford HVDC converter station. *IEEE Transactions on Power Delivery*, 4(3):1876 – 1881, 1989.

[57] R. P. Kendig and S. E. Wright. Validation of acoustic intensity measurements for power transformers. *IEEE Transactions on Power Delivery*, 6(4):1524–1530, 1991.

[58] H. W. Kerr and S. Palmer. Developments in the design of large power transformers. *Proceedings of the Institution of Electrical Engineers*, 111(4):823 – 832, 1964.

[59] W. Kitagawa, Y. Ishihara, T. Todaka, and A. Nakasaka. Analysis of structural deformation and vibration of a transformer core by using magnetic property of magnetostriction. *Electrical Engineering in Japan*, 172(1):19–26, July 2010.

[60] M. Kohtoh, S. Kaneko, S. Okabe, and T. Amimoto. Aging effect on electrical characteristics of insulating oil in field transformer. *IEEE Transactions on Dielectrics and Electrical Insulation*, 16(6):1698–1706, December 2009.

[61] A. V. Lambert. Audio noise in transformers in residential areas. *Transactions of the American Institute of Electrical Engineers*, 70(2):1589 – 1598, 1951.

[62] Y. Langhame and J. Castonguay. Low temperature performance of naphthenic and paraffinic oils in transformers and automatic circuit reclosers. *IEEE Transactions on Power Apparatus and Systems*, PAS-104(April):1985, 1985.

[63] Y. Langhame, J. Castonguay, J.-P. Crine, M. Duval, and H. St-Onge. Physical Behavior of Paraffinic Oils at Low Temperatures. *IEEE Transactions on Electrical Insulation*, EI-20(3):629–638, June 1985.

[64] A. W. Leissa. *Vibration of plates*. National aeronautics and space administration, Washington, D.C., 1969.

[65] A. W. Leissa. The free vibration of rectangular plates. *Journal of Sound and Vibration*, 31(3):257–293, 1973.

[66] J. P. López, P. Mutjé, M. À. Pèlach, N.-E. El Mansouri, S. Boufi, and F. Vilaseca. Analysis of the tensile modulus of polypropylene composites reinforced with stone groundwood fibers. *BioResources*, 7(1):1310–1323, 2012.

[67] D. Martin, W. Guo, N. Lelekakis, and N. Heyward. Using a remote system to study the thermal properties of a vegetable oil filled power transformer: How does operation differ from mineral oil. *2011 IEEE PES Innovative Smart Grid Technologies*, pages 1–5, November 2011.

[68] D. N. May, editor. *Handbook of noise assessment*. Van Nostrand Reinhold Company, 1978.

[69] C. McLean. Confinement of transformer noise. *Electrical Engineering*, 70(4):325–330, 1951.

[70] I. S. Mendenhall and F. L. Taylor. Quiet Transformer Installations—A Problem for Both Equipment and Substation Designers. *Transactions of the American Institute of Electrical Engineers*, 69(2):1148 – 1153, 1950.

[71] A. K. Mitchell and C. R. Hazell. A simple frequency formula for clamped rectangular plates. *Journal of Sound and Vibration*, 118(2):271–281, 1987.

[72] C. S. Murray. Transformer Audio Noise Problems on an Electric Power System. *Transactions of the American Institute of Electrical Engineers*, 68(1):740–752, 1949.

[73] H. Nagaoka. The inductance coefficients of solenoids. *Journal of the college of science, Imperial university, Tokyo, Japan*, 27(6):33, 1909.

[74] H. F. Olson. The Measurement of Loudness. *Audio*, (February):18–22, 1972.

[75] C. H. Page and P. Vigoureux. *The international system of units (SI)*. 1974.

[76] W. Peng and J. Shengchang. Study on an Audible Noise Reduction Measure for Filter Capacitors Based on Compressible Space Absorber. *IEEE Transactions on Power Delivery*, 26(1):438–445, 2011.

[77] W. Peng, J. Shengchang, C. Tao, L. Yanming, L. Xiaolin, and L. Yan. Study on an Audible Noise Reduction Measure for the Filter Capacitors in the HVDC Converter Station Based on the MPP Absorber. *IEEE Transactions on Power Delivery*, 24(4):1756–1762, October 2009.

[78] C. Perrier, A. Beroual, and J. L. Bessede. Improvement of power transformers by using mixtures of mineral oil with synthetic esters. *IEEE Transactions on Dielectrics and Electrical Insulation*, 13(3):556–564, 2006.

[79] L. W. Pierce. An investigation of the thermal performance of an oil filled transformer winding. *IEEE Transactions on Power Delivery*, 7(3):1347–1358, 1992.

[80] R. L. St. Pierre and D. J. Maguire. The Impact of A-weighting Sound Pressure Level Measurements during the Evaluation of Noise Exposure. In *NOISE-CON 2004*, pages 1–8, 2004.

[81] T. D. Rossing. *The Science of Sound*. Addison-Westley Publishing Company, Inc., second edition, 1989.

[82] S. A. Ryder. Diagnosing transformer faults using frequency response analysis. *IEEE Electrical Insulation Magazine*, 19(2):16–22, 2003.

[83] M. W. Schulz and R. J. Ringlee. Some characteristics of audible noise of power transformers and their relationship to audibility criteria and noise ordinances. *Power Apparatus and Systems, Part III. Transactions of the American Institute of Electrical Engineers*, 79(3):316 – 322, 1960.

[84] K. Sezawa. On the Lateral Vibration of a rectangular plate clamped at four edges.pdf. *Report of the Aeronautical Research Institute, Tokyo Imperial University*, 70, 1931.

[85] P. Shao, L. Luo, Y. Li, and C. Rehtanz. Electromagnetic Vibration Analysis of the Winding of a New HVDC Converter Transformer. *IEEE Transactions on Power Delivery*, 27(1):123–130, 2012.

[86] J. Shengchang, W. Peng, Z. Qiaogen, and L. Yanming. Study on the Noise-Level Calculation Method for Capacitor Stacks in HVDC Converter Station. *IEEE Transactions on Power Delivery*, 25(3):1866–1873, July 2010.

[87] T. J. Singal. *Wireless Communications*. Tata McGraw Hill Education Private Limited, New Delhi, 2010.

[88] H. Smede and C. G. Johansson. Design of HVDC converter stations with respect to audible noise requirements. *IEEE Transactions on Power Delivery*, 10(2), 1995.

[89] SteelSS. Data Table for:Mould steel:UNS S40900. *Internet site of the manufacturer*, (http://www.steelss.com/Mould-steel/uns-s40900.html).

[90] C.-C. Sung and J. T. Jan. The response of and sound power radiated by a clamped rectangular plate. *Journal of Sound and Vibration*, 207(3):301–317, 1997.

[91] D. Susa, M. Lehtonen, and H. Nordman. Dynamic thermal modelling of power transformers. *IEEE Transactions on Power Delivery*, 20(1):197–204, 2005.

[92] The British Boardcasting Corporation Engineering Division. The assessment of noise in audio-frequency circuits. Technical report, 1968.

[93] The ITU Radiocommunication Assembly. Measurement of audio-frequency noise voltage level in sound broadcasting. Technical report, 1986.

[94] S. Tomotika. On the Transverse Vibration of a Square Plate with Four Clamped Edges. *Report of the Aeronautical Research Institute, Tokyo Imperial University*, 10:301, 1935.

[95] S. Tomotika. LX. The transverse vibration of a square plate clamped at four edges. *Philosophical Magazine*, 21(142):745–760, 1936.

[96] G. O. Usry and P. Saha. Prediction of far field sound radiation from transformers. *IEEE Transactions on Power Apparatus and Systems*, PAS-99(1):358–364, 1980.

[97] R. S. Vedam and M. S. Sarma. *Power Quality - VAR Compensation in Power Systems*. Taylor & Francis, Boca Raton (FL), 2009.

[98] I. L. Ver and D. W. Andersen. Field study of sound radiation by power transformers. *IEEE Transactions on Power Apparatus and Systems*, PAS-100(7):3513 – 3524, 1981.

[99] L. Verbruggen. Vibrations and sound of dry-type air-core reactors. Master's thesis, Helsinki University of Technology. Department of Electrical and Communications Engineering. Power Systems and High Voltage Engineering, Espoo, Finland, 2007.

[100] J. H. Vivian and R. R. Peck. An Investigation of Audio Noise in Substation-Type Transformers. *Transactions of the American Institute of Electrical Engineers*, 70(1), 1951.

[101] G. B. Warburton. The vibration of rectangular plates. *Proceedings of the institution of mechanical engineers*, 168(12):371–384, 1954.

[102] B. M. Weedy and B. J. Cory. *Electric Power Systems*. John Wiley & Sons, Inc., 2001.

[103] H. A. Wheeler. Simple inductance formulas for radio coils. *Proceedings of the Institute of Radio Engineers*, 16(10):1398–1400, 1928.

[104] S. Yasufuku. General Properties of Mixtures of Paraffinic Insulating Oil with Alkylbenzenes. *IEEE Transactions on Electrical Insulation*, EI-15(5):429 – 433, 1980.

[105] D. Young. Vibration of rectangular plates by the Ritz method. *Journal of applied mechanics*, 17:448–453, 1950.

Aalto-DD 155/2013

ISBN 978-952-60-5361-5
ISBN 978-952-60-5362-2 (pdf)
ISSN-L 1799-4934
ISSN 1799-4934
ISSN 1799-4942 (pdf)

Aalto University
School of Electrical Engineering
Department of Electrical Engineering
www.aalto.fi

BUSINESS +
ECONOMY

ART +
DESIGN +
ARCHITECTURE

SCIENCE +
TECHNOLOGY

CROSSOVER

DOCTORAL
DISSERTATIONS